AWARD NUMBER: W81XWH-17-1-0241

TITLE: *Plk1 Spatial Synchronization in Prostate Epithelial Cells during Mitosis*

PRINCIPAL INVESTIGATOR: Heidi Hehnly

CONTRACTING ORGANIZATION: Syracuse University, Syracuse, NY

REPORT DATE: January 2021

TYPE OF REPORT: Final

PREPARED FOR: U.S. Army Medical Research and Materiel Command
Fort Detrick, Maryland 21702-5012

DISTRIBUTION STATEMENT: Approved for Public Release;
Distribution Unlimited

The views, opinions and/or findings contained in this report are those of the author(s) and should not be construed as an official Department of the Army position, policy or decision unless so designated by other documentation.

# REPORT DOCUMENTATION PAGE

*Form Approved*
*OMB No. 0704-0188*

Public reporting burden for this collection of information is estimated to average 1 hour per response, including the time for reviewing instructions, searching existing data sources, gathering and maintaining the data needed, and completing and reviewing this collection of information. Send comments regarding this burden estimate or any other aspect of this collection of information, including suggestions for reducing this burden to Department of Defense, Washington Headquarters Services, Directorate for Information Operations and Reports (0704-0188), 1215 Jefferson Davis Highway, Suite 1204, Arlington, VA 22202-4302. Respondents should be aware that notwithstanding any other provision of law, no person shall be subject to any penalty for failing to comply with a collection of information if it does not display a currently valid OMB control number. **PLEASE DO NOT RETURN YOUR FORM TO THE ABOVE ADDRESS.**

| 1. REPORT DATE | 2. REPORT TYPE | 3. DATES COVERED |
|---|---|---|
| January 2021 | Final | 01Aug2017-31Oct2020 |

**4. TITLE AND SUBTITLE**

*Plk1 Spatial Synchronization in Prostate Epithelial Cells during Mitosis*

**5a. CONTRACT NUMBER**

**5b. GRANT NUMBER**
W81XWH-17-1-0241

**5c. PROGRAM ELEMENT NUMBER**

**6. AUTHOR(S)**

Heidi Hehnly, PhD

E-Mail: hhehnly@syr.edu

**5d. PROJECT NUMBER**

**5e. TASK NUMBER**

**5f. WORK UNIT NUMBER**

**7. PERFORMING ORGANIZATION NAME(S) AND ADDRESS(ES)**

Syracuse University
900 Crouse Ave. Ste 620
Syracuse, NY 13244

**8. PERFORMING ORGANIZATION REPORT NUMBER**

**9. SPONSORING / MONITORING AGENCY NAME(S) AND ADDRESS(ES)**

U.S. Army Medical Research and Materiel Command
Fort Detrick, Maryland 21702-5012

**10. SPONSOR/MONITOR'S ACRONYM(S)**

**11. SPONSOR/MONITOR'S REPORT NUMBER(S)**

**12. DISTRIBUTION / AVAILABILITY STATEMENT**

Approved for Public Release; Distribution Unlimited

**13. SUPPLEMENTARY NOTES**

**14. ABSTRACT**

Cell division is a process whereby genetic material is duplicated, separated, and packaged to yield two daughter cells. This process relies on spatial and temporal synchronization of protein kinase activity at the mitotic spindle, a macromolecular machine that segregates chromosomes towards the daughter cells. A major generator of this machine and organizer of mitotic signaling is the centrosome. Interphase cells have a single centrosome that nucleates microtubules for cellular material to transport on. When cells decide to divide into two, they duplicate their genetic material and their centrosomes to make two mitotic spindle poles, which function to nucleate microtubules to capture duplicated genetic material and distribute it equally to each daughter cell. We propose a testable model that defects in centrosome number and function lead to genomic instability causing a normal prostate epithelial cell genome to behave like a cancer genome. To test this, we are determining the mechanism of centrosome amplification in prostate cancer cells and its impact on genome stability. Our studies will address the overall hypothesis that deregulation of centrosome based signaling events leads to genomic instability and subsequent metastasis in prostate cancer.

**15. SUBJECT TERMS**

Chromosome instability, Centrosome based PLK1 signaling, Kinase activity

| 16. SECURITY CLASSIFICATION OF: | | | 17. LIMITATION OF ABSTRACT | 18. NUMBER OF PAGES | 19a. NAME OF RESPONSIBLE PERSON |
|---|---|---|---|---|---|
| a. REPORT | b. ABSTRACT | c. THIS PAGE | | | USAMRMC |
| Unclassified | Unclassified | Unclassified | Unclassified | 64 | 19b. TELEPHONE NUMBER *(include area code)* |

## TABLE OF CONTENTS


| | Page |
|---|---|
| 1. Introduction | 1 |
| 2. Keywords | 2 |
| 3. Accomplishments | 2 |
| 4. Impact | 6 |
| 5. Changes/Problems | 6 |
| 6. Products | 6 |
| 7. Participants & Other Collaborating Organizations | 7 |
| 8. Special Reporting Requirements | 8 |
| 9. Appendices | 9 |

## 1. INTRODUCTION:

Prostate cancer is the most common cancer in men, with a lifetime risk of one in seven, and it is the second leading cause of cancer death in men. In 2007, 97.5% of Veterans Affairs (VA) cancers were diagnosed among men with the most frequent being prostate cancer (31.8%) (Zullig *et al.*, 2012). Hormone therapy is an option for men with androgen sensitive prostate cancer who are not candidates for surgery, radiation, or have failed these therapies. However, hormone therapy is ineffective for androgen insensitive tumors. Here we examine prostate cancer samples from patients who failed hormone therapy with the goal of identifying molecular targets that can slow prostate cancer cell growth. Most control cells contain one centrosome, but in cancer cells supernumerary centrosomes are very common and have been positively associated with advanced tumor metastasis (Pihan *et al.*, 2001). However, the mechanisms determining whether supernumerary centrosomes lead to increased metastatic behavior in prostate cancer have not been determined. The overall goal of this proposal was to determine the impact of centrosome deregulation on genome stability and tissue architecture. Specifically, we tested the hypothesis that the mitotic kinase, polo-like kinase 1 (PLK1), centrosome-based signaling events regulate centrosome function, genome stability, and metastasis. My laboratory made several contributions to these goals (Colicino and Hehnly, 2018; Colicino *et al.*, 2018; 2019). Specifically, We determined that centrosome localized signaling events regulate genomic stability to subsequently influence tissue architecture and cellular behavior. Our findings demonstrated that primary patient cell lines with supernumerary centrosomes display abnormalities in several PLK1 scaffold protein expression and in PLK1 itself (Fig 1). Thus, we proposed a scenario where PLK1-centrosome-localized scaffolds, such as cenexin and/or Gravin, are disrupted causing a deregulation in PLK1-activity at specific sub-centrosome locales. Abnormal Plk1 signaling has been linked to genomic instability, which can result in copy number alteration and chromosomal rearrangements that are associated with prostate cancer. Several key regulatory genes are thought to be lost due to chromosomal rearrangements, such as PTEN at 10q23. With our long-term studies we hope to identify specific chromosomal fragile sites (CFSs) to determine how a normal genome is reorganized to produce a prostate cancer genome. This may reveal a mechanism for specific genomic rearrangements in prostate cancer, identify new cancer-associated genes, and provide early diagnostic tools to predict cancer development. Our long-term goal is to provide an explanation for how prostate cells with abnormal centrosomes could conceivably contribute to disease development and progression through abnormal PLK1 signaling.

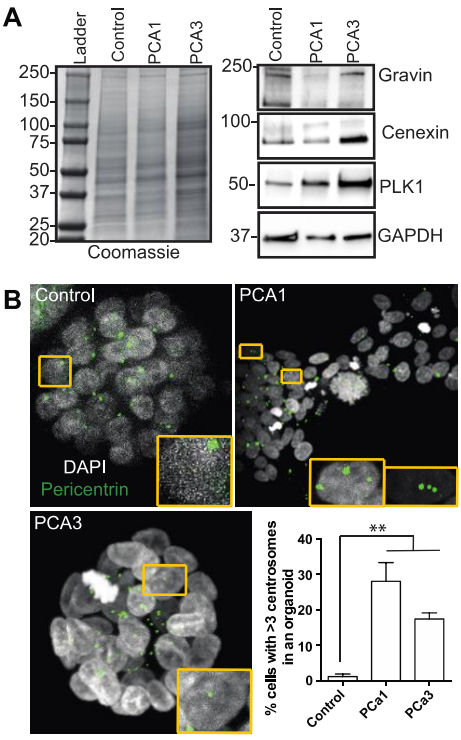



Figure 1. ***The use of primary 3D cultures to examine the role of centrosomes and PLK1 in prostate cancer.*** (A) Protein expression patterns of two PLK1 scaffolds, Gravin and cenexin, and PLK1. (B) Characterization of supernumerary centrosomes in organoids.

**2. KEYWORDS:**

Scaffolds
Kinases
PLK1: Polo-Like Kinase 1
Centrosome
Mitosis
Signaling
Spindle
Chromosome-instability
Aneuploidy
Gravin
Cenexin
Mitosis
Cytokinesis

**3. ACCOMPLISHMENTS:**

***The major accomplishments are described below in accordance with our approved SOW and discusses major activities, specific objectives, and significant results with resulting publication.***

- ***What were the major goals of the project?***

**Aim 1:** Determine mechanisms of centrosome amplification and determine its impact on genome stability.

**1)** *Determining the mechanism of centrosome amplification.* This task is still underway.

**2)** *Determine whether supernumerary centrosomes lead to increased genetic instability.* This task is still underway.

**3)** *Determine whether supernumerary centrosomes lead to increased cellular invasion.* This task is still underway.

**Aim 2:** Determine whether loss of specific PLK1 scaffolds affect PLK1 activity.

**Task 1 from this aim has been completed and published in two manuscripts (Colicino et al. MBoC 2018, 2019).** Where we completed tasks 1 in our presented SOW outlined below.

**1)** *Determine whether loss of specific PLK1 scaffolds affect PLK1 activity*

**2)** *Determine whether supernumerary centrosomes disrupt PLK1 distribution and subsequent activity.* This task is currently underway, and we hope to be preparing it for publication.

- ***What was accomplished under these goals?***

**Goals of AIM 1 we accomplished:**

In our submitted SOW we proposed for our first aim to accomplish the optimization of 3-D culture for fixed and live-cell imaging to determine the mechanism of centrosome amplification, optimize organoid growth for super resolution imaging (e.g. SIM), and processing and quantification of all imaging experiments. We have optimized 3-D primary prostate cancer cell organoid growth (featured in (Colicino *et al.*, 2018); refer to appendix). We have quantified the percentage of cells that have supernumerary centrosomes (~25-30%, Figure 1). We are currently in the process of trying to express a centrosome marker in primary prostate cancer samples but have yet to efficiently do so. We have successfully done this in immortalized prostate cancer cells, which we are also using for our studies. We have successfully optimized super resolution imaging for organoids with either SIM (Zeiss's Elyra at Cornell University, Figure 2E) or with STED (a purchased microscope by the Cancer Center at Upstate Medical). A STED micrograph was included in (Colicino *et al.*, 2018)(refer to appendix).

**Goals for AIM 2 we accomplished:**

My student Erica Colicino has made giant strides in examining the impact of centrosome-based PLK1 scaffolds on PLK1 dynamics, activity, and downstream PLK1-driven signaling events. Her first manuscript ((Colicino *et al.*, 2018), see appendix) discovered that a gene (down-

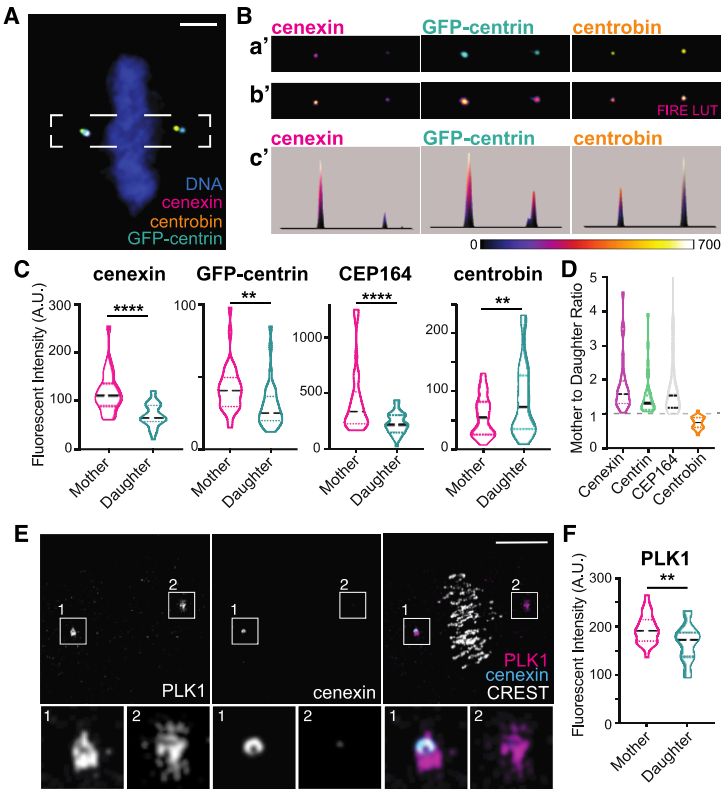



Figure 2. ***PLK1 distribution between the oldest (mother) and youngest (daughter) spindle poles.*** **(A)** Immunofluorescence staining of HeLa GFP-centrin cells at metaphase, centrioles (centrin, cyan), cenexin (magenta), centrobin (gold), and DNA (blue). Bar = 3□m **(B)** Insets from **(A)** showing cenexin (magenta), GFP-centrin (cyan), and centrobin (gold) **(Ba')**. FIRE LUT depicting intensities of cenexin, GFP-centrin, and centrobin **(Bb')**. 3D profile plot of each pole. Heat map of intensity ranges **(Bc')**. **(C)** The intensity of cenexin, GFP-centrin, CEP164, and centrobin was measured at the mother and daughter spindle pole. Violin plot shown, black dashed line at median. Representative of n=3 experiments, n>30 cells measured/group. Student's paired t-test, **p<0.01, ****p<0.0001. **(D)** Measured fluorescent intensities were used to calculate a ratio for each metaphase cell where the mother spindle pole intensity was divided by that of the daughter spindle pole. Violin plot shown, black dashed line at median. Representative of n=3 experiments, n>30 cells/group. **(E)** Structured illumination micrograph (SIM) volumetric projection of a single metaphase HeLa cell immunolabeled for PLK1 (magenta), cenexin (cyan), and CREST (grey). Mother spindle pole (M) and daughter spindle pole (D). White insets depict single mitotic centrosomes. Bar = 5μm. **(F)** PLK1 fluorescent intensity was measured at the mother and daughter spindle pole (determined by GFP-centrin) across n=30 cells). Violin plot shown, black dashed line at median. Student's paired t-test, **p<0.01.

regulated in cancer) Gravin, which is a PLK1-scaffold, causes an increase in genomic instability by inducing micronuclei formation. She developed a biosensor to examine PLK1 activity specifically at centrosomes. Her studies identified that Gravin-loss resulted in an increased PLK1 mobile fraction, causing the redistribution of active PLK1, which leads to increased defocusing and phosphorylation of the mitotic centrosome protein CEP215 at serine-613. Our findings demonstrated that disruption of a Gravin-PLK1 interface leads to inappropriate PLK1 activity contributing to chromosome segregation errors, formation of micronuclei, and subsequent DNA damage.

Erica completed her second manuscript ((Colicino *et al.*, 2019), see appendix) where she examined a second PLK1 scaffold, cenexin. Erica's studies identified an inherent asymmetry of PLK1 localization and activity between the two mitotic centrosomes. This asymmetry is dependent, at least in part, on mitotic centrosome age. We hypothesize this dependence is because the oldest mitotic centrosome is positive for the known PLK1 binding scaffold cenexin compared to the youngest mitotic centrosome (Figure 2). Our studies found that PLK1 asymmetrically localizes between spindle poles under conditions of chromosome misalignment, and chromosomes tend to misalign toward the oldest spindle pole in a cenexin- and PLK1-dependent manner (Figure 3). During chromosome misalignment, PLK1 activity is increased specifically at the oldest spindle pole, and this increase in activity is lost in cenexin-depleted cells (Figure 3 and 4). We propose a model where PLK1 activity elevates in response to misaligned chromosomes at the oldest spindle pole during metaphase to possibly fix

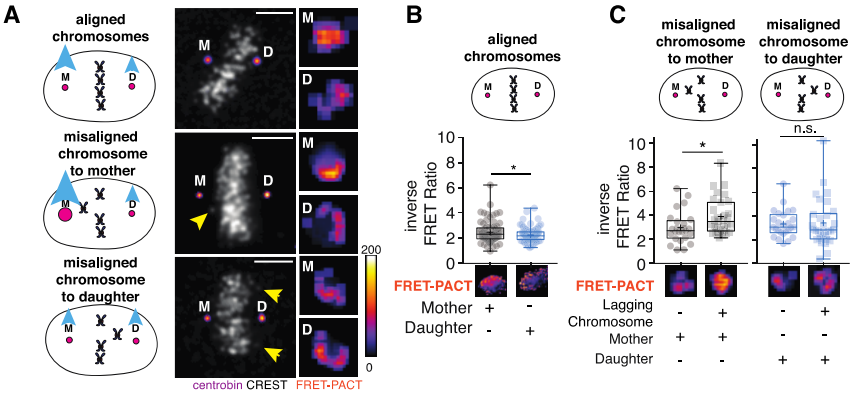



Figure 3. ***PLK1 activity increases at the oldest spindle pole (mother) when a misaligned chromosome is in close proximity.*** **(A)** Models depicting conditions of normal chromosome alignment (top), misaligned chromosome to the mother spindle pole (center), and misaligned chromosome to the daughter spindle pole (bottom). Representative maximum confocal projections of metaphase HeLa cells immunostained for centrobin (magenta) and DAPI (white). Insets show inverse FRET ratio of the PLK1-FRET biosensor (right, Fire-LUT (ImageJ)). The mother (M) and daughter (D) spindle pole labeled respectively. Bars = 5μm. **(B)** Significantly greater PLK1 activity FRET ratios are measured at the mother (gray) spindle pole compared to the daughter (blue) under conditions of normal chromosome alignment. n=79 cells over n=3 experiments, Data shown as box and whisker plot, + indicating mean, and each data point representing a single spindle pole. Student's paired t-test, p=0.0139. **(C)** Greater PLK1 activity FRET ratios are measured at the mother (gray) spindle pole when there is a misaligned chromosome in close proximity, but no change in PLK1 activity is measured when chromosomes misalign towards the daughter (blue). n>20 cells over n=3 experiments, data shown as box and whisker plot, + indicating mean, and each data point representing a single spindle pole. Student's unpaired t-test, lagging chromosomes to mother (p=0.0022), lagging chromosomes to daughter (p=0.7044).

misaligned chromosomes. Thus, it's interesting to speculate in prostate cancer cells that lack cenexin expression (Figure 1) whether they have a higher possibility for chromosome misalignment.

With both of these studies we have completed tasks of Aim 2, which contributes to our understanding whether loss of specific PLK1 scaffolds affect PLK1 activity and have resulted in two publications (Colicino *et al.*, 2018; 2019) and a review article (Colicino and Hehnly, 2018).

- ***What opportunities for training and professional development has the project provided?***

Nothing to report.

- ***How were the results disseminated to communities of interest?***

A subset of these findings was recently published in Molecular Biology of the Cell (MBoC), and our additional unpublished findings have been presented at American Society for Cell Biologists Annual Meeting (ASCB) (2017-2019) and will be presented this year (2020); I have also discussed these studies at the Gordon Research Conference on Polarity. I have given invited seminars on this work at Syracuse University, SUNY Buffalo, University of Nebraska Medical College, University of Toronto, Villanova University, University of Rochester, Ithaca College, Gettysburg College, Clarkson University, and University of Iowa. My laboratory also has a joint mitosis micro-symposium at University of Rochester with Dan Bergstralh's laboratory, where we meet and share data twice a year.

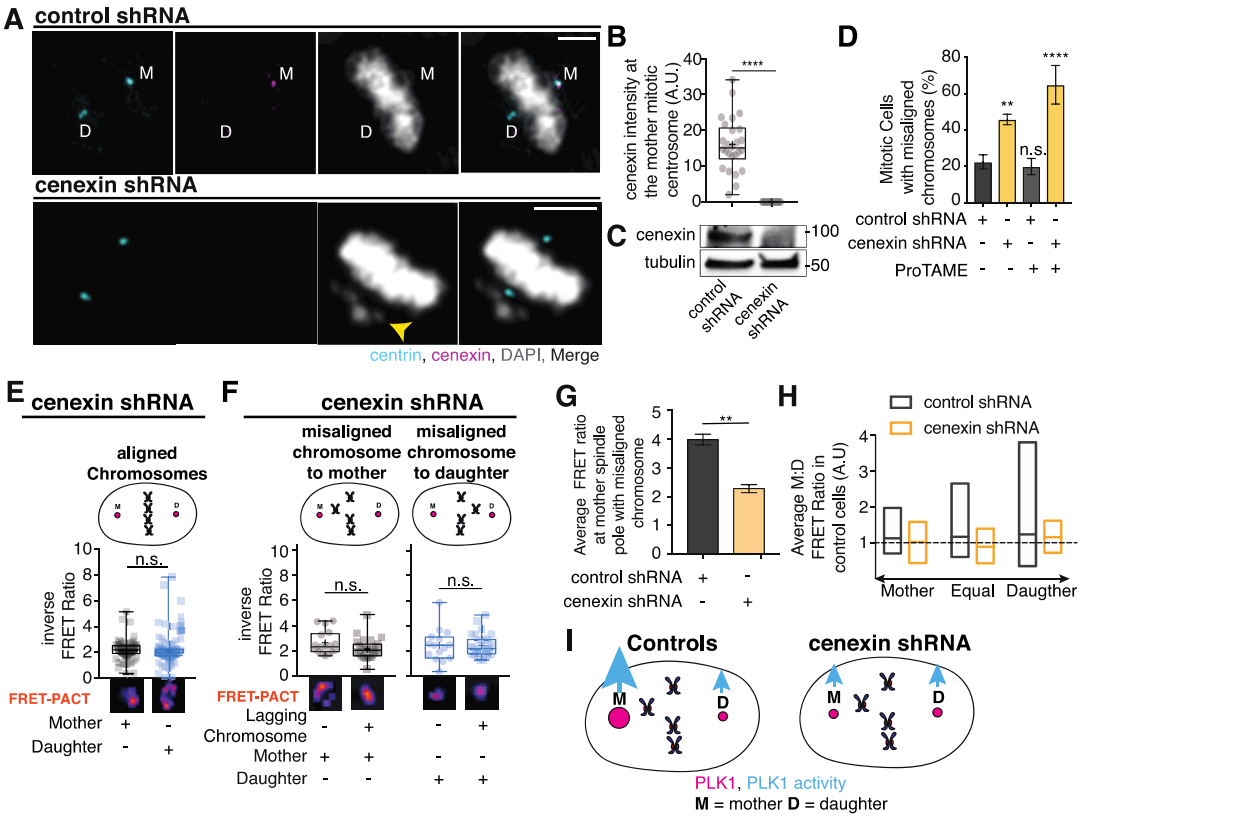



Figure 4. ***An increase in PLK1 activity at the oldest spindle pole (mother) in the event of a misaligned chromosome is cenexin dependent.*** **(A)** Maximum confocal projections of control shRNA and cenexin shRNA HeLa cells immunostained for centrin (cyan), cenexin (magenta), and DAPI (gray). Yellow arrowhead indicates misaligned chromosomes. Bars = 5□m. **(B)** Cenexin fluorescence intensity at the mother spindle pole in control shRNA and cenexin shRNA HeLa cells. Data shown as a box and whisker plot over n>26 cells, + indicating mean, and each data point representing a single spindle pole. Representative from n=3 experiments. Student's t-test p<0.0001. **(C)** Western blot of HeLa cells expressing a control non-targeting shRNA or a cenexin shRNA. Tubulin loading control shown below. **(D)** Bar graph depicting percent (%) metaphase cells with misaligned chromosomes in control and cenexin-depleted cells under control conditions or after ProTAME (10 μM) synchronization in metaphase. n=3 experiments ± S.E.M. With a one-way ANOVA applying multiple comparisons to control shRNA, cenexin shRNA treated (**, p=0.0023) and cenexin shRNA treated plus proTAME (****, p<0.0001) are significant. **(E)** PLK1 activity FRET ratios between the mother (gray) and daughter (blue) spindle pole in cenexin-depleted cells when chromosomes are properly aligned. n>80 cells over n=3 experiments, data shown as box and whisker plot, + indicating mean, and each data point representing a single spindle pole. Student's paired t-test, p=0.3504. **(F)** PLK1 activity in cenexin-depleted cells in the presence of a misaligned chromosome toward the mother (gray) spindle pole or the daughter (blue) spindle pole. n>40 cells over n=3 experiments, data shown as box and whisker plot, + indicating mean, and each data point representing a single spindle pole. Student's unpaired t-test, misaligned chromosome to mother (p=0.0719), misaligned chromosome to daughter (p=0.9415). **(G)** Bar graph representing average PLK1 FRET ratio at the mother spindle pole in cenexin-depleted cells compared to controls in the event of a misaligned chromosome toward the mother spindle pole across n=3 experiments ± S.E.M., Student's t-test, p=0.0018. **(H)** Ratio of PLK1 FRET between the mother and daughter (FRET ratios at mother/FRET ratios at daughter) were compared in control cells (gray) and cenexin-depleted cells (gold) under conditions of equal chromosome misalignment toward both spindle poles, asymmetry in misaligned chromosomes toward the mother spindle pole, or asymmetry in misaligned chromosomes toward the daughter spindle pole. Black dotted line at y=1 represents equal FRET ratios between mother and daughter spindle poles. n>56 cells in graph measured over n=3 experiments. Range of data shown as box plot, center bar represents mean. **(I)** Model illustrating an increase in PLK1 activity (magenta) in control cells, which does not occur in cenexin-depleted cells.

***References:***

Colicino, E. G., and Hehnly, H. (2018). Regulating a key mitotic regulator, polo-like kinase 1 (PLK1). Cytoskeleton (Hoboken) *75*, 481–494.

Colicino, E. G., Garrastegui, A. M., Freshour, J., Santra, P., Post, D. E., Kotula, L., and Hehnly, H. (2018). Gravin regulates centrosome function through PLK1. Mol. Biol. Cell *29*, 532–541.

Colicino, E. G., Stevens, K., Curtis, E., Rathbun, L., Bates, M., Manikas, J., Amack, J., Freshour, J., and Hehnly, H. (2019). Chromosome misalignment is associated with PLK1 activity at cenexin-positive mitotic centrosomes. Mol. Biol. Cell, mbcE18120817.

Hehnly, H., Canton, D., Bucko, P., Langeberg, L. K., Ogier, L., Gelman, I., Santana, L. F., Wordeman, L., and Scott, J. D. (2015). A mitotic kinase scaffold depleted in testicular seminomas impacts spindle orientation in germ line stem cells. Elife *4*, e09384.

Pihan, G. A. (2013). Centrosome dysfunction contributes to chromosome instability, chromoanagenesis, and genome reprograming in cancer. Front Oncol *3*, 277.

Pihan, G. A., Purohit, A., Wallace, J., Malhotra, R., Liotta, L., and Doxsey, S. J. (2001). Centrosome defects can account for cellular and genetic changes that characterize prostate cancer progression. Cancer Res. *61*, 2212–2219.

Zullig, L. L., Jackson, G. L., Dorn, R. A., Provenzale, D. T., McNeil, R., Thomas, C. M., and Kelley, M. J. (2012). Cancer incidence among patients of the U.S. Veterans Affairs Health Care System. Mil Med *177*, 693–701.

**4. IMPACT**

- ***The impact on the principal discipline and other disciplines.*** The studies Erica has published in MBoC (2018, 2019) and the work that is currently being preparing for publication will have significant impact on how the field thinks about kinase signaling, specifically PLK1. For instance, in prostate cancer it is commonly reported that one of PLK1's scaffolds Gravin is downregulated. However, we did not know how this downregulation could affect PLK1 activity. Erica's work demonstrated that loss of Gravin or cenexin causes spatial abnormalities in PLK1 activity at mitotic centrosomes leading to abnormal mitotic spindle formation and chromosome missegregation errors. Thus, it is important to understand how loss of scaffolding proteins can affect mitotic kinases in a spatial and temporal manner, and the impact this has on chromosome instability. These studies have a broad impact in understanding how chromosome instability may come about in prostate cancer. These studies also touch on other disciplines, such as cell biology, where we are identifying the role of scaffolding PLK1 at the centrosome and what downstream targets PLK1 has at this site.
- ***The impact on technology transfer:*** Nothing to Report
- ***The impact on society beyond science:*** Nothing to Report

**5. CHANGES/PROBLEMS**

Nothing to Report

**6. PRODUCTS**

- ***Publications:***

Colicino, E. G., Garrastegui, A. M., Freshour, J., Santra, P., Post, D. E., Kotula, L., and Hehnly, H. (2018). Gravin regulates centrosome function through PLK1. Mol. Biol. Cell *29*, 532–541.

PMID:29282278

Colicino, E.G., Hehnly, H. (2018). Regulating a key mitotic regulator, polo-like kinase 1 (PLK1). Cytoskeleton 75, 481-494

Colicino, E.G., Stevens K, Curtis E, Rathbun L, Bates M, Manikas J, Amack J, Freshour J, Hehnly H. (2019). Chromosome misalignment is associated with PLK1 activity at cenexin-positive mitotic centrosomes. Mol. Biol. Cell 30, 1598-1609. PMID:31042116

- ***Conferences & invited presentations:***
  - State University of New York at Buffalo State, Buffalo, NY, invited by Dr. Derek Beahm, October 2017
  - Villanova University, Philadelphia, PA, invited by Drs. Elaine Youngman and James Wilson, December 2017
  - Syracuse University, Syracuse NY, invited by Dr. Jessica McDonald, February 2018
  - Gettysburg College, Gettysburg PA, invited by Dr. Steven James, March 2018
  - University of Rochester, invited by Dan Bergstralh, May 2018
  - GRC Polarity Conference, Mount Snow, invited by Dr. Ulrich Tepass, June 2018
  - University of Nebraska Medical Center, invited by Dr. Steve Caplan, October 2018
  - University of Toronto, invited by Dr. Ashley Bruce, November 2018
  - Clarkson University, invited by Dr. Kenneth Wallace, December 2018
  - University of Iowa, invited by Dr. Mark Stamnes, September 2019
  - University of Rochester Medical School, invited by Dr. John Lueck, January 2020

- ***Technologies/Techniques:***

We developed a way to specifically examine PLK1-activity at centrosomes live. These studies have been published in two manuscripts (Colicino et al. MBoC 2018, 2019) and PLK1-FRET activity vectors distributed for sharing on addgene.

## 7. PARTICIPANTS & OTHER COLLABORATING ORGANIZATIONS

- ***Individuals that have worked on this project:***

| | |
|---|---|
| Name: | *Erica Colicino* |
| Project Role: | *Graduate Student* |
| Researcher Identifier (e.g. ORCID ID): | 0000-0002-3333-1370 |
| Nearest person month worked: | *12 months* |
| Contribution to Project: | Erica performed has performed all studies on PLK1 activity in live cells, the role of scaffolds, and chromosome instability. |
| Funding Support: | Erica's salary was funded by the State of New York through SUNY Upstate. |

| | |
|---|---|
| Name: | *Heidi Hehnly* |

| | |
|---|---|
| Project Role: | *Principal Investigator* |
| Researcher Identifier (e.g. ORCID ID): | 0000-0001-6660-5254 |
| Nearest person month worked: | 16 months |
| Contribution to Project: | I have managed all aspects of this award, written up manuscripts, and reviewed preliminary data. |
| Funding Support: | My salary was supported by the state of NY and is currently supported by Syracuse University, and 2 months supported on DOD award W81XWH-17-1-0241. |

| | |
|---|---|
| Name: | *Judy Freshour* |
| Project Role: | *Lab Manager* |
| Researcher Identifier (e.g. ORCID ID): | 0000-0003-3235-093X |
| Nearest person month worked: | 36 months |
| Contribution to Project: | Judy performs cloning and other molecular biology in the lab. She manages lab stocks, supplies, and assists with budgeting. |
| Funding Support: | Judy's salary was supported by DOD award W81XWH-17-1-0241 |

| | |
|---|---|
| Name: | *Leszek Kotula* |
| Project Role: | Collaborator |
| Researcher Identifier (e.g. ORCID ID): | 0000-0002-7977-7124 |
| Nearest person month worked: | *3 months* |
| Contribution to Project: | Leszek provided cell lines and expertise on primary prostate cell culture methods. |
| Funding Support: | Leszek's salary was funded by the State of New York through SUNY Upstate. |

- ***Change in active support:***

Nothing to Report.

- ***Other Organizations involved:***

Nothing to Report.

**8. SPECIAL REPORTING REQUIREMENTS**

Nothing to Report.

**9. APPENDICES.**

*Included is a copy of Erica Colicino's two studies and review directly relevant to this award.*

# Gravin regulates centrosome function through PLK1

Erica G. Colicino[a], Alice M. Garrastegui[a,b], Judy Freshour[a], Peu Santra[a], Dawn E. Post[c], Leszek Kotula[c,d], and Heidi Hehnly[a,c,*]

[a]Department of Cell and Developmental Biology, [c]Department of Urology, and [d]Department of Biochemistry, Upstate Medical University, Syracuse, NY 13202, [b]Department of Biology, Syracuse University, Syracuse, NY 13244

**ABSTRACT** **We propose to understand how the mitotic kinase PLK1 drives chromosome segregation errors, with a specific focus on Gravin, a PLK1 scaffold. In both three-dimensional primary prostate cancer cell cultures that are prone to Gravin depletion and Gravin short hairpin RNA (shRNA)–treated cells, an increase in cells containing micronuclei was noted in comparison with controls. To examine whether the loss of Gravin affected PLK1 distribution and activity, we utilized photokinetics and a PLK1 activity biosensor. Gravin depletion resulted in an increased PLK1 mobile fraction, causing the redistribution of active PLK1, which leads to increased defocusing and phosphorylation of the mitotic centrosome protein CEP215 at serine-613. Gravin depletion further led to defects in microtubule renucleation from mitotic centrosomes, decreased kinetochore-fiber integrity, increased incidence of chromosome misalignment, and subsequent formation of micronuclei following mitosis completion. Murine Gravin rescued chromosome misalignment and micronuclei formation, but a mutant Gravin that cannot bind PLK1 did not. These findings suggest that disruption of a Gravin–PLK1 interface leads to inappropriate PLK1 activity contributing to chromosome segregation errors, formation of micronuclei, and subsequent DNA damage.**

**Monitoring Editor**
Yukiko Yamashita
University of Michigan

Received: Aug 22, 2017
Revised: Dec 19, 2017
Accepted: Dec 23, 2017

## INTRODUCTION

The focus of this study is on understanding the spatial regulation of the mitotic kinase Polo-like kinase 1 (PLK1) during mitosis. This question remains enigmatic due to a multiplicity of PLK1 interactions and substrates located at distinct subcellular sites. Here we examine a PLK1 scaffold protein, Gravin/AKAP12/SSeCKS, that localizes to pericentriolar material (PCM) and cytosol (Gelman, 2010; Hehnly *et al.*, 2015). Gravin has been defined as a scaffold for several kinases (Gelman, 2010). Canton et al. demonstrated in vitro that PLK1 interacts with Gravin through a phosphorylated threonine at 766 (Canton *et al.*, 2012), which validated an earlier proteomics screen that identified Gravin as a possible PLK1 scaffold (Lowery *et al.*, 2007). Gravin depletion was then shown to cause prometaphase delay and chromosome instability through FISH analysis of chromosome 18 (Canton *et al.*, 2012). Gravin also interacts with Aurora A kinase, evidence that Gravin, similarly to CEP192 (Joukov *et al.*, 2014) and Bora (Chan *et al.*, 2008), has the potential to facilitate a mitotic signaling cascade between Aurora A and PLK1 (Hehnly *et al.*, 2015). The direct interactions and localization patterns of Gravin and PLK1 were previously characterized (Canton *et al.*, 2012; Hehnly *et al.*, 2015). However, these studies did not thoroughly examine or definitively determine how, in live cells, Gravin regulates PLK1 distribution, activity, or downstream function, which is the main focus of this study.

PLK1 misregulation can drive chromosome missegregation and subsequent formation of micronuclei (Lera and Burkard, 2012). Micronuclei are structures formed as a result of lagging chromosomes that contain either whole or partial chromosomes outside of the

This article was published online ahead of print in MBoC in Press (http://www.molbiolcell.org/cgi/doi/10.1091/mbc.E17-08-0524) on December 27, 2017.

The authors declare that they have no conflict of interest.

Author contributions: E.C., P.S., and A.G. designed and conducted experiments and analyzed the data under the supervision of H.H.; J.F. constructed all viral vectors; D.P. maintained primary prostate cancer cell lines and is under the supervision of L.K.; technical expertise was provided by L.K. and D.P.; E.C. and H.H. wrote the manuscript; all authors critically read and contributed to the manuscript.

*Address correspondence to: Heidi Hehnly (hehnlyh@upstate.edu).

Abbreviations used: DAPI, 4,6-diamidino-2-phenylindole; EGF, epidermal growth factor; EGTA, ethylene glycol-bis(β-aminoethylether)-*N*,*N*,*N*′,*N*′-tetraacetic acid; FRAP, fluorescence recovery after photobleaching; FRET, fluorescence resonance energy transfer; HEK, human embryonic fibroblasts; LB, lysis buffer; MEF, mouse embryonic fibroblasts; PACT, pericentrin-AKAP450-centrosomal targeting domain; PCM, pericentriolar material; PLK1, Polo-like kinase 1; RPE, retinal pigmented epithelium; shRNA, short hairpin RNA; SIM, structured illumination microscopy; STED, stimulated emission depletion microscopy.

© 2018 Colicino *et al.* This article is distributed by The American Society for Cell Biology under license from the author(s). Two months after publication it is available to the public under an Attribution–Noncommercial–Share Alike 3.0 Unported Creative Commons License (http://creativecommons.org/licenses/by-nc-sa/3.0).

"ASCB®," "The American Society for Cell Biology®," and "Molecular Biology of the Cell®" are registered trademarks of The American Society for Cell Biology.

macronucleus (Crasta *et al.*, 2012). Abnormal mitotic kinase expression and activity, such as with PLK1, has been linked to genomic instability in prostate cancer (Deeraksa *et al.*, 2013). Microarray-based studies demonstrated a 3- to 10-fold reduction in relative Gravin mRNA levels in breast, prostate, lung, ovarian, testicular, and other cancer types compared with controls (Gelman, 2010). One plausible mechanism to generate substantial local mutagenesis observed in prostate cancer is physical isolation of one or two chromosomes and their partition into micronuclei. Chromosomes in micronuclei can be subject to massive DNA damage (Holland and Cleveland, 2012). Here we are testing the hypothesis that Gravin loss inappropriately distributes PLK1 signaling during mitosis, driving chromosome missegregation that leads to formation of micronuclei.

## RESULTS AND DISCUSSION

### Gravin loss is associated with increased formation of micronuclei in primary prostate cancer cells

We first analyzed primary hormone therapy–resistant prostate epithelial cells in three-dimensional (3-D) cultures (derived from Gao *et al.*, 2014) in parallel with an immortalized prostate epithelial cell line, RWPE-1. Using this system, we found that Gravin can be significantly down-regulated in primary prostate cancer cells. By comparing two primary patient samples, PCa1 and PCa3, with an immortalized prostate epithelial cell line, RWPE-1, or a control primary prostate epithelial cell line, 26Na, we found that Gravin expression is diminished in PCa1 (Figure 1A). When 3-D primary cultures (Figure 1, A–E) and prostate epithelial cells genetically modified using Gravin short hairpin RNA (shRNA) (Figure 1, F–H) were compared, an increase in mitotic delay or formation of micronuclei was noted in cells that lacked Gravin. Specifically, PCa1 cells that display a significant reduction in Gravin expression (Figure 1A) had an increase in mitotic index compared with both control and PCa3 cells (Figure 1, B and D). PCa1 also contained 25.04 ± 2.35% of cells containing micronuclei compared with 2.65 ± 1.10% in controls and 10.43 ± 3.93% in PCa3 (Figure 1, C and E). These results suggest that Gravin loss contributes to formation of micronuclei in PCa1. From this, we wanted to know whether the effects of Gravin loss on micronuclei formation are the result of inappropriate PLK1 distribution and/or activity causing chromosome missegregation.

### Gravin loss disrupts PLK1 dynamics predominately at mitotic centrosomes

It is unclear how the loss of Gravin impacts PLK1 in live cells during mitosis. One possibility is that scaffold proteins, such as Gravin, help coordinate the appropriate spatial organization of PLK1 to direct the flow of molecular information. Previous studies identified that Gravin phosphorylation at T766 primes it for PLK1 binding (modeled in Figure 2A) and this interaction takes place, at least in part, at mitotic centrosomes (Canton *et al.*, 2012; Hehnly *et al.*, 2015). However, these studies did not examine how this interaction regulates the spatial and temporal dynamics of PLK1 in live cells. By structured illumination microscopy (SIM), we confirmed the finding of our previous studies (Hehnly *et al.*, 2015) that Gravin localizes to mitotic centrosomes (Figure 2B, a′, orange arrows*) along with PLK1 (Figure 2B, b′, orange arrows). Additionally, PLK1 localizes to kinetochores (Figure 2B, b′, magenta arrow) and later in mitosis at the cytokinetic midbody (Figure 2C). Owing to the similar localization patterns of Gravin and PLK1 at mitotic centrosomes, we predict that Gravin loss may disrupt PLK1 dynamics at this locale in live cells during mitosis.

We first examined whether there was a difference in PLK1 dynamics between the mitotic centrosomes, kinetochores, and cytokinetic midbody. A previous study carefully compared the fluorescence recovery after photobleaching (FRAP) kinetics of PLK1 at each of these locales by overexpression of GFP-PLK1 and analysis at 30°C in a human osteosarcoma cell line, U2OS (Kishi *et al.*, 2009). Instead of transiently expressing PLK1, we utilized a cell line with normal ploidy expressing a PLK1 shRNA to eliminate endogenous PLK1 and exogenously expressed an shRNA resistant GFP-PLK1 at endogenous levels (RPE cells, Figure 2C). In addition, FRAP analysis was performed at 37°C. Similarly to the previous study (Kishi *et al.*, 2009), we found significantly different dynamics between mitotic centrosomes, kinetochores, and the cytokinetic midbody for GFP-PLK1 (Figure 2, C and D; Supplemental Figure S1A). However, the half-life of PLK1 at each of these locales was considerably shorter than reported in Kishi *et al.* (2009) (Figure 2D). We predict that this is the case due to endogenous expression levels of PLK1 and 37°C incubation.

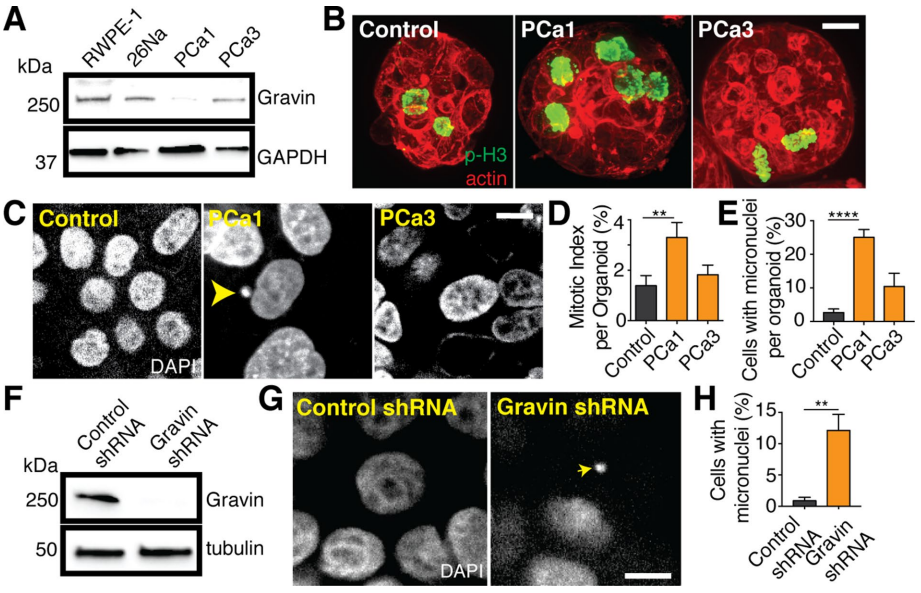



FIGURE 1: Gravin loss is associated with increased micronuclei formation in primary prostate cancer cells. (A) Immunoblot analysis showing decreased Gravin expression in PCa1 and PCa3 cancer cells in comparison with RWPE-1 and normal patient prostate epithelium cells (26Na). (B) Control (RWPE-1), PCa1, and PCa3 3-D acini cultures fluorescently labeled for p-H3 (green) and actin (red). (C) Control (RWPE-1), PCa1, and PCa3 3-D acini labeled for DAPI (gray) displaying micronuclei within a single cell (yellow arrowhead). Confocal micrographs for B and C are presented as maximum projections. Bar, 5 μm. (D, E) Quantification of the mitotic index (D) and cells (%) with micronuclei (E) for control (RWPE), PCa1, and PCa3 in 3-D acini was calculated. $n = 30$ organoids over $n = 3$ experiments ± SEM, Student's $t$ test $p = 0.0099$ (D) and $p < 0.0001$ (E). (F) Immunoblot analysis of Gravin expression in RWPE-1 cells expressing a control GAPDH shRNA or a Gravin shRNA. Tubulin was used as loading control. (G) Control shRNA and Gravin shRNA RWPE-1 3-D acini cultures stained for DAPI displaying micronuclei within a single cell (yellow arrow). Bar, 5 μm. (H) Quantification of Gravin shRNA and control shRNA treated cells with micronuclei (%) over $n = 3$ experiments ± SEM. Student's $t$ test $p = 0.0097$.

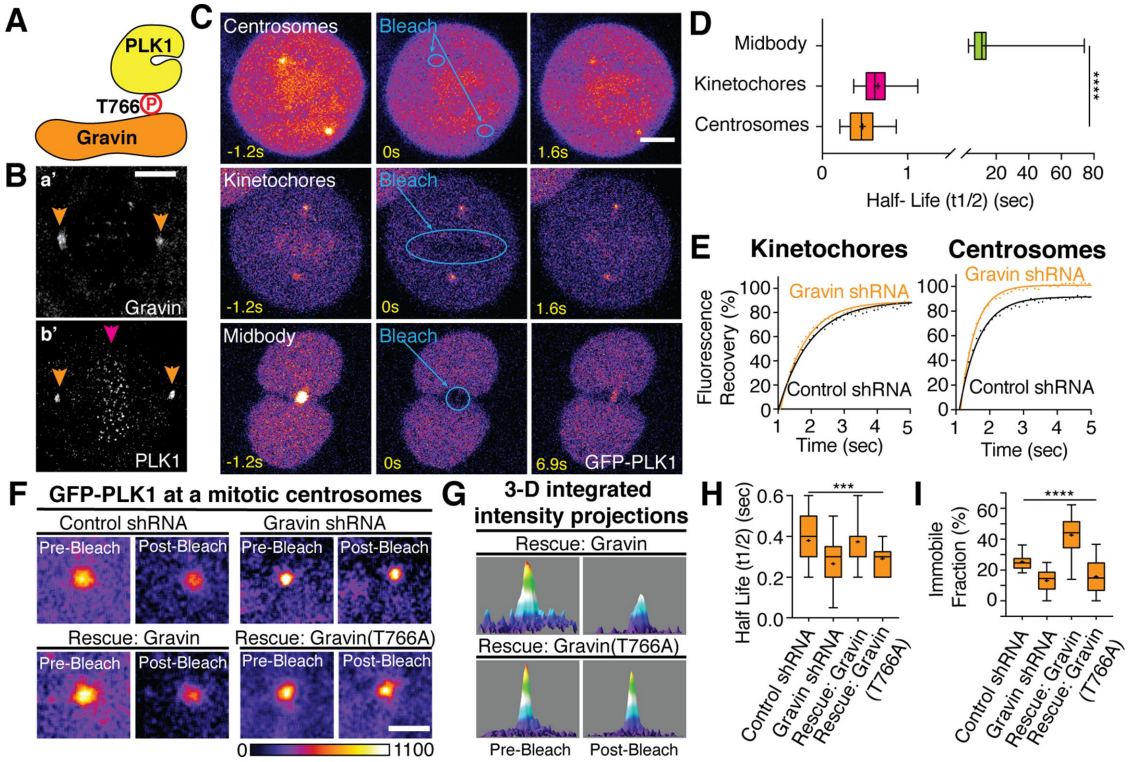



FIGURE 2: Gravin loss disrupts PLK1 dynamics predominately at mitotic centrosomes. (A) Model depicting Gravin (orange) binding PLK1 (yellow) at phosphorylated T766 (Canton *et al.*, 2012). (B) Maximum projection of structured illumination microscopy (SIM) micrographs of Gravin (a') and PLK1 (b') localizing to mitotic centrosomes (orange arrows) in metaphase cells. Magenta arrow represents PLK1 localization at kinetochores in b'. (C) Representative images of fluorescence recovery after photobleaching (FRAP) of GFP-PLK1 (Fire LUT, ImageJ) RPE cells at mitotic centrosomes, kinetochores, and cytokinetic midbodies. Bar, 5 μm. (D) Quantification presented as box-and-whisker plot of half-life for GFP-PLK1 in control and Gravin-shRNA treated cells (+ indicates mean, $n > 20$ cells across $n = 3$ experiments, ANOVA indicates significance of $p < 0.0001$). (E) A curve was fitted using one-phase decay of PLK1 fluorescence recovery at kinetochores (left) and mitotic centrosomes (right) in metaphase cells treated with control or Gravin shRNAs ($n > 20$ cells over $n = 3$ experiments). (F) GFP-PLK1 at a single metaphase mitotic centrosome in control shRNA- or Gravin shRNA-treated cells rescued with full-length wild-type Gravin, or T766A mutant Gravin prior to and 3 s after bleaching events. Confocal micrographs at a single mitotic centrosome are shown (Fire LUT, Image J, bar indicates gradient of integrated fluorescence intensity values, A.U.). Bar, 2 μm. (G) Integrated intensity profiles for GFP-PLK1 at a single mitotic centrosome before and 3 s after bleaching events are presented. (H, I) The average (H) half-life ($t_{1/2}$) and (I) immobile fraction of GFP-PLK1 at metaphase spindle poles was calculated and presented as box-and-whisker plots with + indicating mean ($n > 20$ cells over $n = 3$ experiments). One-way ANOVA indicates significance between $p < 0.001$ (H) and $p < 0.0001$ (I).

We next compared GFP-PLK1 dynamics in Gravin-depleted RPE cells (Gravin shRNA) and in control RPE cells (control shRNA; Supplemental Figure S1B). Gravin-depleted cells had a significant decrease in GFP-PLK1 half-life at kinetochores (Figure 2E; Supplemental Figure S1, C and D) and mitotic centrosomes (Figure 2, E and H) and no significant difference at cytokinetic midbodies (Supplemental Figure S1, F and G). We then compared the immobile fraction of GFP-PLK1 at each locale, that is, the fraction of GFP-PLK1 that remained after photobleaching. Gravin-depleted cells demonstrated a 12% decrease in the immobile fraction at mitotic centrosomes when compared with controls (Figure 2, E and I). However, no difference in the immobile fraction was observed at kinetochores or at the cytokinetic midbody (Figure 2E; Supplemental Figure 1, E and H).

Using control and Gravin-depleted cells rescued ectopically with wild-type Gravin or Gravin (T766A) that cannot bind PLK1 (Canton *et al.*, 2012), we repeated the FRAP experiments at individual mitotic centrosomes (Figure 2, F and G; expression levels following rescues in Supplemental Figure S1B). A significant proportion of GFP-PLK1 fluorescence was not recovered at mitotic centrosomes in control shRNA and Gravin-rescued cells, representing the immobile fraction of PLK1. In Gravin-depleted and Gravin (T766A) rescue cells, GFP-PLK1 fluorescence is almost fully recovered 3 s post-bleach (Figure 2, F and G). From analysis of multiple metaphase cells, rescue with Gravin (T766A) caused a significant decrease in the immobile fraction and in the half-life of GFP-PLK1 compared with wild-type Gravin rescue (Figure 2, H and I). With wild-type Gravin rescue there is a slight increase in total Gravin expression compared with that in controls, which is likely causing the significant increase in the immobile fraction of GFP-PLK1 (42.68% immobile) compared with that for control shRNA (25.33% immobile, Figure 2I). Collectively, these findings suggest that GFP-PLK1 dynamics at mitotic centrosomes is partly regulated by its binding scaffold Gravin.

### Gravin-depleted cells redistribute active PLK1, causing increased phosphorylation events at mitotic centrosomes

We utilized a fluorescence resonance energy transfer (FRET)-based phosphorylation sensor (Macůrek *et al.*, 2008) to test whether Gravin loss causes a change in PLK1 activity. The PLK1 biosensor is

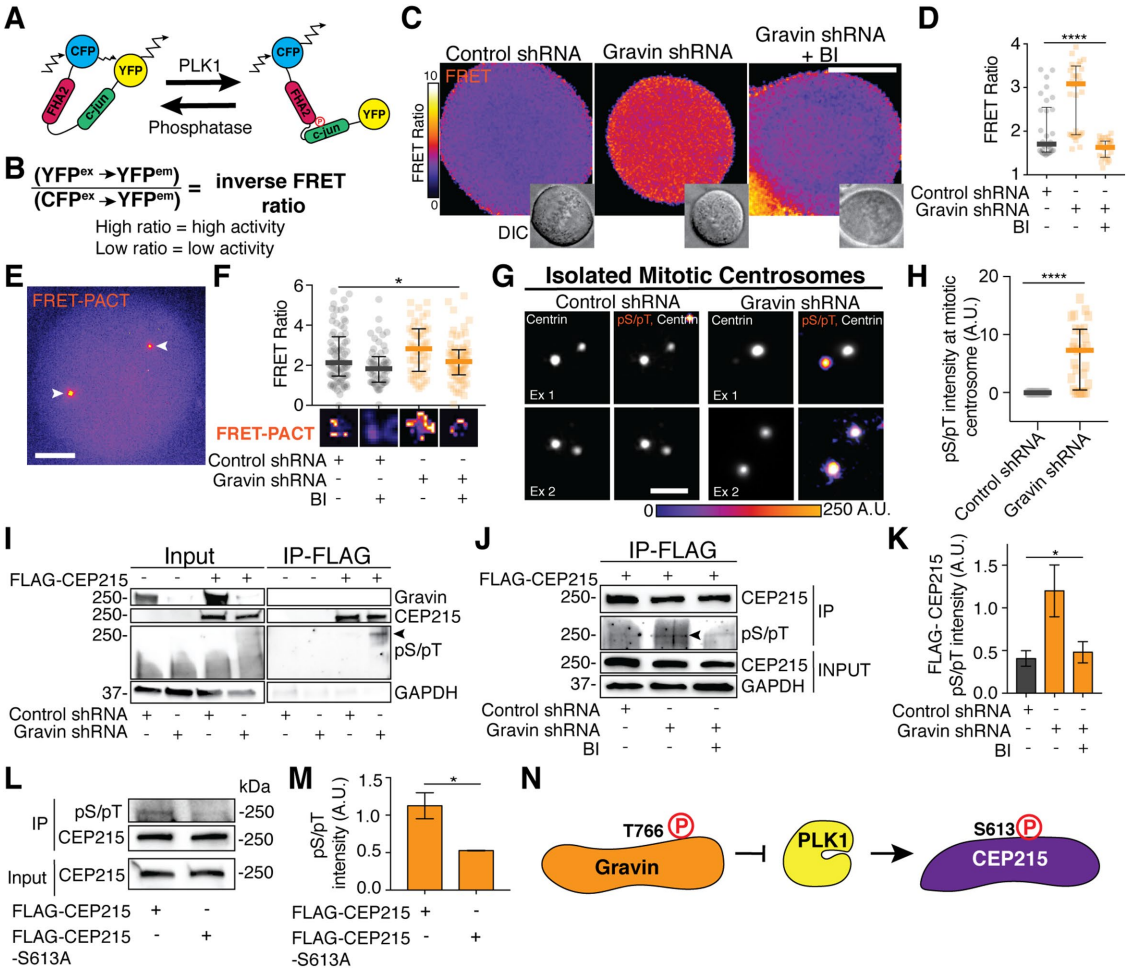



FIGURE 3: Gravin-depleted cells redistribute active PLK1, causing increased phosphorylation events at mitotic centrosomes. (A) Model of PLK1 biosensor showing how increased PLK1 activity causes a conformational change in the biosensor through phosphorylation of c-jun (green) and binding of the FHA2 domain (magenta), resulting in a loss of FRET. When there is increased phosphatase activity, the PLK1 biosensor is in a relaxed state, allowing FRET. (B) Equation for determining the inverse FRET ratio by dividing the $YFP^{EX} \rightarrow YFP^{EM}$ by the $CFP^{EX} \rightarrow YFP^{EM}$. When the inverse FRET ratio is calculated, high ratios correspond with high levels of PLK1 activity while low ratios correspond to low levels of PLK1 activity. (C) Relative PLK1 activity shown as an inverse FRET ratio (Fire LUT, ImageJ, bar indicates gradient of FRET ratio values) and DIC images taken from nocodazole synchronized and released cells in metaphase. Control shRNA, Gravin shRNA, and Gravin shRNA cells plus BI2536 are shown. Bar, 5 µm. (D) Quantification of the inverse FRET efficiency nocodazole-released cells in metaphase that were treated with control shRNA, Gravin shRNAs, and/or BI2536 (BI) is presented as a scatterplot. $n > 30$ cells over $n = 3$ experiments, median with interquartile range shown, one-way ANOVA $p < 0.0001$. (E) PLK1-FRET-PACT biosensor localization in metaphase cells. Arrows depict mitotic centrosomes (Fire LUT). Bar, 5 µm. (F) The inverse FRET-efficiency of the PLK1-FRET-PACT probe was quantified from nocodazole synchronized and released metaphase cells treated with control shRNA, Gravin shRNA, and/or BI2536 (BI) and presented as a scatterplot. Representative single mitotic centrosome inverse FRET ratios shown below graph (FIRE-LUT). $n > 50$ cells over $n = 4$ experiments, median with interquartile range shown, one-way ANOVA $p = 0.0371$. (G) Isolated mitotic centrosomes from control shRNA and Gravin shRNA HEK293 cells immunolabeled for centrin (white) and phosphoserine/phosphothreonine (pS/pT; FIRE LUT). Bar, 2 µm. (H) Quantification of pS/pT intentsity at mitotic centrosomes in G presented as a scatterplot. $n = 27$ centrioles for each treatment, median with interquartile range shown, Student's $t$ test $p < 0.0001$. (I, J) FLAG IP of Mock or FLAG-CEP215 transfected control shRNA- or Gravin shRNA ± BI2536-treated HEK293 cells as indicated. Protein expression and immunoprecipitation was analyzed by immunoblot for Gravin, CEP215, pS/pT, and GAPDH (as loading control). Black arrowhead indicates pS/pT band at 250 kDa. (K) Quantification of pS/pT intensities normalized over total FLAG-CEP215 IP ($n = 3$ experiments ± SEM, one-way ANOVA $p = 0.0353$). (L) Immunoblot analysis of FLAG-CEP215 and FLAG-CEP215-S613A IP from HEK293 cells. (M) Quantification of pS/pT expression levels from FLAG-IP normalized over total FLAG-CEP215 ($n = 3$ experiments ± SEM, Student's $t$ test $p = 0.0264$). (N) Working model depicting that phosphorylated Gravin (orange) inhibits PLK1 (yellow) from phosphorylating CEP215 (purple) during mitosis.

composed of a monomeric CFP and YFP flanking a PLK1 specific c-jun substrate sequence tethered by a flexible linker to an FHA2 phosphothreonine binding domain (Liu *et al.*, 2012). The phosphorylation of the PLK1 substrate triggers an intramolecular clamp with the FHA2, causing a conformational change that decreases the amount of FRET from CFP to YFP (Figure 3A). The FRET biosensor

provides a fluorometric readout for PLK1 phosphorylation, and a decrease in FRET is measured upon increased activity of PLK1. For ease of interpretation, we plotted an inverse ratio of $YFP^{EX}\rightarrow YFP^{EM}$ over $CFP^{EX}\rightarrow YFP^{EM}$ (Figure 3B), so that an increase in the inverse FRET ratio represents an increase in PLK1 activity. To determine whether anchoring of PLK1 by Gravin affected PLK1's activity, we monitored either the PLK1 biosensor in cycling cells (Supplemental Figure S2, A and B) or cells synchronously released from mitotic arrest by nocodazole (Figure 3, C and D; Supplemental Figure S2C). For these studies we utilized HEK293 cells treated with either a control shRNA or Gravin shRNA with or without addition of the PLK1 inhibitor BI2536. In control cells treated with BI2536 a significant decrease in the inverse FRET ratio was calculated (Supplemental Figure S2C), suggesting that we accurately measured PLK1 activity. In cells depleted of Gravin, a significant increase in the inverse FRET ratio was calculated when compared with that in control cells (median of 1.703 compared with 3.09 for Gravin-depleted cells, Figure 3, C and D), and the increase was lost after treatment with the PLK1 inhibitor BI2536, indicating that the increase requires PLK1 kinase activity (median of 1.63, Figure 3, C and D). Previous studies reported that an upstream PLK1 kinase, Aurora A, activates PLK1 during mitosis by phosphorylating it at T210 (Macůrek *et al.*, 2008). This is facilitated by these two kinases forming a complex with Gravin. We confirmed that Gravin loss resulted in a modest decrease in T210 phosphorylation (Hehnly *et al.*, 2015; Supplemental Figure S2, D and E). However, Gravin loss caused a significant increase in the FRET-biosensor fluorometric readout (Figure 3, C and D). One possibility is that Gravin-depleted cells display a slight decrease in global PLK1 activity, shown by decreased phosphorylation at T210; however, a population of active PLK1 is redistributed in cells, allowing increased phosphorylation and unregulated access to its substrates. Thus, we conclude that we are not causing an increase in overall activity of PLK1, but a change in distribution of already active PLK1 with Gravin loss.

Since Gravin and PLK1 likely interact on mitotic centrosomes (Figure 2, B and E; Hehnly *et al.*, 2015), we tested for changes in PLK1 centrosome substrate phosphorylation with loss of Gravin. To mimic the localization of possible endogenous PLK1 centrosome substrates, we attached a pericentrin-AKAP450-centrosomal-targeting domain (PACT) to the c-terminus of the FRET biosensor (FRET-PACT), which successfully targets the PLK1 biosensor to mitotic centrosomes (Figure 3E). To examine FRET-PACT response to changes in PLK1 activity in living cells, we imaged mitotic HEK293 cells treated with a control shRNA, Gravin shRNA, and/or the PLK1 inhibitor, BI2536. As with the cytosolic PLK1 FRET biosensor, the centrosome-targeted biosensor demonstrated a significant increase in the inverse FRET ratio in Gravin-depleted cells (median of 2.83) compared with controls (median of 2.13; Figure 3F). Treatment with BI2536 decreased the FRET ratio for both control cells (median of 1.84) and Gravin-depleted cells (median of 2.18; Figure 3F).

We confirmed the increase in phosphorylation seen with the FRET-PACT biosensor by isolating mitotic centrosomes (Hung *et al.*, 2015) from control and Gravin-depleted cells. Gravin-depleted mitotic centrosomes displayed a significant increase in phosphoserine/phosphothreonine (pS/pT) compared with controls (Figure 3, G and H). We next examined a putative centrosome-localized PLK1 substrate, CEP215 (Santamaria *et al.*, 2011), for increased phosphorylation in Gravin-depleted cells compared with controls (Figure 3I). Immunoblot analysis detected a threefold increase in PLK1-dependent pS/pT levels in FLAG-CEP215 isolated from Gravin shRNA–treated cell lysate compared with control lysate or lysates treated with BI2536 (Figure 3, I–K). A previous phosphoproteomics screen of PLK1 substrates identified a PLK1 phosphorylation site on CEP215 at its serine-613 residue (Santamaria *et al.*, 2011). Through sequence alignment, we found that this serine is conserved between human and murine CEP215 (Supplemental Figure S2F). We immunoprecipitated a FLAG-tagged nonphosphorylatable mutant, CEP215 (S613A), or wild-type FLAG-CEP215, and FLAG-CEP215-S613A presented with decreased pS/pT phosphorylation compared with FLAG-CEP215 (Figure 3, L and M), suggesting that serine-613 is phosphorylated. Collectively, these data support the idea that Gravin constrains a subset of PLK1 to be released at the right time and place. When Gravin is depleted, this subset of PLK1 is now free to inappropriately phosphorylate downstream substrates, one of which is CEP215 at serine 613 (modeled in Figure 3N).

### Gravin loss results in CEP215 disorganization and disrupted mitotic centrosome function

Since CEP215 phosphorylation is increased in Gravin-depleted cells, we examined if its organization at the mitotic centrosomes was affected in HEK293 cells treated with Gravin shRNA. Using stimulated emission depletion microscopy (STED), CEP215 in control cells clustered into a ring-like structure at both mitotic centrosomes (Figure 4A). In Gravin-depleted cells, we found that CEP215 no longer organized symmetrically across the two poles. One pole contained more CEP215 that was no longer organized in a ring and the other pole contained diffusely arranged CEP215. Line scans across multiple cells that bisected the mitotic centrosomes demonstrated a specific decrease in CEP215 organization on one pole over the other in Gravin-depleted cells compared with controls (Figure 4A). We then measured the fluorescence intensity of CEP215 at mitotic centrosomes in cells treated with either control or Gravin shRNA. Gravin-depleted cells contained significantly less CEP215 at mitotic centrosomes than controls (Figure 4B). When the ratio of the mitotic centrosome with the highest CEP215 fluorescence intensity to the mitotic centrosome with the lowest was calculated, Gravin-depleted cells had a significantly higher ratio (Figure 4C). Together, these data suggest that Gravin loss causes decreased CEP215 organization and localization at mitotic centrosomes, leading to an asymmetric distribution of CEP215 between the two mitotic centrosomes.

To determine whether Gravin loss and subsequent CEP215 disorganization and distribution lead to defects in centrosome function, we performed a functional test to monitor mitotic centrosome–mediated MT-nucleating activity over time in HEK293 cells. Spindles were disassembled with nocodazole and examined at different times after nocodazole washout for MT nucleation. At 0 min there was less tubulin at mitotic centrosomes in Gravin-depleted cells than in controls. At 2 min of regrowth, mitotic centrosomes in control cells showed an increased ability to nucleate MTs (Figure 4, D and E). This activity was modestly impaired at first in Gravin-depleted cells, but by 5 min both Gravin-depleted cells and control cells were nucleating MTs to a similar degree, and by 20 min Gravin-depleted cells formed a complete spindle, whereas control cells were still recovering from the regrowth (Figure 4D). This finding suggests that the initial defects in nucleation at 0 and 2 min could be caused by downstream defects in PLK1 target organization, such as CEP215, which is known to organize the γ-tubulin ring complex (Fong *et al.*, 2008). Following this, the redistribution of active PLK1 caused by Gravin loss likely contributes to the rapid increase in nucleation and spindle assembly after nocodazole washout (Figure 4, D and E). One possible consequence for defects in centrosome function and/or abnormal PLK1 activity is a loss in kinetochore fiber integrity (Paschal *et al.*, 2012; Hehnly and Doxsey, 2014). To test whether Gravin loss affects kinetochore fiber integrity, we employed

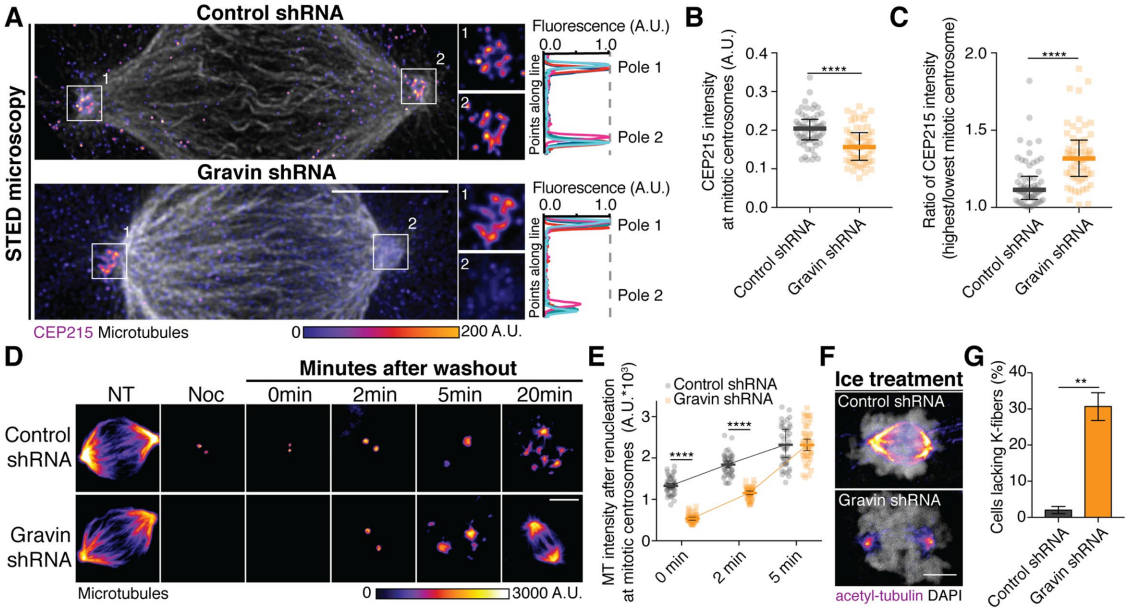



FIGURE 4: Gravin loss results in CEP215 disorganization and disrupted mitotic centrosome function. (A) STED (stimulated emission–depletion) micrographs of metaphase control and Gravin shRNA HEK293 cells are presented as maximum projections. Cells were immunostained for CEP215 (Fire-LUT, ImageJ, bar indicates gradient of integrated fluorescence intensity values, A.U.) and tubulin (white). Bar, 5 μm. Inserts (white boxes) depict 2× magnification of CEP215 at mitotic centrosomes. A line scan through the mitotic centrosomes is drawn and the normalized fluorescence intensity of CEP215 is plotted (right, each line represents a single line scan over $n = 5$ cells for each treatment). (B) Quantification of total CEP215 fluorescence intensity at mitotic centrosomes in control and Gravin shRNA–treated HEK293ad cells. $n = 3$ experiments, $n = 60$ cells, median with interquartile range shown, Student's $t$ test, $p < 0.0001$. (C) Ratio of highest CEP215 intensity over lowest CEP215 intensity between the two mitotic centrosomes within a single cell. $n = 60$ cells over $n = 3$ experiments, median with interquartile range shown, Student's $t$ test $p < 0.0001$. (D) A series of confocal micrographs demonstrating MT regrowth (α-tubulin, Fire-LUT, bar indicates gradient of integrated fluorescence intensity values, A.U.) at mitotic centrosomes for a time course following nocodazole washout in HEK293 cells treated with Gravin or control shRNAs. Micrographs presented as maximum projections. Bar, 5 μm. (E) The integrated α-tubulin intensity at mitotic centrosomes was quantified and presented as a scatterplot at indicated times following washout. $n = 50$ poles for each time and treatment, median with interquartile range shown, representative of $n = 3$ experiments, Student's $t$ test for 0 min ($p < 0.0001$), 2 min ($p < 0.0001$), and 5 min ($p = 0.60$). (F) Maximum confocal projections of control shRNA and Gravin shRNA mitotic HEK293 cells treated for 5 min on ice. Cells were immunostained for acetylated tubulin (Fire-LUT, ImageJ) and DAPI (white). (G) Quantification of cells (%) lacking K-fibers in HEK293 cells treated with control or Gravin shRNAs calculated over $n = 3$ experiments ± SEM (Student's $t$ test $p = 0.0020$).

cold treatment to specifically eliminate dynamic microtubules from mitotic HEK293 cells. Kinetochore fibers in control cells were well organized and robust (Figure 4F). Following Gravin depletion, kinetochore fibers were completely lost in 31 ± 3.84% of mitotic cells (Figure 4G). A previous study reported that an active form of PLK1, PLK1 T210D, resulted in labile kinetochore fibers, in contrast to wild-type controls (Paschal *et al.*, 2012). This finding, in combination with our findings, suggests that redistribution of active PLK1 caused by Gravin loss disrupts centrosome function and kinetochore fiber integrity.

### Gravin loss and increased phosphorylation of CEP215 results in higher incidence of cells containing micronuclei

PLK1 is an essential kinase in the regulation of mitotic progression by allowing the passage of cells through the G2/M cell cycle checkpoints (Zitouni *et al.*, 2014). Premature passage of these checkpoints through overactive PLK1 has been shown to cause genomic instability in cells through lagging chromosomes and DNA damage (Pan *et al.*, 2009). In addition, a disruption in centrosome function through the loss of centrioles also results in increased lagging chromosomes and micronuclei formation (Sir *et al.*, 2013). Thus, we examined whether Gravin-depleted cells, which have decreased centrosome function (Figure 4, D and E), present with lagging chromosomes. Comparing 3-D prostate epithelial cells depleted of Gravin with controls, we noted an increase in lagging chromosomes (Supplemental Figure S3A). To monitor this quantitatively in live cells, we utilized a GFP-H2B HeLa cell line stably depleted of Gravin (Gravin shRNA; Supplemental Figure S3, B–D), where only 42.28 ± 11.20% of Gravin-depleted cells displayed normal chromosome alignment, compared with 81.16 ± 6.90% of control cells. Of the remaining cells, 32.37 ± 6.17% of dividing Gravin-depleted cells presented with lagging chromosomes compared with 7.95 ± 3.44% in control cells (Supplemental Figure 3, B and C). These findings suggest that Gravin loss contributes to increased chromosome segregation defects. We further tested whether lagging chromosomes can be rescued in cells when Gravin is reintroduced (Figure 5, A and B; Supplemental Figure S3D). We found that cells lacking Gravin or expressing Gravin T766A contained lagging chromosomes compared with rescue cells with wild-type Gravin, suggesting that the binding of Gravin to PLK1 is essential for proper chromosome alignment during metaphase.

Since chromosome misalignment can result in formation of micronuclei (Crasta *et al.*, 2012), we examined whether disrupting the

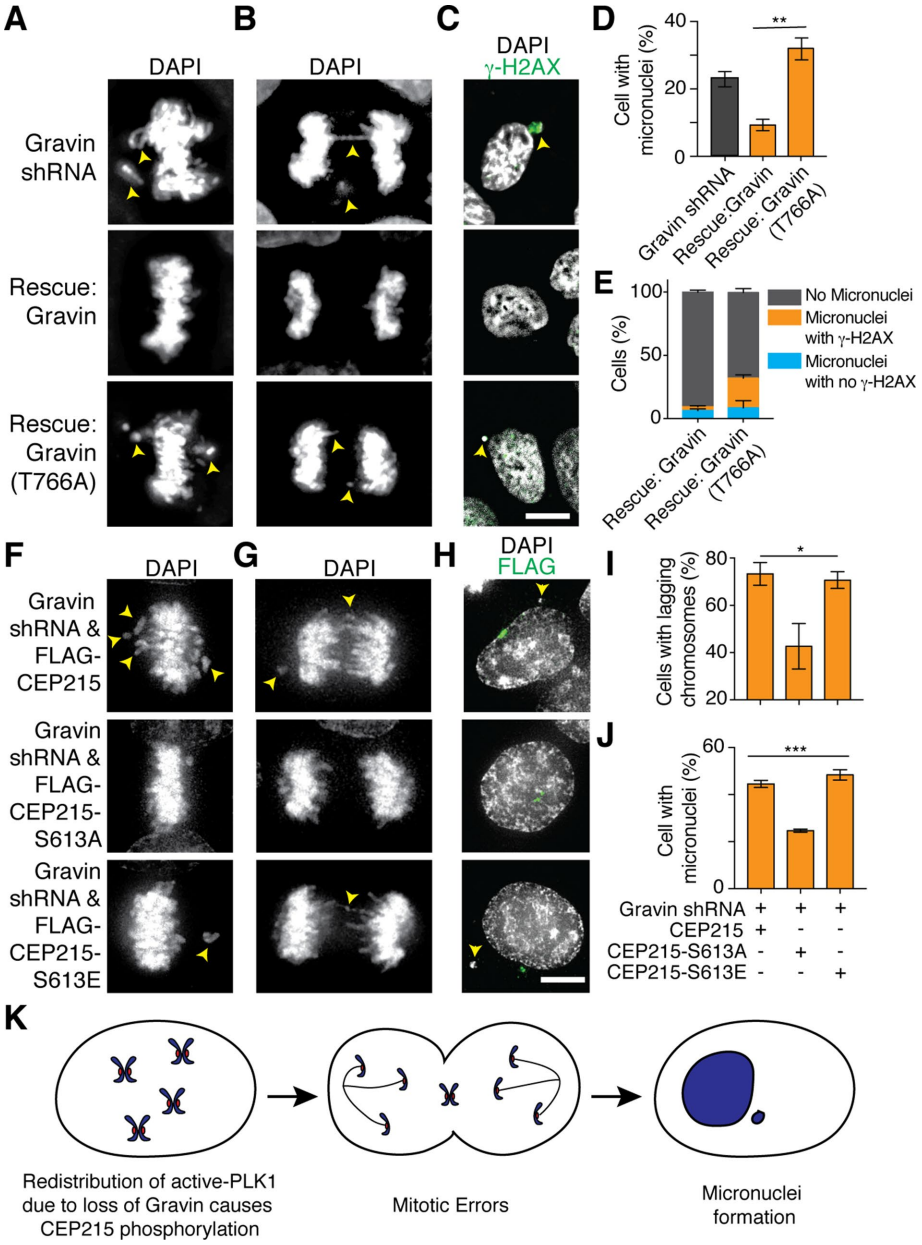



**FIGURE 5:** Gravin loss and increased phosphorylation of CEP215 results in higher incidence of cells containing micronuclei. (A–C) Wide-field deconvolved micrographs of Gravin shRNA, full-length Gravin rescue, and mutant T766A Gravin cells are presented as maximum projections. Cells were immunostained for DAPI (A, B, C white) and γ-H2AX (C, green). Bar, 5 μm. (D) Quantification of cells containing micronuclei (%) in Gravin shRNA–treated cells rescued with full-length Gravin or Gravin (T766A) over $n = 3$ experiments ± SEM; Student's $t$ test $p$ value = 0.0034. (E) Quantification of cells containing micronuclei with γ-H2AX (%) in Gravin shRNA cells rescued with full-length Gravin or Gravin (T766A) over $n = 3$ experiments ± SEM. (F–H) Deconvolved wide-field micrographs of Gravin shRNA–treated cells expressing FLAG-CEP215, FLAG-CEP215-S613A, or FLAG-CEP215-S613E presented as maximum projections. Cells were immunolabeled for DAPI (F, G, H, white) and FLAG (H, green). Bar, 5 μm. (I, J) Quantification of cells containing lagging chromosomes (I) and micronuclei (J) (%) in Gravin shRNA cells expressing FLAG-CEP215, FLAG-CEP215-S613A, or FLAG-CEP215-S613E. $n = 3$ experiments ± SEM, $n > 300$ cells, one-way ANOVA $p = 0.0290$ (I), $p = 0.0003$ (J). (K) Model summarizing that when Gravin is lost, a redistribution of active PLK1 leads to mitotic errors and subsequent formation of micronuclei.

Gravin–PLK1 interface resulted in increased formation of micronuclei. In Gravin-depleted cells we found that 22.87 ± 3.92% of cells formed micronuclei, whereas rescue with full-length wild-type Gravin led to a significant reduction in micronuclei formation (down to 9.3 ± 2.88%, Figure 5, C and D). When Gravin-depleted cells were rescued with Gravin-T766A, 32.03 ± 5.61% of cells displayed formation of micronuclei. To confirm that loss of Gravin resulted in increased formation of micronuclei, we compared wild-type and Gravin-null MEFs (Supplemental Figure S3, E and F). Gravin-null MEFs resulted in a twofold increase in formation of micronuclei compared with controls (Supplemental Figure S3F). These data suggest that disruption of the Gravin–PLK1 interface results in lagging chromosomes and micronuclei formation (modeled in Figure 5K). Previous studies suggested that micronuclei formed from lagging chromosomes develop DNA breaks (Leibowitz *et al.*, 2015). Since disrupting the Gravin–PLK1 binding interaction causes an increase in chromosome missegregation and formation of micronuclei (Figure 5, A–D), we examined whether these micronuclei had an increased incidence in developing DNA breaks by staining for γ-H2AX (Figure 5, C and E). Of cells rescued with Gravin-T766A that contained micronuclei, 76.37 ± 24.66% contained γ-H2AX-positive micronuclei compared with 33.33 ± 11.55% of wild-type Gravin rescue cells (Figure 5E).

CEP215 phosphorylation by PLK1 at serine-613 when Gravin is depleted (Figure 3, I–M) results in CEP215 disorganization at mitotic centrosomes (Figure 4, A–C). Thus, we tested in Gravin-depleted cells whether CEP215-S613A can alleviate chromosome missegregation errors and micronuclei formation compared with a phospho-mimetic mutant CEP215-S613E or wild-type CEP215 (Figure 5, F–J; Supplemental Figure S3G). The FLAG-tagged nonphosphorylatable mutant (S613A) and the FLAG-tagged phosphomimetic mutants (S613E) localize to mitotic spindle poles in control and Gravin-depleted cells (Supplemental Figure S3G) and to the interphase centrosome in Gravin-depleted cells (Figure 5H). We found that 73.33 ± 4.81% of cells expressing FLAG-CEP215 and 70.67 ± 3.53% of cells expressing FLAG-CEP215-S613E presented with lagging chromosomes, compared with 42.67 ± 9.62% in cells expressing FLAG-CEP215-S613A (Figure 5I). The cells expressing FLAG-CEP215 (47 ± 2.65%) or FLAG-CEP215-S613E (48.33 ± 2.19%) contained significantly more micronuclei than cells expressing FLAG-CEP215-S613A (24.67 ± 0.67%, Figure 5J). These data suggest that PLK1-dependent CEP215 phosphorylation at S613 leads to increased chromosome instability through the formation of lagging chromosomes and formation of micronuclei. Together, our findings suggest that blocking the ability

of Gravin to scaffold PLK1 causes an increase in DNA damage (Figure 5K). This is a potential mechanism by which chromosome instability can arise upon PLK1 deregulation in prostate cancer.

## MATERIALS AND METHODS

### Cell culture

3-D RWPE human prostate epithelial cells were grown in Keratinocyte SFM combo from Life Technologies/Fisher (cat. no. 17-005-042) with 60% Matrigel (Fisher cat. no. CB40234C; Corning no. 356237). 2-D PLK1-GFP RPE, GFP-H2B HeLa (Hehnly and Doxsey, 2014), mouse embryonic fibroblasts (MEFs) isolated from wild type and Gravin null mice, and human embryonic kidney (HEK) 293ad cells were grown in 1× DMEM (Life Technologies) supplemented with 10% Seradigm fetal bovine serum (FBS; VWR) and 1% penicillin–streptomycin (10,000 U/ml) (Life Technologies). Phoenix-AMPHO cells were used for viral production in Gravin rescue experiments, grown in 1X DMEM (Life Technologies) supplemented with 10% FBS (Sigma) and 1% penicillin–streptomycin (10,000 U/ml) (Life Technologies). All cultures were maintained at 37°C with 5% $CO_2$.

Human primary prostate cancer epithelial cells (PCa1, PCa3) were grown as 3-D-organoid cultures (Gao *et al*., 2014). Cells were plated in 200-µl DMEM/F12 containing supplements in a multiwell plate (Ibidi cell chambers #80827; PCa1 and PCa3 at 3000 cells/well) coated with collagen type II. Media supplements included epithelial growth factor (EGF), R-spondin 1, noggin, FGF10, FGF2, dihydrotestosterone (DHT), nicotinamide, the TGF-b/Alk inhibitor A83-01, the p38 MAK kinase inhibitor SB202190, the ROCK inhibitor Y-27632, B27 additive, *N*-acetyl-L-cysteine, glutamax, HEPES, and primocin. Following seeding, media were removed and cells overlaid with 200 µl of 50% GFR (growth factor–reduced) matrigel (GFR-matrigel from Fisher cat. no. CB40230C; Corning no. 356231) and 50% mixture.

### shRNA and FRET constructs

Cells depleted of Gravin were made using a lentivirus-infected shRNA specific to Gravin (AKAP12 [Gravin] shRNA sc-40305-v). Control cells were treated with control shRNA (sc-108080). Gravin rescue experiments were performed using the wild-type and phospho-dead mutant T766A of the murine Gravin (SSECKS) gene. FRET experiments were performed using a PLK1 FRET biosensor containing a PLK1 specific c-jun substrate (Liu *et al*., 2012). To examine PLK1 activity specifically at mitotic centrosomes, a localized PLK1 FRET-biosensor was constructed by fusing the above FRET biosensor to the PACT domain (human pericentrin-kendrin) using a 10–amino acid linker (R-A-Q-A-S-N-S-G-R-P) as done for kinetochores in Liu *et al*. (2012). All constructs were verified through sequencing.

### Antibodies and chemical inhibitors

For Western blot analysis and immunofluorescence imaging, the following antibodies were used: phospho-Histone H3 (Ser10, 1:200; Cell Signaling 9701S), mouse anti-PLK1 (E-2, 1:250; Santa Cruz sc-55504), rabbit anti-PLK1 (1:100; Cell Signaling #4513S), mouse anti-Centrin (1:1,000; EMD Millipore 04-1624), mouse anti-Gravin (1:250; Sigma Aldrich 45-G3795), anti–α-tubulin conjugated with FITC (1:250; Sigma Aldrich F2168), Actinred 555vReady Probes reagent (Thermo Fisher Scientific R37112), NucBlue fixed cell stain from Ready Probes (Thermo Fisher Scientific R37606), rabbit anti–γ-histone H2A.X (Ser 139, γ-H2AX, 1:500; Cell Signaling 9718S), anti-CEP215 (1:500; Bethyl Laboratories IHC-00063), anti–acetylated tubulin (1:500; Sigma 45-T6793), and phosphoserine/phosphothreonine (1:40; Fisher Scientific 01-672-764). Horseradish peroxidase (HRP)-conjugated antibodies included donkey anti-mouse immunoglobulin G (IgG) (H+L; Jackson ImmunoResearch Labs 715-035-150), donkey anti-rabbit IgG (H+L; Jackson ImmunoResearch Labs 711-035-152), and mouse anti-GAPDH (1:10,000; Sigma Aldrich 45-G9295). Fluorescent secondary antibodies included AlexaFluor donkey anti-mouse 488 (Life Technologies A21202), 568 (Life Technologies A10037), and 647 (Life Technologies A31571) and AlexaFluor donkey anti-rabbit 488 (Life Technologies A21206), 568 (Life Technologies A10042), and 647 (Life Technologies A31573).

### Immunofluorescence for 3-D cultures/2-D cultures

Using a pipette, as in Hung *et al*. (2016), media were carefully removed from cultures. Cultures were rinsed with PBS and fixed with 4% paraformaldehyde (PFA) at room temperature for 30 min with light shaking. The PFA was carefully removed and replaced with fresh PFA for an additional 30 min with light shaking. After the PFA was removed, 50 mM $NH_4Cl$ was added for 10 min. Cells were washed with PBS for 30 min with light shaking and then treated for 5 min with 0.1% Triton-X, blocked with PBSΔT (PBS, 1% BSA, 0.5% Triton X-100), and incubated with primary antibodies for 4 h at room temperature. Cultures were washed three times with PBSΔT and incubated with secondary antibodies for 4 h at room temperature. Cultures were kept in PBS containing DABCO (1,4-diazabicyclo[2.2.2] octane) antifade reagent (200 mM) for imaging.

Cells were plated on #1.5 coverslips until they reached 90% confluence and fixed using methanol (–20°C). Cells were rehydrated in PBS before blocking in PBSΔT for 30 min. Primary antibodies diluted in PBSΔT were added to coverslips and incubated for 1 h at room temperature, followed by 10 washes with PBSΔT, secondary antibodies for 1 h at room temperature, and then 10 washes with PBSΔT. Coverslips were rinsed with di$H_2O$ and mounted on glass slides using Prolong Diamond with 4,6-diamidino-2-phenylindole (DAPI) mounting media.

### Imaging

Cells were imaged using either a Leica DMi8 STP800 (Leica, Bannockburn, IL) equipped with a Lumencor SPECTRA X with a Hamamatsu ORCAflash 4.0 V2 CMOS C11440-22CU camera using either a 40 × 1.15 N.A. Lambda S LWD objective or 100 ×/1.4 N.A. HC Pl Apo oil emersion objective and Metamorph software to acquire images or a PerkinElmer Ultraview VoX spinning disc confocal system on a Nikon Eclipse Ti-E microscope using a Hammamatsu C9100-50 EMCCD camera and a 100 ×/1.4 N.A. Apo oil emersion objective using Volocity software. Superresolution 3D-SIM images were acquired on a DeltaVision OMX V4 (GE Healthcare) equipped with a 60 ×/1.42 N.A. PlanApo oil immersion lens (Olympus), 405-, 488-, 568-, and 642-nm solid-state lasers, and sCMOS cameras (pco.edge). Image stacks of 5–6 µm with 0.125-µm-thick *z*-sections and 15 images per optical slice (three angles and five phases) were acquired using immersion oil with a refractive index 1.518. Images were reconstructed using Wiener filter settings of 0.003 and optical transfer functions measured specifically for each channel with SoftWoRx 6.1.3 (GE Healthcare). Images from different color channels were registered using parameters generated from a gold grid registration slide (GE Healthcare) and SoftWoRx 6.1.3 (GE Healthcare). STED imaging was performed using a Leica TCS SP8 (Leica, Bannockburn, IL) equipped with STED 3X, a supercontinuum laser (white light laser 470–670 nm) for excitation, 592/546/600-nm STED depletion lasers, and an HCS PL APO 100x/1.40 oil STED white objective. Images were acquired using the Leica LAS software and postimage processing of STED images was performed using SVI Huygens deconvolution software.

FRAP experiments were performed using a Leica SP5 scanning confocal microscope (Leica, Bannockburn, IL) with an HCX Plan Apochromat 63 ×/1.40-0.06 N.A. OIL objective or the PerkinElmer Ultraview VoX spinning disc confocal system on a Nikon Eclipse Ti-E microscope. With the Leica SP5 the LAS AF (Leica application suite advanced fluorescence) software (Leica) FRAP wizard was used to acquire images. The ImageJ FRAP calculator macro plug-in was used to generate FRAP curves and generate half-life and immobile fraction values. Graphs were then produced in Prism GraphPad software.

### Fluorescence resonance energy transfer

HEK293ad cells were transfected with a PLK1 FRET or a PLK1 FRET-PACT sensor using Mirus Bio TransIT-LT1 transfection reagent (Hukasova *et al.*, 2012; Liu *et al.*, 2012; Bruinsma *et al.*, 2015). After 24 h, cells were synched for 8 h using 100 nM nocodazole and released. To inhibit PLK1 cells were treated with 100 nM BI2536 for 20 min. Images were acquired on a Leica DMi8 STP800 (Leica, Bannockburn, IL) using a 63 ×/1.4 N.A. HC Pl Apo oil emersion objective. The $YFP^{ex} \rightarrow YFP^{em}$/$CFP^{ex} \rightarrow YFP^{em}$ emission ratio in each image was calculated after background subtraction and averaged over multiple cells. The FRET ratio was calculated using an ImageJ Ratio-Plus plugin. Experiments were repeated multiple times with similar results.

### Mitotic centrosome isolation

HEK 293ad cells were treated with 100 nM nocodazole for 18 h. A mitotic shake-off was then performed, and centrosome isolation was carried out as described in Hung *et al.* (2015). In short, HEK293ad cells were treated with 20 µg/ml cytochalasin D and 10 µg/ml nocodazole for 2 h. Cells were then washed with the following buffers in order: 1X PBS, 0.1%PBS:8% wt/wt sucrose, 8% wt/wt sucrose, lysis buffer (LB) (1 mM Tris-HCl, 8 mM BME). Cells were then treated with 1 ml (per 100 mm plate) LB + 0.5% NP40 containing phosphatase inhibitors at 4°C for 2 min on rocker. Supernatants were collected and centrifuged at 1500 × *g* for 6 min at 4°C. The supernatants were then transferred to tubes containing 5 ml Ficoll (20% diluted in PE buffer [10 mM PIPES, 1 mM EDTA, 8 mM BME]) and centrifuged at 13,000 × *g* for 15 min at 4°C, and the Ficoll-PE interface (~150 µl) was collected. The interface was diluted in PE buffer containing phosphatase inhibitors and isolated onto coverslips by centrifugation. Mitotic centrosomes were fixed with ice-cold methanol and immunostained for pS/pT and centrin.

### Immunoprecipitation

HEK293ad cells were transfected with 5 µg (per 100 mm plate) FLAG-CEP215. After 48 h, cells were lysed using ice-cold HEPES lysis buffer (25 mM HEPES, 150 mM NaCl, 0.5% Triton X-100, 1 mM EDTA, 1 mM ethylene glycol-bis(β-aminoethylether)-*N*,*N*,*N*′,*N*′-tetraacetic acid [EGTA], 2% glycerol, 10 mM NaF) and then incubated on ice for 10 min, and postnuclear supernatant was collected. A quantity of 600 µg–1 mg protein was incubated with anti-FLAG M2 affinity gel beads (Sigma) for 1.5 h at 4°C on rotator. Beads were washed twice with lysis buffer, and isolated beads were boiled in 30-µl sample buffer before Western blot analysis.

### Ice treatment

HEK293ad cells treated with either control shRNA or Gravin shRNA were placed in Leibovitz's L-15 media (ThermoFisher #21083027) and placed on ice. After 5 min, the cells were washed in PBS and fixed in ice-cold methanol at –20°C for 10 min. Cells were then immunolabeled and imaged for analysis.

### Microtubule renucleation assay

HEK293ad cells were treated with 10 µg nocodazole in media for 1 h. Cells were then washed three times with PBS before being placed in media at 37°C for times indicated. Cells were fixed using ice-cold methanol at –20°C, immunolabeled, and imaged for analysis.

### Image analysis

A series of 0.2 µm Z-steps of cell volumes are presented as maximum projections using ImageJ. AutoQuant deconvolution was used on wide-field images using Metamorph software. Integrated intensities were measured on sum projections as described in Hoffman *et al.* (2001). To measure integrated intensity on either isolated centrosomes or mitotic centrosomes, circular regions of interest (ROIs) were drawn. The larger ROI ($ROI^L$) is used to measure background whereas the center smaller ROI ($ROI^S$) measures signal. The following equation was used: integrated intensity of $ROI^L$ – ((integrated intensity of $ROI^S$ – integrated intensity of $ROI^L$)×(area $ROI^L$/(area $ROI^S$– area $ROI^L$))) (Hehnly and Doxsey, 2014). Line scans were performed by calculating the normalized fluorescence intensity across a single line. Graphs and statistical analysis (unpaired Student's *t* tests or analysis of variance [ANOVA] as labeled) were completed using Graphpad Prism software. Error bars represent ± SEM; $p < 0.05$ was considered to be statistically significant. All images were set to a resolution of 300 DPI or greater after image analysis from raw data.


## ACKNOWLEDGMENTS

The work was supported by National Institutes of Health Grant R00GM107355 (to H.H.), Department of Defense Grant PC160083 (to H.H.), the Carol Baldwin Foundation of Central New York (to H.H.), National Cancer Institute R01 CA161018 (to L.K.), and Department of Health Prostate Cancer Hypothesis Development RFA 1410200115 (to L.K. and H.H.). We thank René Medema for providing us with the PLK1-FRET biosensor plasmid, Patrina Pellett (previously at G.E., currently at Oxford Nanoimaging) for assistance obtaining SIM images, and Geoff Daniels and Jessica Shivas (Leica) for assistance obtaining STED images. We thank Wenyi Feng (Upstate Medical University) and Jeff Amack (Upstate Medical University) for critical feedback.


## REFERENCES


Bruinsma W, Aprelia M, Kool J, Macurek L, Lindqvist A, Medema RH (2015). Spatial separation of Plk1 phosphorylation and activity. Front Oncol 5, 1–8.

Canton DA, Keene CD, Swinney K, Langeberg LK, Nguyen V, Pelletier L, Pawson T, Wordeman L, Stella N, Scott JD (2012). Gravin is a transitory effector of Polo-like kinase 1 during cell division. Mol Cell 48, 547–559.

Chan EHY, Santamaria A, Silljé HHW, Nigg EA (2008). Plk1 regulates mitotic Aurora A function through betaTrCP-dependent degradation of hBora. Chromosoma 117, 457–469.

Crasta K, Ganem NJ, Dagher R, Lantermann AB, Ivanova EV, Pan Y, Nezi L, Protopopov A, Chowdhury D, Pellman D (2012). DNA breaks and chromosome pulverization from errors in mitosis. Nature 482, 53–58.

Deeraksa A, Pan J, Sha Y, Liu X-D, Eissa N, Lin S-H, Yu-Lee L-Y (2013). Plk1 is upregulated in androgen-insensitive prostate cancer cells and its inhibition leads to necroptosis. Oncogene 32, 2973–2983.

Fong K-W, Choi Y-K, Rattner JB, Qi RZ (2008). CDK5RAP2 is a pericentriolar protein that functions in centrosomal attachment of the γ-tubulin ring complex. Mol Biol Cell 19, 115–125.

Gao D *et al.* (2014). Organoid cultures derived from patients with advanced prostate cancer. Cell 159, 176–187.

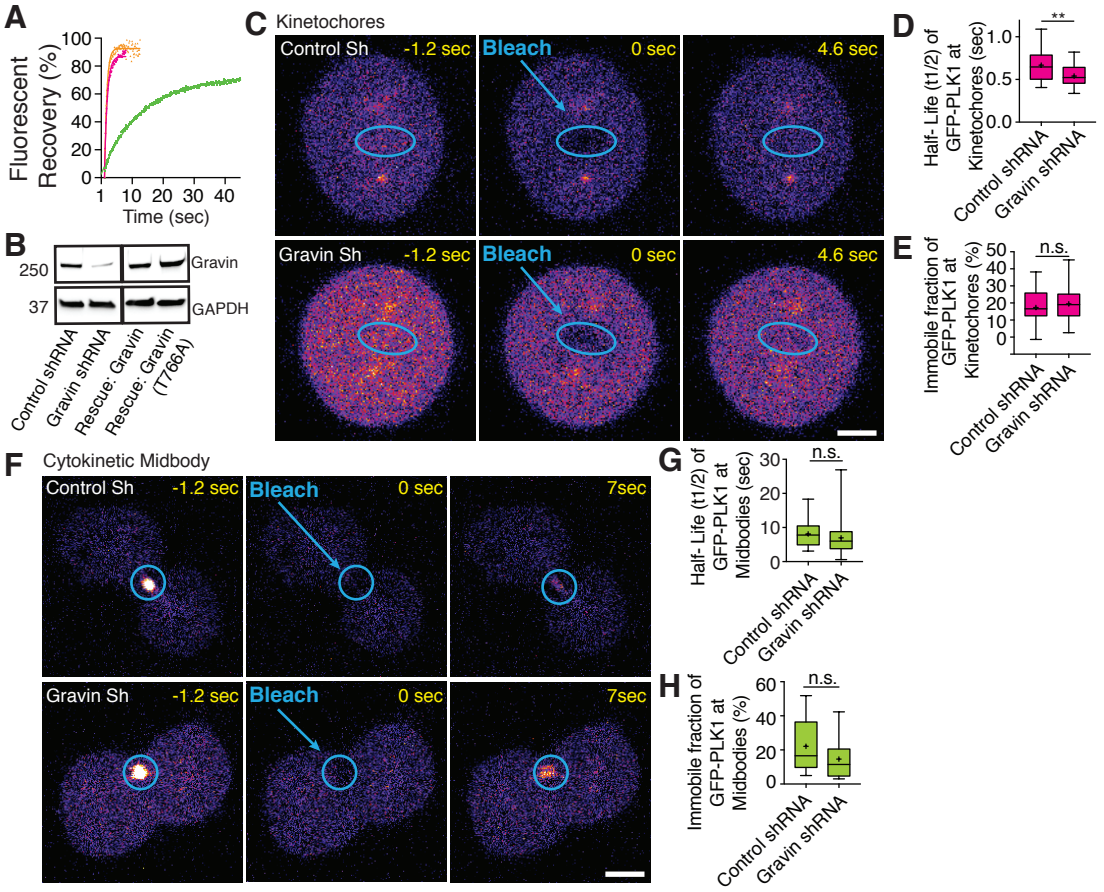
Gelman IH (2010). Emerging roles for SSeCKS/Gravin/AKAP12 in the control of cell proliferation, cancer malignancy, and barriergenesis. Genes Cancer 1, 1147–1156.

Hehnly H, Canton D, Bucko P, Langeberg LK, Ogier L, Gelman I, Santana LF, Wordeman L, Scott JD (2015). A mitotic kinase scaffold depleted in testicular seminomas impacts spindle orientation in germ line stem cells. Elife 4, e09384.
Hehnly H, Doxsey S (2014). Rab11 endosomes contribute to mitotic spindle organization and orientation. Dev Cell 28, 497–507.
Hoffman DB, Pearson CG, Yen TJ, Howell BJ, Salmon ED (2001). Microtubule-dependent changes in assembly of microtubule motor proteins and mitotic spindle checkpoint proteins at PtK1 kinetochores. Mol Biol Cell 12, 1995–2009.
Holland AJ, Cleveland DW (2012). Chromoanagenesis and cancer: mechanisms and consequences of localized, complex chromosomal rearrangements. Nat Med 18, 1630–1638.
Hukasova E, Silva Cascales H, Kumar SR, Lindqvist A (2012). Monitoring kinase and phosphatase activities through the cell cycle by ratiometric FRET. J Vis Exp e3410.
Hung H-F, Hehnly H, Doxsey S (2015). Methods to analyze novel liaisons between endosomes and centrosomes. Biophys Methods Cell Biol 130, 47–58.
Hung HF, Hehnly H, Doxsey S (2016). The mother centriole appendage protein cenexin modulates lumen formation through spindle orientation. Curr Biol 26, 793–801.
Joukov V, Walter JC, De Nicolo A (2014). The Cep192-organized Aurora A-Plk1 cascade is essential for centrosome cycle and bipolar spindle assembly. Mol Cell 55, 578–591.
Kishi K, van Vugt MATM, Okamoto K, Hayashi Y, Yaffe MB (2009). Functional dynamics of Polo-like kinase 1 at the centrosome. Mol Cell Biol 29, 3134–3150.
Leibowitz ML, Zhang C-Z, Pellman D (2015). Chromothripsis: a new mechanism for rapid karyotype evolution. Annu Rev Genet 49, 183–211.
Lera RF, Burkard ME (2012). High mitotic activity of Polo-like kinase 1 is required for chromosome segregation and genomic integrity in human epithelial cells. J Biol Chem 287, 42812–42825.
Liu D, Davydenko O, Lampson MA (2012). Polo-like kinase-1 regulates kinetochore-microtubule dynamics and spindle checkpoint silencing. J Cell Biol 198, 491–499.
Lowery DM, Clauser KR, Hjerrild M, Lim D, Alexander J, Kishi K, Ong S-E, Gammeltoft S, Carr SA, Yaffe MB (2007). Proteomic screen defines the Polo-box domain interactome and identifies Rock2 as a Plk1 substrate. EMBO J 26, 2262–2273.
Macůrek L, Lindqvist A, Lim D, Lampson MA, Klompmaker R, Freire R, Clouin C, Taylor SS, Yaffe MB, Medema RH (2008). Polo-like kinase-1 is activated by aurora A to promote checkpoint recovery. Nature 455, 119–123.
Pan S-H, Tai C-C, Lin C-S, Hsu W-B, Chou S-F, Lai C-C, Chen J-Y, Tien H-F, Lee F-Y, Wang W-B (2009). Epstein–Barr virus nuclear antigen 2 disrupts mitotic checkpoint and causes chromosomal instability. Carcinogenesis 30, 366–375.
Paschal CR, Maciejowski J, Jallepalli P V (2012). A stringent requirement for Plk1 T210 phosphorylation during K-fiber assembly and chromosome congression. Chromosoma 121, 565–572.
Santamaria A, Wang B, Elowe S, Malik R, Zhang F, Bauer M, Schmidt A, Silljé HHW, Körner R, Nigg EA (2011). The Plk1-dependent phosphoproteome of the early mitotic spindle. Mol Cell Proteomics 10, M110.004457.
Sir JH, Pütz M, Daly O, Morrison CG, Dunning M, Kilmartin JV, Gergely F (2013). Loss of centrioles causes chromosomal instability in vertebrate somatic cells. J Cell Biol 203, 747–756.
Zitouni S, Nabais C, Jana SC, Guerrero A, Bettencourt-Dias M (2014). Polo-like kinases: structural variations lead to multiple functions. Nat Rev Mol Cell Biol 15, 433–452.

# Supplemental Materials

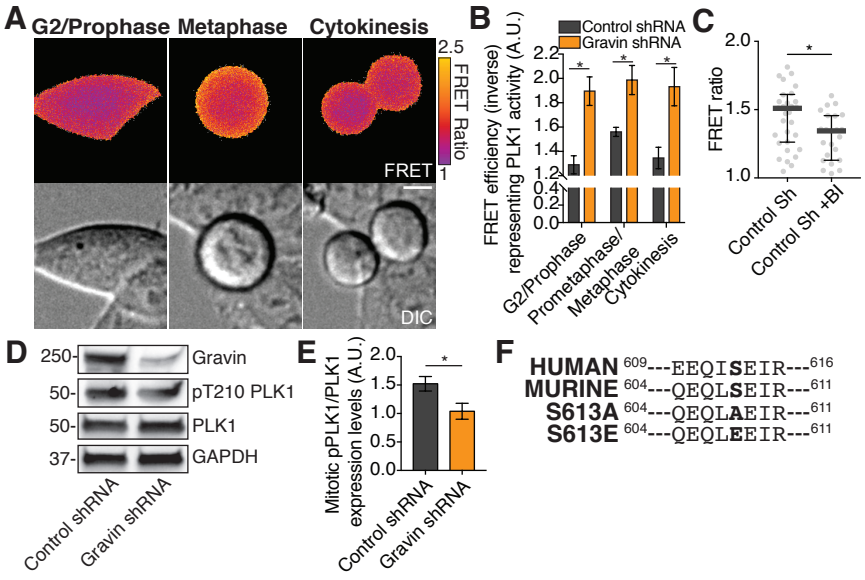
***Molecular Biology of the Cell***

Colicino et al.



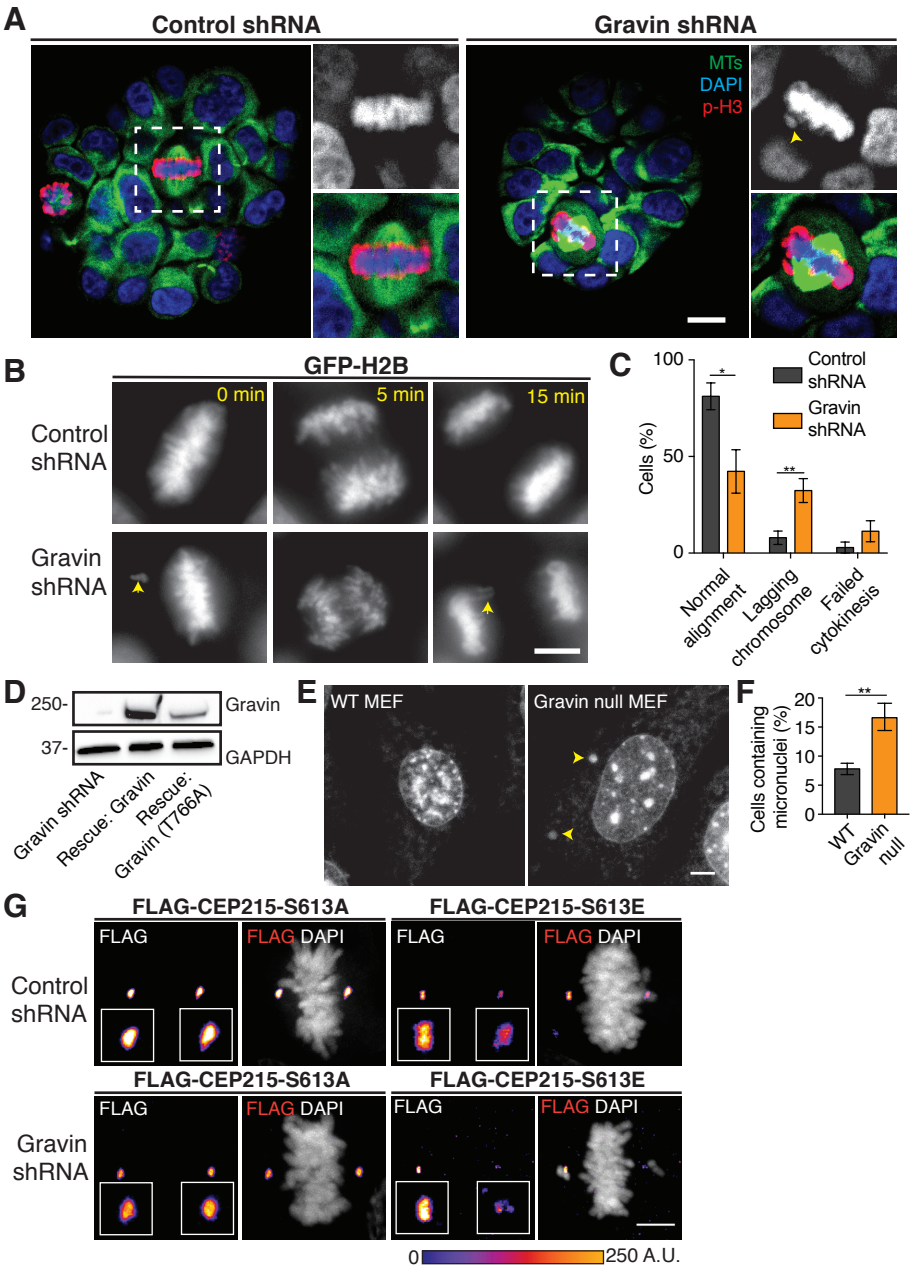

**Supplementary Figure 1. Gravin dynamics disrupts PLK1 dynamics predominantly at mitotic centrosomes.**

(A) A curve was fit using one-phase decay of GFP-PLK1 normalized fluorescence intensity recovery after FRAP of mitotic centrosomes (orange), kinetochores (magenta), and cytokinetic midbodies (green) (n > 20 cells over n = 3 experiments). (B) Immunoblot analysis showing Gravin-depletion by shRNA knockdown and rescue of this depletion by full-length wild-type murine Gravin and the phospho-dead mutant murine Gravin T766A. (C) Representative confocal micrographs of FRAP at kinetochores in control and Gravin shRNA treated GFP-PLK1 RPE cells. (D, E) (D) Half-life and (E) immobile fraction of GFP-PLK1 at kinetochores (box-and-whisker plot of n>20 cells over n=3 experiments, + indicates mean, Student's t-test p=0.0095 (D), Student's t-test p=0.4876 (E)). (F) Representative images of FRAP at cytokinetic midbodies in control and Gravin shRNA treated GFP-PLK1 RPE cells. (G,H) (G) Half-life and (H) immobile fraction of GFP-PLK1 at cytokinetic midbodies measured (box-and-whisker plot of n>25cells over n=3 experiments, + indicates mean. Student's t-test p=0.3211 (H), Student's t-test p=0.1887 (I)).




**Supplementary Figure 2. Gravin-depleted cells redistribute active-PLK1 causing increased phosphorylation events at mitotic centrosomes.**

(A) Relative PLK1 activity for a control shRNA treated cell passing through mitosis is shown as an inverse FRET ratio (Fire LUT, top), corresponding DIC images below. Bar, 5µm. (B) Quantification of PLK1 activity in cells treated with Gravin shRNA or control shRNA, ($n > 5$ cells ± SEM, Student's t-test $p = 0.0109$). (C) Quantification of the inverse FRET-efficiency nocodazole released cells in metaphase that were treated with control shRNA ±BI2536 (BI) is presented as a scatter plot ($n>20$ cells, scatterplot with median and interquartile range shown, Student's t-test $p=0.0118$). (D) Immunoblot analysis of mitotic lysate showing Gravin, PLK1 pT210, and PLK1 expression levels in control shRNA and Gravin shRNA HEK293 cells. GAPDH used as loading control. (E) Quantification of pPLK1 expression normalized to PLK1 expression in HEK293 cells treated with control and Gravin shRNAs. ($n=3$ experiments ±SEM, Student's t-test $p=0.0431$). (F) Alignment of Human and Murine CEP215 showing conservation of PLK1 serine phosphorylation site. Non-phosphorylatable mutant (S613A) and a phosphomimetic (S613E) were constructed.




**Supplementary Figure 3. Gravin loss results in higher incidence of cells containing micronuclei.**

(A) Control shRNA (left) and Gravin shRNA (right) RWPE-1 3-D acini cultures immunostained for microtubules (green), pH3 (red), and DAPI (blue) showing lagging chromosomes in Gravin-depleted acini. Inset is at 2x magnification. Bar, 5 µm. (B) Live-cell imaging of GFP-H2B HeLa cells from metaphase through telophase to visualize lagging chromosomes (yellow arrow). Bar, 5µm. (C) Quantification of control shRNA and Gravin shRNA mitotic cells (%) from (B) that display normal chromosome alignment during metaphase, lagging chromosomes, and

failed cytokinesis over n=3 experiments ±SEM, Student's t-test p=0.0176 for normal alignment and Student's t-test p=0.0022 for lagging chromosomes. (D) Immunoblot analysis from Gravin shRNA treated HeLa cells rescued with Gravin or Gravin (T766A). Proteins were identified using antibodies against Gravin and GAPDH loading control. (E) Immunofluorescent images of wild-type (WT) and Gravin null MEFs stained for DAPI. Yellow arrows depicting micronuclei. Bar, 5µm. (F) Quantification of MEFs (%) containing micronuclei from n=4. (G) Confocal micrographs of control shRNA or Gravin shRNA HEK293 cells expressing FLAG-CEP215-S613A or FLAG-CEP215-S613E are presented as maximum projections. Cells were immunostained for FLAG (Fire-LUT, ImageJ, bar indicates gradient of integrated fluorescent intensity values (A.U.)) and DAPI (white). Insets (white boxes) of individual mitotic centrosomes magnified 3x. Bar, 5µm.

Received: 3 September 2018 | Revised: 8 October 2018 | Accepted: 26 October 2018

DOI: 10.1002/cm.21504

WILEY

REVIEW ARTICLE

# Regulating a key mitotic regulator, polo-like kinase 1 (PLK1)

Erica G. Colicino[1] | Heidi Hehnly[1,2]

[1]Department of Cell and Developmental Biology, Upstate Medical University, Syracuse, New York

[2]Department of Biology, Syracuse University, Syracuse, New York

**Correspondence**
Heidi Hehnly, Department of Biology, Syracuse University 236 Life Sciences Complex Syracuse, NY 13210.
Email: hhehnly@syr.edu

**Funding information**
Carol M. Baldwin Breast Cancer Research Fund; U.S. Department of Defense, Grant/Award Number: W81XWH-17-1-0241; NIH Grants, Grant/Award Numbers: R00GM107355, R01GM127621

## Abstract

During cell division, duplicated genetic material is separated into two distinct daughter cells. This process is essential for initial tissue formation during development and to maintain tissue integrity throughout an organism's lifetime. To ensure the efficacy and efficiency of this process, the cell employs a variety of regulatory and signaling proteins that function as mitotic regulators and checkpoint proteins. One vital mitotic regulator is polo-like kinase 1 (PLK1), a highly conserved member of the polo-like kinase family. Unique from its paralogues, it functions specifically during mitosis as a regulator of cell division. PLK1 is spatially and temporally enriched at three distinct subcellular locales; the mitotic centrosomes, kinetochores, and the cytokinetic midbody. These localization patterns allow PLK1 to phosphorylate specific downstream targets to regulate mitosis. In this review, we will explore how polo-like kinases were originally discovered and diverged into the five paralogues (PLK1-5) in mammals. We will then focus specifically on the most conserved, PLK1, where we will discuss what is known about how its activity is modulated, its role during the cell cycle, and new, innovative tools that have been developed to examine its function and interactions in cells.

**KEYWORDS**

biosensor, cell division, centrosome, chemical genetics, FRET, kinetochore, midbody, mitosis, polo-like kinase 1, scaffolds

## 1 | INTRODUCTION

Mitosis incorporates a multitude of protein interactions and macromolecular machinery to successfully segregate sister chromatids into new daughter cells (Nigg & Stearns, 2011). The fidelity of mitotic progression requires regulatory and signaling proteins to be dynamically recruited and constrained at centrosomes. The centrosome is a structure that is composed of two centrioles that start their duplication cycle during S-phase (reviewed in Nigg & Stearns, 2011). Once the centrosome has duplicated into two mitotic centrosomes, they will then drive the assembly of the microtubule-based spindle. The assembly of the microtubule-based spindle requires the recruitment of microtubule nucleating components (e.g., pericentrin, γ-tubulin, CEP215, γ-turc, CEP170, CEP68, AKAP450, etc.) (Choi, Liu, Sze, Dai, & Qi, 2010; Doxsey, Steln, Evans, Calarco, & Kirschnefi, 1994; Fabbro et al., 2005; Kolobova et al., 2017; Zimmerman, Sillibourne, Rosa, & Doxsey, 2004). The recruitment of these components require activated mitotic signaling cascades involving the mitotic kinases Aurora A, polo-like kinases (PLKs), and cyclin-dependent kinase 1 (CDK1) to name a few (Bruinsma et al., 2015; Hehnly et al., 2015; Lee et al., 2018; Sanhaji et al., 2014; Thomas et al., 2016). One kinase that seems to be at the center of this process from a single cell eukaryote to a multi-cellular vertebrate is polo-like kinase 1 (PLK1).

PLK, in mammals, has diverged into five paralogues, PLK1-5 (De Cárcer, Manning, & Malumbres, 2011). Unlike its alternative mammalian paralogues (PLK2-5), PLK1 function is evolutionarily conserved persisting in *Schizosaccharomyces pombe* (fission yeast), *Drosophila melanogaster* (fruit flies), and *Caenorhabditis elegans* (PLK-1) where it acts broadly throughout mitosis from G2 until the final stage of cytokinesis, abscission (Nasmyth & Nurse, 1981; Sunkel & Glover, 1988). While these initial studies defined an essential and conserved role for PLK1 during the cell cycle, it has been difficult to delineate the spatial and temporal regulation of PLK1. However, with the onset of chemical genetics and biosensors to analyze PLK1 activity in live cells, giant

This is an open access article under the terms of the Creative Commons Attribution License, which permits use, distribution and reproduction in any medium, provided the original work is properly cited.
© 2018 The Authors. *Cytoskeleton* published by Wiley Periodicals, Inc.

strides have been made, and likely will still be made, in understanding PLK1 activity and function during the cell cycle (Bruinsma et al., 2014, 2015; Burkard et al., 2007; Lera & Burkard, 2012; Liu, Davydenko, & Lampson, 2012; Macůrek et al., 2008). In this review, we will touch briefly on how polo-like kinases were discovered, as well as its evolutionary conservation and divergence in mammals. We will then specifically focus on PLK1, where we will explore its diverse functions, subcellular localizations, scaffold–protein interactions, and its known downstream phosphorylation substrates. Finally, we will discuss the intramolecular tools that will facilitate future advancements in understanding PLK1's role throughout the cell cycle.

## 2 | DISCOVERY OF POLO-LIKE KINASES

Polo-like kinase was first identified in budding yeast (*Saccharomyces cerevisiae*) through the screening of various cell division cycle (cdc) mutants (Hartwell, Mortimer, L O, CuLo, & Esposito, 1973). Hartwell et al. defined and characterized previously identified temperature-sensitive mutants, which perturbed the progression of the cell cycle. They determined that *cdc5*, a homologue of mammalian PLK1, specifically caused cytokinetic defects when cells were shifted to a restrictive temperature, resulting in a significant increase in bi-nucleated cells. Strikingly, if the cells were shifted to restrictive temperatures following cytokinesis completion, cells would then arrest during the second cell cycle. This work demonstrated that the temporal regulation of cdc5/PLK1 is necessary for the initiation and proper progression of mitosis (Hartwell et al., 1973). PLK1's role in mitotic progression was later confirmed in *Drosophila melanogaster* (Sunkel & Glover, 1988). In *Drosophila*, the homologue is called *polo*. Homozygous *polo* mutant flies were found to arrest in development, failing to form a fully developed embryo. This was due to cells of *polo* embryos arresting at the same stage of the cell cycle, prometaphase and metaphase, where they presented with multipolar spindles, aneuploidy, and abnormal centrosome structure and microtubule aster formation (Sunkel & Glover, 1988). This suggested that the gene *polo* was a vital mitotic regulator that assists in the proper establishment of the mitotic spindle through microtubule nucleation from the mitotic centrosomes. When this process is disrupted, a functional bipolar spindle cannot be formed and chromosome mis-segregation occurs, resulting in increased aneuploidy (Sunkel & Glover, 1988).

While it was becoming clear that PLK1 is a vital regulator of mitosis, scientists were unclear as to ***how*** PLK1 regulated this process. By further examining the *Drosophila polo* sequence, it was found that *polo* contains an N-terminal sequence consistent with serine–threonine kinases such as SNF1, KIN1, and KIN2 in budding yeast (Llamazares et al., 1991). It was later discovered through indirect protein kinase analysis of *polo* from mitotic *Drosophila* lysates, that PLK1 was capable of phosphorylating the protein casein, further supporting the role of PLK1 as a kinase (Fenton & Glover, 1993). A later study confirmed that this PLK1 kinase activity was specific during mitosis by performing in vitro kinase assays with cells released into prometaphase after nocodazole treatment. Casein phosphorylation by PLK1 was specific to lysates for 50 min after nocodazole release (Lee, Yuan, Kuriyama, & Erikson, 1995). Over time, it was found that this kinase was highly conserved between vertebrates, invertebrates, and single-celled organisms alike. This includes *Caenorhabditis elegans* PLK-1 (Ouyanga, Wangb, & Daia, 1999), *Xenopus* (*Plx1*) (Descombes & Nigg, 1998), and mammals (*PLK1*) (Lee & Erikson, 1997). The evolutionary conservation of this gene and role as a mitotic kinase strengthened the notion that this is a vital component of cellular division.

## 3 | FUNCTIONS OF THE DIVERGENT MAMMALIAN PLKS (1–5)

Mammals contain five paralogues (PLK1-5) that are distinct in localization, expression patterns, and function within cells. Despite this divergence, each of the paralogues retained the canonical PLK domains, the N-terminal kinase domain and the C-terminal polo-box domain (PBD) (depicted in Figure 1). The kinase domain is a catalytic T-loop domain which allows PLKs to convert ATP to ADP, transferring the phosphate group to any of the numerous PLK downstream phosphorylation targets (Kothe et al., 2007). The PBD domain is unique in that it recognizes specific phosphorylation motifs on PLK binding scaffolds (Elia, Rellos, et al., 2003; Elia, Cantley, & Yaffe, 2003). The main difference between the five PLK paralogues is the number of PBDs they contain, their expression patterns within particular cell types, and/or their expression patterns throughout the cell cycle. For instance, PLK4 has diverged to contain a cryptic polo-box domain (CPB) and a single polo-box region within the PBD overtime (Figure 1; De Cárcer, Escobar, et al., 2011; Habedanck, Stierhof, Wilkinson, & Nigg, 2005). Due to the presence of the cryptic polo-box and single PBD, PLK4 homodimerizes, altering its structural conformation and causing regulated spatial activity in cells (Leung et al., 2002; Sillibourne & Bornens, 2010). This localizes the kinase to the centrosome during S-phase to bind scaffolds, such as CEP192 and CEP152 (Park et al., 2014; Slevin et al., 2012; Sonnen, Gabryjonczyk, Anselm, Stierhof, & Nigg, 2013), which restricts its localization and activity to the centrosome allowing for precise spatial regulation of centrosome duplication (Leung et al., 2002; Sillibourne & Bornens, 2010; Sonnen et al., 2013). This led researchers to further try and understand how either a specific PBD or the number of polo-box regions leads to scaffold-binding specificity and PLK localization patterns. To answer this question, PLK2-4

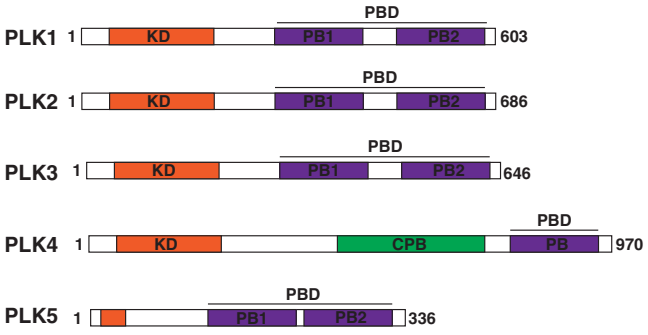


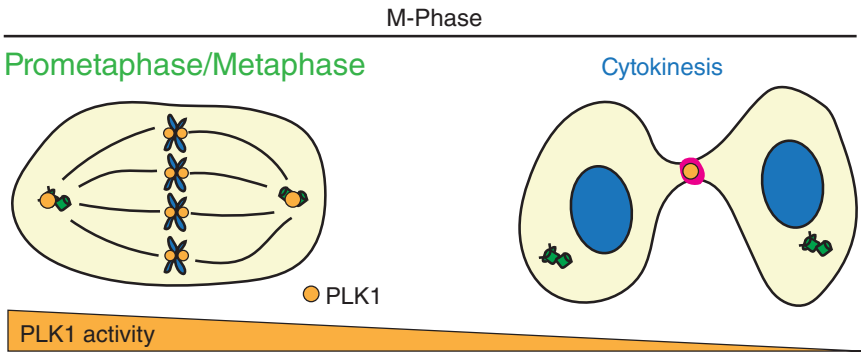

**FIGURE 1** There are five mammalian polo-like kinase paralogues. The five mammalian paralogues contain an N-terminal catalytic kinase domain (orange) and a C-terminal polo-box domain (PBD, purple). The PLK4 cryptic polo-box domain (CPB) is shown in green. Adapted from (De Cárcer, Manning, et al., 2011)

chimeras containing PLK1 kinase domains were expressed in cells depleted of endogenous PLK1. These chimeric PLKs were able to rescue phenotypes that are present with PLK1-depletion (Van De Weerdt et al., 2008), supporting the idea that, through the PBDs, specific scaffolding of polo-kinases is required for PLK spatial localization and temporal phosphorylation of downstream phosphorylation targets. A schematic representation of the five PLKs containing both their kinase and PBDs are demonstrated in Figure 1. The PBD is highly conserved between PLK1-3 (36–43% homology) and is less so in PLK4 (16% homology) (Park et al., 2010). Thus, this brings up the question, what is it about these different PLKs that allow directed localization and subsequent downstream function?

One possibility is that the expression patterns within a cell and within an organism varies between PLKs. PLK2, PLK3, and PLK5 are expressed predominantly during interphase and play a variety of functions. PLK2 has been implicated in neuronal synapse function and signal transduction (Seeburg, Pak, & Sheng, 2005). Additionally, PLK2 has been implicated during S-phase of the cell cycle, phosphorylating the protein CPAP and allowing for subsequent centriole assembly (Chang, Cizmecioglu, Hoffmann, & Rhee, 2010). PLK5 is unique in humans in that it has lost the kinase domain, but retained the conserved PBD-domain characteristic of the PLK-family kinases, gaining its membership into this family (Andrysik et al., 2010; De Cárcer, Escobar, et al., 2011). Like PLK2, PLK5 functions exclusively within quiescent brain cells where it aids in the formation of neuritic processes (De Cárcer, Escobar, et al., 2011). Even less is currently known about PLK3, but studies have implicated it during G0/G1, during apoptosis, and later during S/G2-phase as a component of p53-dependent DNA damage checkpoint (Zimmerman & Erikson, 2007). PLK1 and PLK4 are expressed predominantly during S/G2 and M-phase of diving cells.

PLK1 and PLK4 are the most heavily studied PLKs. PLK1 is the most highly conserved through single celled eukaryotes up to vertebrates where it is expressed during the G2/M-phases of the cell cycle (Figure 2a). This expression is the result of p53-dependent transcription which follows the upregulation of two key factors during division, CDK1 and Cyclin B (Martin & Strebhardt, 2006). These proteins work in concert with PLK1 to ensure proper mitotic progression. CDK1/Cyclin B phosphorylates specific serine/threonine residues on

(a)




(b)

| Stage of Mitosis | Sub-cellular Localization | Potential Role at Locale | Known Scaffolds | References |
|---|---|---|---|---|
| Prophase | Nucleus/ Cytoplasm | Mitotic entry and CDK1 activation | Bora | (Seki et al., 2008) |
| Prometaphase | Kinetochores Centrosomes | K-MT attachments MT nucleation Recruitment of PCM components (pericentrin, γ-tubulin, γ-turc) | Gravin (centosome) cenexin (centosome) BubR1 (kinetochore) | (Canton et al., 2012; Colicino et al., 2018; Qi, Tang, & Yu, 2006a; Nak-Kyun Soung et al., 2006) |
| Metaphase | Centrosomes Kinetochores | SAC Passage MT attachments Chromosomes alignment at Metaphase plate | Gravin (centosome) cenexin (centosome) BubR1 (kinetochore) | (Canton et al., 2012; Colicino et al., 2018; Qi et al., 2006a; Nak-Kyun Soung et al., 2006) |
| Cytokinesis/ Abscission | Midbody | Suppression of CEP55 prior to recruitment of ESCRT-complex | PRC1 | (Hu et al., 2012; Neef et al., 2007) |

**FIGURE 2** PLK1 subcellular distribution and function during metaphase in mammalian cells. (a) PLK1 (orange) localizes during M-phase to the mitotic centrosomes, kinetochores, and cytokinetic midbody (magenta) to ensure mitotic progression, microtubule attachments, and anaphase onset, as well as proper cytokinesis and abscission. Gradient below (orange) represents relative PLK1 activity changes between prometaphase/metaphase and cytokinesis. (b) Table outlining PLK1 localization patterns with corresponding functions and known binding scaffolds during M-phase

PLK1-binding scaffolds, with the sequence motif of Ser-pSer/pThr-Pro/X, allowing PLK1 to directly bind. Known PLK1 scaffold proteins include Bora (Seki, Coppinger, Jang, Yates, & Fang, 2008), cenexin (Soung et al., 2006), Gravin (Canton et al., 2012), BubR1 (Qi, Tang, & Yu, 2006), PRC1 (Hu, Özlü, Coughlin, Steen, & Mitchison, 2012) to name a few, and localize subcellularly to the nucleus, centriole appendages, pericentriolar matrix (PCM), kinetochores, and cytokinetic midbody, respectively (Figure 2b). These scaffolds aid PLK1 in its regulation of centrosome maturation and microtubule nucleation, as well as regulating its role as a component of the spindle assembly checkpoint, during which it ensures proper end-on microtubule attachments at kinetochores and activation of the anaphase promoting complex (APC). The APC is an E3-ubiquitin ligase that degrades mitotic proteins, allowing sister chromatids to separate and cells to progress through the end of mitosis and enter G1 (Eckerdt & Strebhardt, 2006). Since PLK1 regulates the onset of this complex, PLK1 is known as a major regulator of the metaphase to anaphase transition of division.

PLK4 is exclusively expressed during S-phase of the cell cycle. The expression and localization of PLK4 at the centrioles triggers centriole duplication and procentriole formation (Habedanck et al., 2005). Following PLK4 localization, PLK4 is able to recruit, phosphorylate, and bind the protein STIL (Ohta et al., 2014). This leads to the recruitment of additional centriole components such as SAS6, CEP135, and γ-tubulin, allowing for centriole duplication and assembly to begin (Kleylein-Sohn et al., 2007; Ohta et al., 2014; Shyang Fong, Kim, Tony Yang, Liao, & Bryan Tsou, 2014). Centriole duplication produces two mitotic centrosomes, required for the formation of the microtubule-based bipolar spindle during M-phase. In the event of PLK4 overexpression or an S-phase mitotic delay during this process, such as DNA damage, persistent PLK4 activity can cause centriole overduplication, or reduplication to occur (Habedanck et al., 2005). In contrast, when PLK4 is absent, either through knockdown or drug inhibition by centrinone, centriole duplication fails causing complete centriole loss after two or more consecutive cell cycles (Habedanck et al., 2005; Wong et al., 2015). This centriole loss eventually leads to p53-dependent G1 cell cycle arrest. Together, this suggests that PLK4 has specific and timely roles in centriole duplication during S-phase, and if the threshold expression of PLK4 is disrupted, either due to over- or under-expression, centriole duplication is impacted.

PLK1 is also involved in centriole duplication, where its signaling allows for centriole disengagement, allowing for centriole duplication (Lon Carek, Hergert, & Khodjakov, 2010). Thus, a likely relationship exists between PLK1 and PLK4, where active-PLK1 is required for centriole disengagement and maturation to occur during S-phase, and PLK4 is required for duplication. The inherent nature of the relationship between PLK1 and PLK4, though, is not completely understood. Despite PLK4 being the major kinase responsible for centriole duplication, as described above, PLK1-depletion has been implicated in causing a centriole duplication delay (Hatano et al., 2012; Lon Carek et al., 2010; Shukla, Kong, Sharma, Magidson, & Loncarek, 2015). It has been suggested that the reason for this delay is the inability of the cell to recruit centriole maturation factors, such as γ-tubulin (Lon Carek et al., 2010). Alternatively, if PLK1 activity is elevated, the centrioles prematurely disengage, which allows the daughter centriole to recruit centriole proteins and nucleation factors, such as cenexin and γ-tubulin, triggering an additional round of centriole duplication during S-phase (Bryan Tsou et al., 2009; Kong et al., 2014; Lon Carek et al., 2010; Shukla et al., 2015). These studies support the idea that PLK1 and PLK4 are tightly regulated kinases with distinctly choreographed functions that work to ensure proper centriole disengagement, duplication, and recruitment of microtubule nucleating factors allowing for the assembly of a robust mitotic spindle.

## 4 | FUNCTION OF PLK1

As shown in Figure 1, PLK1 contains two polo-box regions, forming a PBD sufficient for localizing PLK1 to centrosomes, kinetochores and the cytokinetic midbody during mitosis (Figures 2 and 3). PLK1 spatial and temporal localization throughout division is shown using structured illumination microscopy (SIM) in Figure 3, illustrating its transition from centrosomes and kinetochores during early M-phase to the midzone and cytokinetic midbody during the final stages of mitosis (Figure 3). By expressing the PLK1 kinase domain alone, it is insufficient to localize PLK1 at the mitotic centrosomes or kinetochores, whereas expressing the PBD alone localizes PLK1 robustly to mitotic centrosomes and, to a lesser extent, at kinetochores (Kishi, van Vugt, Okamoto, Hayashi, & Yaffe, 2009). Together, this suggested that even though the kinase domain was not required for PLK1 localization to mitotic centrosomes, it likely assists in PLK1 localization to kinetochores.

The PBD provides specific PLK1 binding through defined pS/pT sequences on binding scaffold proteins (Elia, Cantley, et al., 2003). This binding specificity requires PLK1 to contain both the two polo-box regions within the PBD and the protein linker sequence separating the kinase domain from the PBD. To determine this PLK1-specific binding sequence, a phospho-peptide library was utilized. This library comprised of motifs known to be phosphorylated by alternative mitotic kinases, including CDKs and mitogen activated protein kinases (MAPKs). Using this library, the specific PLK1 PBD binding sequence was identified to be Ser-pSer/pThr-Pro/X (Elia, Rellos, et al., 2003). Once this sequence was determined, it was later used to identify greater than 600 potential putative PLK1 scaffolds to be further examined. This library of putative scaffolds are potential regulators of PLK1 that likely control PLK1's spatial distribution and activity throughout the cell cycle (Lowery et al., 2007).

While only a select few PLK1 binding scaffolds have been confirmed, studies have clearly demonstrated that the subcellular distribution of PLK1 is tightly regulated through scaffold proteins. The regulation of these interactions relies heavily on the ability of these scaffolds to be phosphorylated by the mitotic kinase CDK1. The CDK1 kinase domain recognizes the motif Ser–Ser/Thr–Pro/X on PLK1-binding scaffolds and is able to phosphorylate the second amino acid, known as priming, allowing for PLK1–PBD interactions (Enserink & Kolodner, 2010). Some of the identified scaffolds that require this priming by CDK1 are Bora, Gravin, and cenexin (Canton et al., 2012; Soung et al., 2009; Thomas et al., 2016). PLK1 also has the ability to phosphorylate its own scaffold, such as PBIP1 and BubR1 at the centromeres, a mechanism commonly used to maintain

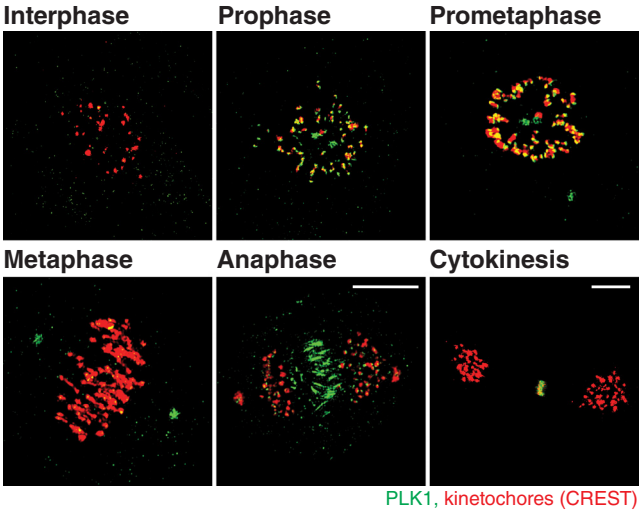



**FIGURE 3** PLK1 distribution throughout mitosis. Structured illumination microscopy (SIM) volumetric projection micrographs of RPE cells showing localization of PLK1 (green) from interphase through cytokinesis. Kinetochore marker: CREST (red). Unpublished SIM micrographs from Dr. Heidi Hehnly's lab, performed by Erica Colicino

its localization at kinetochores (Elowe, Hümmer, Uldschmid, Li, & Nigg, 2007; Lee, Oh, Kang, & Park, 2008). These PLK1-scaffold interactions allow for the localization and regulation of PLK1 dynamics, activity, and function at its subcellular locales.

Through differential regulation at numerous subcellular locales, PLK1 displays a variety of functions as a major regulator of mitotic entry. For instance, PLK1 localizes to the nucleus during G2-phase where it has been implicated as a DNA damage checkpoint regulator (Hyun, Hwang, Hwan, & Jang, 2014; Smits et al., 2000; Van Vugt, Brá, & Medema, 2004; Wakida et al., 2017). During this process, PLK1 is required to recruit initial components of the DNA Damage Response (DDR), including ATM/ATR (Hyun, Hwang, et al., 2014). PLK1 is then dephosphorylated in an ATM-Chk1 dependent manner, effectively inactivating the kinase. Thus, PLK1 is downregulated until the completion of the DDR, in which newly active-PLK1 then works as a checkpoint regulator, allowing division to progress into M-phase (Hyun, Hwan, & Jang, 2014; Lee, Hwang, & Jang, 2010). One possibility is that while DDR occurs, PLK1 is unable to recruit MT-nucleating components to the centrosome so mitotic spindle formation cannot occur. An additional possibility that has yet to be examined is whether a population of PLK1 that acts within the nucleus can be exchanged to act on mitotic centrosomes. In this case, it is interesting to predict that PLK1 acts as a sensor that relays messages between the nucleus and mitotic centrosomes.

Since PLK1 depletion is lethal, it has been difficult to study its acute role at different cell-cycle stages. For instance, PLK1 is thought to be necessary for cytokinesis, but it is difficult to test its direct contributions to this process because early mitotic defects caused by PLK1-depletion triggers the spindle assembly checkpoint (SAC), preventing cells from entering cytokinesis and hindering these direct observations of PLK1 during this specific cell cycle stage. One solution has been to use small-molecules that rapidly inhibit PLK1 during anaphase, after the SAC has been satisfied. ATP-analogues that target and inhibit the PLK1 kinase domain in vitro include BI2536 and BI6727 (Lenart et al., 2007; Steegmaier, Hoffmann, Baum, Ter Lé Ná Rt, et al., 2007). However, the specificity of these drugs to specifically inhibit PLK1 in vivo is either poorly understood or unknown. In addition, based on the strong conservation of the PLK-kinase domains, none of these compounds are expected to be selective for individual PLK-homologues, complicating their use.

To overcome this issue, a chemical genetics system was developed in order to acutely inhibit specifically PLK1 at select times during division. A technique was developed based on traditional studies performed in yeast, where monospecific-kinase inhibition could be achieved by replacing the target enzyme-of-interest with a variant, whose catalytic pocket was genetically modified to accept bulky purine analogues to inhibit kinase activity (Bishop et al., 2000). A similar approach can now be taken with mammalian tissue culture, where gene-targeting and transgenic complementation can be used to establish somatic cell lines exclusively expressing an analogue-sensitive PLK1 (PLK1$^{as}$) (Figure 4; Burkard et al., 2007). These PLK1$^{as}$ cells grow in culture similarly to wild-type cells expressing endogenous PLK1. However, PLK1$^{as}$ cells displayed heightened sensitivity to purine analogues, whereas wild-type cells do not. PLK1$^{as}$ cells, in the presence of purine analogues, display defects in mitotic spindle assembly, centrosome maturation, and chromosome alignment. These cells were then used to demonstrate and confirm PLK1's involvement during cytokinesis, where treatment with a purine-analogue during anaphase prevented cleavage furrow formation and abscission (Burkard et al., 2007). The system was also used to determine that PLK1 kinase functions that are separable by an activity threshold where titrating PLK1 activity leads to specific mitotic defects (Lera & Burkard, 2012). Together, these studies demonstrated the power of chemical genetics in dissecting complex, but short-term, events in dividing cells.

While PLK1 is expressed at its peak level during metaphase (Golsteyn, Mundt, Fry, & Nigg, 1995), there are still small amounts of PLK1 at other cell cycle stages. For instance, at G1/G0 there is small but significant amount of PLK1 that may regulate cilia function (Wang et al., 2013). Such that PLK1 association with the BBsome, an octameric protein complex that localizes at the centrosome/basal body and is involved in trafficking cargoes to the primary cilium, is required for cilia disassembly as cells re-enter the cell cycle. It is suggested that cilia disassembly can occur through two PLK1-dependent pathways: (1) PLK1-Dvl2 dependent AuroraA-HEF1 recruitment to the ciliary base, leading to cilia disassembly through the noncanonical Wnt pathway (Lee et al., 2012) and (2) PLK1-dependent phosphorylation DAZ-

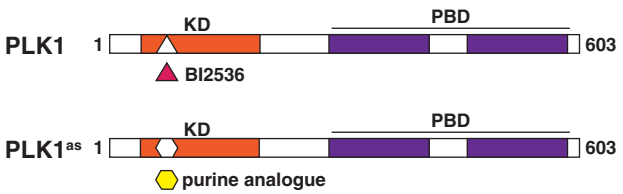



**FIGURE 4** Model of PLK1 chemical genetics. The catalytic domain of PLK1 can be inhibited by treatment with an ATP analogue, such as the drug BI2536. By mutating and enlarging this catalytic domain, PLK1 can be inhibited in cells expressing this mutant using a purine analogue. Adapted from Burkard et al. (2007)

interacting protein 1 (Dzip1), causing its dissociation from the BBsome and subsequent cilia disassembly (Zhang et al., 2016). Through the first pathway, PLK1 is recruited to cilia through Dvl2, a PLK1 scaffold that is primed for binding by Wnt5a. Once PLK1 binds Dvl2, it was shown that Aurora A and HEF1 expression increases, allowing a complex to form and be recruited to the cilia, leading to ciliary disassembly (Lee et al., 2012). In the secondary pathway, PLK1 phosphorylates Dzip1 at S210, allowing for its removal from the centriolar satellite, or ciliary base, triggering BBsome removal and eventual ciliary disassembly (Zhang et al., 2016). This suggests that while mitotic entry requires a robust amount of active-PLK1 for mitotic fidelity, small amounts of precisely localized active-PLK1 likely regulates essential, nonmitotic processes.

## 5 | ROLE OF PLK1 AT CENTROSOMES, KINETOCHORES, AND CYTOKINETIC MIDBODIES

### 5.1 | PLK1 at kinetochores

PLK1's localization and function has been heavily studied at kinetochores, a complex of proteins associated with the centromere of a chromosome, where microtubules attach during cell division (reviewed in Saurin, 2018). PLK1-localization at kinetochores is highest during prometaphase, where it is recruited initially by Bub1 (Qi et al., 2006), NudC (Nishino et al., 2006), and BubR1 (Elowe et al., 2007; Suijkerbuijk, Vleugel, Teixeira, & Kops, 2012). This localization is significantly reduced as the cell enters metaphase, similar to many other checkpoint signaling proteins, but PLK1 is not, in fact, required for spindle checkpoint function. PLK1 reduction at kinetochores results from SAC satisfaction during metaphase, where the CUL3-based E3-ligase ubiquitinates PLK1, resulting in its dissociation and the stabilization of kinetochore–microtubule attachments (reviewed in Liu & Zhang, 2017). This suggests that PLK1 activity suppresses kinetochore–microtubule dynamics. A potential mechanism by which PLK1 achieves this is through stabilizing initial microtubule attachments during prometaphase, such as through CLASP-phosphorylation (Maia et al., 2012) and Kif2b (Hood, Kettenbach, Gerber, & Compton, 2012), while PLK1 removal during metaphase maintains dynamic microtubules (Liu et al., 2012). When there are no proper end-on attachments at kinetochores, PLK1 can then act on BubR1 to recruit Mad2, preventing the passage of the SAC until proper end-on attachments form (Wong & Fang, 2007). Once proper kinetochore–microtubule attachments are made, PLK1 activity decreases at kinetochores, allowing for passage of the SAC and initiation of the APC/Cyclosome, concluding metaphase (Beck et al., 2013). After cells enter anaphase/telophase, PLK1 is thought to transition from kinetochores into the midzone, where it recruits RhoGEF Ect2, allowing for proper cleavage furrow and cytokinetic bridge formation (Burkard et al., 2007; PLK1 at midzone shown in SIM micrograph in Figure 3).

In general, it is understood that increased PLK1 concentrations are found at kinetochores during prometaphase, but exactly how PLK1 operates within the kinetochore is uncertain. Specifically, it is unclear whether the spatial distribution of PLK1 within the kinetochore controls its accessibility to substrates, and its subsequent downstream functions, at this locale. However, the PLK1 spatial regulation at kinetochores remains enigmatic due to multiple PLK1 interactions and substrates along the kinetochore–centromere axis (Lera et al., 2016). For example, PLK1 interacts with outer kinetochore components, including Bub1, NudC, and BubR1, as well as inner kinetochore components where it is recruited by CENP-U/50 (Kang et al., 2006) and CENP-Q (Park et al., 2015). PLK1 also functions at the inner centromere, 500 nm from the outer kinetochore, through binding INCENP (Goto et al., 2006). A recent study utilized chemical genetics to investigate exactly how PLK1 spatial distribution within kinetochores contributes to its function and access to downstream substrates (Lera et al., 2016). This study was important in determining that pools of PLK1 anchored at one part of the kinetochore axis did not act on substrates localized at another point on the kinetochore axis. Additionally, the PLK1 pool that acts within the inner centromere is distinct in function from its role in stabilizing microtubule attachments at the outer kinetochore (Lera et al., 2016). This supported the idea that multiple pools of PLK1 exist at distinct kinetochore subcompartments, and that PLK1 displays discrete functions at these distinct sites.

### 5.2 | *PLK1 at centrosomes*

PLK1 plays an essential role in the recruitment of MT-nucleating components to mitotic centrosomes, an essential process for building a robust MT-based spindle and ensuring mitotic fidelity. For instance, in *C. elegans*, PLK1 works to organize PCM scaffolding where its activity allows for the recruitment of PCM components SPD-2 and SPD-5. Strikingly, in an in vitro reconstitution environment, these two PCM components can self-assemble into a selective phase PCM that is dependent on PLK1 activity (Woodruff et al., 2017). In vivo, PLK1 assists the assembly of pericentrin (Lee & Rhee, 2011) and CEP215 (Colicino et al., 2018; Santamaria et al., 2011) at the PCM through phosphorylation. Both pericentrin and CEP215 are essential PCM scaffolds required for the recruitment of additional PCM components, including γ-turc. In the case of pericentrin, inhibiting its PLK1 phosphorylation sites, S1235 and S1241, results in the failed recruitment of PCM proteins, including γ-tubulin, CEP192, and γ-turc (Lee & Rhee, 2011). Little is known about CEP215's phosphorylation by PLK1, except for an identified PLK1 phosphorylation site at S613 through a phosphoproteome (Santamaria et al., 2011). Our recent study dissected the role of the PLK1 scaffold Gravin and further explored the implications of CEP215 phosphorylation by PLK1 (Colicino et al., 2018). Interestingly, we found that when PLK1 is unable to be sequestered by Gravin at mitotic centrosomes, increased CEP215 phosphorylation occurred at its S613 site. Thus, we created a phospho-mimetic mutant (CEP215-S613E) to examine the downstream consequences of this phosphorylation. CEP215-S613E expression led to CEP215 defocusing at mitotic centrosomes and caused chromosome missegregation that further resulted in micronuclei formation (Colicino et al., 2018). Our study suggested that CEP215 phosphorylation status is required for mitotic fidelity, providing interesting implications as to when and where this phosphorylation should occur. One potential

possibility is that CEP215 phosphorylation status is increased during metaphase exit, allowing the PCM to efficiently disassemble.

The centrosome proteins Gravin, CEP215, cenexin, pericentrin, primary microcephaly (MCHP2), and PLK1 have all been implicated in regulating the orientation of the mitotic spindle (Chen et al., 2014; Hanafusa et al., 2015; Hehnly et al., 2015; Hung, Hehnly, & Doxsey, 2016; Miyamoto et al., 2017), which can cause downstream consequences such as heart septation defects and microcephaly (Chen et al., 2014; Delaval & Doxsey, 2010; Vertii, Bright, Delaval, Hehnly, & Doxsey, 2015). However, it is unknown how all these molecules act in concert to correctly position the spindle along the division axis. We do know that if we un-couple PLK1 from its scaffold Gravin, increased phosphorylation of its downstream substrate CEP215 occurs, which is associated with a loss of astral microtubules and corresponding spindle positioning defects (Colicino et al., 2018; Hehnly et al., 2015). It is unknown, though, where the mother centriole appendage protein cenexin, or the PCM proteins pericentrin and MCPH2 fits into this possible pathway. In order to better understand the role of PLK1 at the mitotic centrosomes, the chemical genetics system described above could be used to replace endogenous-PLK1 at a single locus with either a kinetochore-targeted or centrosome-targeted PLK1$^{as}$ (PLK1-PACT used in Kishi et al., 2009). This will allow centrosome- or kinetochore-tethered PLK1 to be inhibited using a purine analogue or wild-type PLK1 using a common PLK1 inhibitor (BI 2536) in order to tease out the consequences of PLK1 at the mitotic centrosomes versus the kinetochores. In addition, just as with the kinetochore (Lera et al., 2016), PLK1$^{as}$ could be tethered to subcompartments of the centrosome, where it is known to have a specific function (e.g., PCM, centriole, or mother centriole appendages) (Colicino et al., 2018; Hehnly et al., 2015; Lee & Rhee, 2011; Soung et al., 2009). These studies could elucidate whether PLK1 operates in pools within the centrosome, as it seems to operate at the kinetochore (Lera et al., 2016).

### 5.3 | *PLK1 at the midbody*

PLK1 activity is required for cytokinesis and is regulated, in part, through binding phosphorylated scaffold proteins with distinct subcellular localization. During metaphase, CDK1 predominately creates the phosphorylated docking sites for PLK1, but what controls PLK1 docking post-anaphase and during cytokinesis when less CDK1 activity is present? Similar to kinetochore-localized PLK1 scaffolds, the microtubule-associated protein regulating cytokinesis (PRC1) is phosphorylated by PLK1, creating a PLK1 docking site on PRC1. Interestingly, PRC1 is phosphorylated by CDK1 adjacent to this PLK1 docking site during metaphase to prevent PLK1 binding at this time. PLK1 binding to PRC1 is necessary though for cytokinesis (Hu et al., 2012; Neef et al., 2007), where it phosphorylates MgcRacGAP/Cyk4 on several residues and elicits the binding of epithelial cell transforming sequence 2 (Ect2) (Burkard, Maciejowski, Rodriguez-Bravo, Repka, & Lowery, 2009; Burkard et al., 2007; Wolfe, Takaki, Petronczki, & Glotzer, 2009), a guanine nucleotide exchange factor for the small GTPase RhoA (Somers & Saint, 2003). MgcRacGAP phosphorylation by PLK1 is crucial to trigger the onset of cytokinesis.

Following the completion of the cytokinetic furrow, many of the central spindle components are packaged into a structure known as the cytokinetic midbody. The midbody lies within the intercellular bridge, which connects the two daughter cells. The abscission of the intercellular bridge occurs in the vicinity of the midbody, where numerous abscission proteins are enriched, including PLK1 (reviewed in Chen, Hehnly, & Doxsey, 2012). Thus, the midbody is a likely platform to coordinate abscission machinery where kinases act to ensure faithful abscission. One example of this is with the midbody localized protein CEP55. CEP55 is first phosphorylated by PLK1 where it prevents CEP55's association with the midzone (Bastos & Barr, 2010). Only after the loss of PLK1 activity does CEP55 translocate to and integrate into the midbody. Inhibition of PLK1 causes CEP55 to prematurely translocate to the midbody, causing abscission failure. The likely reason for this failure is that aberrant midbody architecture arises and the inability to target ESCRT-III components to the midbody, such as ALIX and TSG101 (Kamranvar et al., 2016; Morita et al., 2007). Thus, PLK1 seems to regulate cytokinesis progression and faithful abscission through its ability to recruit midbody components in an orderly manner by phosphorylation of substrates.

Three-dimensional structured illumination microscopy (SIM) and electron microscopy tomography were used to examine fluorescently tagged or immunostained components of ESCRT-III [e.g., CHMP4B (charged MVB protein 4B) and VPS4B (vacuolar protein sorting-associated protein 4B)]. This work showed that ESCRT-III concentrates initially at the midbody and then at a separate site in the intercellular bridge (Elia, Sougrat, Spurlin, Hurley, & Lippincott-Schwartz, 2011; Guizetti et al., 2011), where an array of helical filaments are assembled (Agromayor et al., 2009; Guizetti et al., 2011; Yang et al., 2008). The ESCRT-III-dependent helical filaments allow for deformation of the intercellular bridge membrane adjacent to the midbody, allowing the bridge to sever. Recent studies have implicated PLK1-dependent phosphorylation of a proline-rich domain of ALIX is required to transform ALIX from a closed conformation to an open conformation, allowing it to function in cytokinetic abscission (Sun et al., 2016). This suggests a major mechanism for PLK1 in activating ESCRT function of ALIX to induce abscission.

## 6 | PLK1-SCAFFOLD INTERACTIONS

While the function of PLK1 at various locales is intriguing and necessary to understanding its importance during division, it is equally as important to understand how PLK1 is subcellularly localized and regulated. The proteins required to ensure this tightly choreographed regulation and localization are known as binding scaffolds. The binding of PLK1 to its scaffold can assist in regulating PLK1's activity in three possible ways: (1) To augment or enhance its ability to phosphorylate downstream substrates; (2) To insulate or sequester it to a specific locale; (3) To terminate or impede its ability to phosphorylate downstream substrates (Langeberg & Scott, 2015). While there is much known about PLK1 and the mitotic scaffold Bora (Bruinsma et al., 2016; Macůrek et al., 2008; Seki et al., 2008; Thomas et al., 2016), here, we will focus on what is known about PLK1 scaffolds specifically at mitotic centrosomes and our recent study involving PLK1 and its

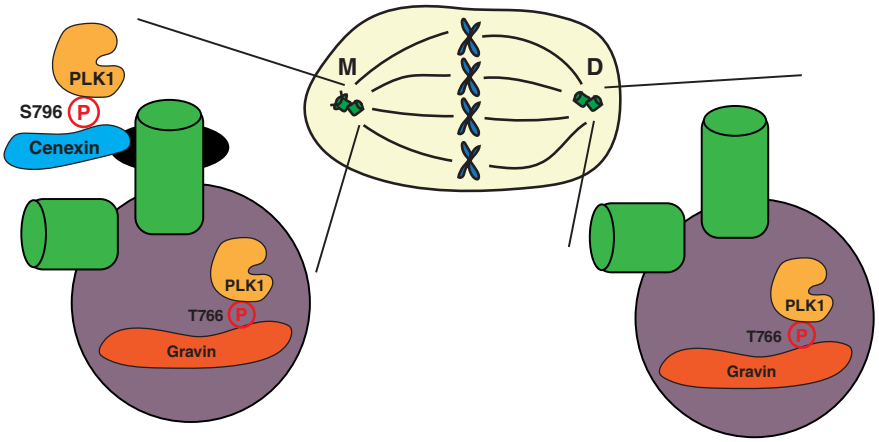



**FIGURE 5** PLK1 scaffolding at the mitotic centrosomes. A model depicting the localization of PLK1 (gold) to the mother centriole appendages (black) and pericentriolar matrix (PCM, purple) through its binding scaffolds, cenexin (blue) and Gravin (red). PLK1 has been shown to bind cenexin, a known mother centriole appendage protein, at its phosphorylated S796 site (Soung et al., 2009). PLK1 has also been shown to bind Gravin, a known PCM component, at its phosphorylated T766 site (Canton et al., 2012). These scaffolds subsequently sequester PLK1 at its subcentrosomal locales, regulating its activity during mitosis

PCM localized scaffold Gravin (Figure 5). Strikingly, the two mitotic centrosomes, which appear to be symmetric in nature, are actually asymmetric structures (Nigg & Stearns, 2011). While there are PLK1 scaffolds within the PCM (Canton et al., 2012; Colicino et al., 2018; Hehnly et al., 2015), a presumably symmetric structure between the two mitotic centrosomes, there is also an identified scaffold that localizes exclusively to one of the two mitotic centrosomes (Figure 5, (Soung et al., 2006). This creates an additional layer of regulation for the amount and activity of PLK1 that can occur between the two centrosomes and suggests interesting roles for PLK1 in regulating spindle orientation and cell differentiation.

The asymmetry between the two mitotic centrosomes derives from the centriole duplication cycle, where one centriole is always inherently older than the other. The oldest centriole, referred to as the mother, is structurally distinct from the youngest centriole, or daughter (Nigg & Stearns, 2011). The mother centriole contains unique proteins that make up the distal and subdistal appendages, one of which has been identified as a PLK1-scaffold protein, cenexin. PLK1 directly binds cenexin at its S796 site after CDK1 phosphorylation (depicted in Figure 5; Soung et al., 2009). This interaction has been implicated in regulating the recruitment of the PCM proteins γ-tubulin and pericentrin to mitotic centrosomes during division. When this interaction is disrupted through mutating the PLK1 binding site (S796A), these components fail to be recruited (Soung et al., 2009). This is interesting to put into context of another study that found a unique set of mother-centriole appendage proteins known to require cenexin for appendage localization that include centriolin and ninein that interact with pericentrin to regulate spindle orientation (Chen et al., 2014). Cenexin regulates both distal and subdistal appendage formation; however, it is unknown whether this process requires cenexin's interaction with PLK1. Additional studies have shown that cenexin is vital to orient the mitotic spindle parallel to the plane of 3D-epithelial expansion (Hung et al., 2016) and mediate the propensity for stem cells to mis-segregate chromosomes towards the mother mitotic centrosome (Gasic, Nerurkar, & Meraldi, 2015). However, it is not clearly understood whether the interaction between cenexin and PLK1 is required for these processes. Together, it is interesting to design a testable model where cenexin phosphorylation during mitotic entry recruits a complex involving pericentrin and CEP215 to the oldest mitotic centrosome to help direct spindle orientation through modulation of the nucleating capacity of the oldest mitotic centrosome.

Another PLK1 scaffold that localizes to mitotic centrosomes, specifically within the PCM, is Gravin (Figure 5). Gravin is a scaffold protein that interacts with numerous kinases, including protein kinase A (PKA), protein kinase C (PKC), Aurora A, and PLK1 at various cell cycle stages. Gravin is specifically phosphorylated at T766 by CDK1, allowing for the direct binding of PLK1 during cell division (depicted in Figure 5, Canton et al., 2012). Gravin sequesters Aurora A and PLK1, facilitating a kinase phosphorylation cascade where Aurora A phosphorylates PLK1 at its T210 site, which subsequently increases PLK1 activity (Hehnly et al., 2015). Our recent studies additionally demonstrated that when Gravin is lost in advanced stage prostate cancers, there is an increased incidence in PLK1-associated errors, including mitotic delay and chromosome instability (Colicino et al., 2018). While these studies provided an understanding that Gravin forms a complex with PLK1 at mitotic centrosomes during mitosis, it was unclear what significance this interaction had on PLK1 spatial and temporal dynamics and subsequent activity. To test this, we utilized a stable GFP-PLK1 cell line along with Fluorescent Recovery After Photobleaching (FRAP) to calculate that Gravin anchors approximately 12% of PLK1 at mitotic centrosomes at metaphase. We next utilized a Fluorescence Resonance Energy Transfer (FRET) biosensor for PLK1 activity (Macůrek et al., 2008) and anchored it to the mitotic centrosomes in order to measure PLK1 activity specifically at mitotic centrosomes (Figure 6). Using this biosensor, we could calculate that when Gravin is removed from cells, there is a significant increase in active-PLK1 at mitotic centrosomes. This suggested that when PLK1 is anchored by Gravin, it is unable to act on its downstream substrates. Thus, when Gravin is lost, increased PLK1-dependent phosphorylation of its downstream centrosome substrate CEP215 (Santamaria et al., 2011) is measured, resulting in the defocusing and disorganization of

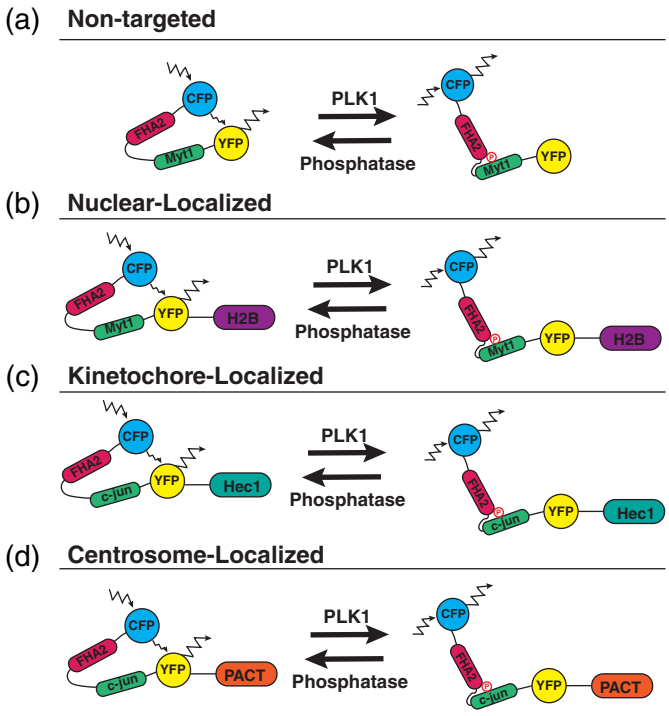



**FIGURE 6** PLK1 FRET biosensors. (a) A nontargeted PLK1 FRET biosensor containing a CFP monomer (blue), FHA2 phospho-binding domain (magenta), Myt1 PLK1-substrate sequence (green), and YFP monomer (yellow). When active-PLK1 is present, it phosphorylates the Myt1 sequence (T495), causing a conformational change in the biosensor, decreasing FRET. When no active-PLK1 is present, the biosensor is in a relaxed state, allowing for FRET (Macůrek et al., 2008). (b) A nuclear-localized PLK1 FRET-biosensor fused to H2B (purple) (Bruinsma, Raaijmakers, & Medema, 2012). **(c)** A kinetochore-localized PLK1 FRET-biosensor containing a c-jun PLK1-susbtrate sequence and fused to Hec1 (cyan). The c-jun substrate sequence was mutated (S17T), allowing for PLK1-specific phosphorylation of the biosensor (Liu et al., 2012). **(d)** A centrosome-localized PLK1 FRET-biosensor containing a c-jun PLK1-substrate sequence and fused to the pericentrin AKAP centrosomal-targeting (PACT) domain (orange) (Colicino et al., 2018)

CEP215 at mitotic centrosomes (Colicino et al., 2018). The downstream consequences of this disorganization includes the loss of centrosome function through decreased microtubule re-nucleation, loss of stable microtubules, and increased incidence of genomic instability measured by micronuclei formation (Colicino et al., 2018). While these studies provide insight as to how PLK1 is regulated at the mitotic centrosomes during division, it is still unclear how additional PLK1 scaffolds regulate PLK1 and how PLK1 is regulated between the two mitotic centrosomes.

## 6.1 | Innovative tools developed to study PLK1 spatial and temporal dynamics, activity, and function during division

The development of a PLK1-FRET biosensor allowed, for the first time, the activity of PLK1 to be examined in an in vivo setting throughout the cell cycle (Bruinsma et al., 2016; Macůrek et al., 2008). By manipulating a previously developed Aurora B kinase activity biosensor (Fuller et al., 2008), a biosensor was developed that possessed a donor (CFP) and acceptor (YFP), a phospho-binding domain (FHA2, Forkhead-Associated Domain 2), and a PLK1 specific phosphorylation sequence (Myt1). When little or no PLK1 activity is present, the biosensor is in a relaxed state, where the excitation and emission of CFP causes energy transfer which causes the excitation and emission of YFP, or FRET (refer to Figure 6a). When PLK1 is present and active, it is able to phosphorylate the Myt1 substrate sequence. This causes the FHA2 domain to bind, leading to a conformational change in the biosensor, so the excitation and emission of CFP no longer causes the excitation/emission of YFP, or a loss of FRET. By taking a ratio of FRET vs no FRET, the user of this biosensor can arbitrarily measure the temporal activity of PLK1 within the cell. It was improved even further by changing PLK1 substrate sequence to the more specific c-jun, and further increasing PLK1 specificity by mutating the PLK1-phosphorylation site from serine to threonine (Figure 6, Liu et al., 2012). While this biosensor was revolutionary in measuring and visualizing PLK1 activity in vivo throughout cell division, it was cytosolically expressed and only provided PLK1 temporal activity. From there, scientists wanted to be able to additionally examine the spatial activity of PLK1 during division.

This biosensor was then targeted to specific locales to examine PLK1 activity at unique sites during the cell cycle such as the nucleus (Figure 6a,b, Bruinsma et al., 2015; Macůrek et al., 2008), kinetochores (Figure 6c, Liu et al., 2012), and then the centrosome (Figure 6d, Colicino et al., 2018). PLK1 activation was first identified to occur several hours before mitotic entry, where it requires Aurora A-dependent phosphorylation of Thr210 in the T-loop of the PLK1 kinase domain (Macůrek et al., 2008). This was identified using a novel PLK1 FRET-biosensor which localized within the nucleus and cytosol (Figure 6a, Macůrek et al., 2008). This study also determined that Aurora A-dependent activation of PLK1 at Thr210 was enhanced when the scaffold Bora was present. A follow-up study used a modified FRET-biosensor fused to histone-2b (H2B), identifying that PLK1 activity is increased within the nucleus during G2 in a Bora-dependent manner (Figure 6b, Bruinsma et al., 2015). Interestingly, a recent study identified a mechanism for nuclear localization of PLK1 where PBD binding to the kinase domain masks a nuclear localization signal in PLK1. Phosphorylation of the kinase domain within the T-loop leads to exposure of an NLS causing the entry of PLK1 into the nucleus during G2 (Kachaner et al., 2017).

The PLK1 FRET-biosensor has also been anchored to kinetochores by fusing to the kinetochore protein Hec1 (Figure 6c, Liu et al., 2012). These studies designed a FRET-based phosphorylation sensor to track phosphorylation changes at the kinetochores during division in live cells. This sensor demonstrated that when PLK1 levels were high on kinetochores, such as when cells are treated with the microtubule-depolymerizing drug nocodazole, that phosphorylation of the kinetochore-targeted biosensor was high. When PLK1 concentration on kinetochores was low, such as during metaphase when chromosomes are aligned along the metaphase plate, phosphorylation of the biosensor was low compared to nocodazole-treated cells. Based on this consistency, where the PLK1 activity biosensor correlated with relative concentrations of PLK1 levels at kinetochores, the biosensor was used to track phosphorylation dynamics as chromosomes align

during metaphase. These studies demonstrated that as the kinetochores aligned at metaphase, the kinetochore-anchored PLK1 biosensor was dephosphorylated in a phosphatase 1 (PP1)-dependent manner. In addition, they found that phosphatase levels are inversely correlated with PLK1 recruitment (Liu et al., 2012). This is consistent with a phosphorylation-dependent mechanism to regulate PLK1 localization, likely through PBD binding to phosphorylated kinetochore scaffolds (Elia, Rellos, et al., 2003). Thus, PLK1-biosensors not only can be utilized to understand PLK1-activity, but also the significance of PLK1-substrate dephosphorylation (Liu et al., 2012).

To examine PLK1-activity specifically at centrosomes, the FRET-biosensor was fused to the pericentrin AKAP450 centrosomal-targeting domain (PACT), allowing for specific localization to centrosomes (Figure 6d, Colicino et al., 2018). Our study utilized PLK1-FRET-PACT to understand how a PLK1 scaffold, in this case Gravin, could spatially coordinate PLK1 activity at centrosomes during metaphase (Colicino et al., 2018). These studies identified that when one specific centrosome-localized scaffold was depleted, there was an increase in PLK1 substrate phosphorylation at the centrosome that correlates with an increase in centrosome disorganization and loss of nucleation potential during prometaphase (Colicino et al., 2018). Together, these studies shed light on the tight regulation of PLK1 at mitotic centrosomes and how this works to ensure proper mitotic centrosome formation and function. With further development of these technologies, it is hopeful that the interactions between PLK1 at its subcellular locales can be thoroughly examined, determining how and when PLK1 responds to cellular cues in an effort to ensure mitotic fidelity.

## 6.2 | PLK1 as a targeted cancer therapeutic

Another major field in PLK1 research is developing PLK1 small-molecule inhibitors as drug therapies in diseases such as cancer (reviewed in Elizabeth, Gutteridge, Ndiaye, Liu, & Ahmad, 2016; Murugan et al., 2011). Numerous studies have tested PLK1 inhibitors, including BI2536, as potential cancer therapeutics for advanced metastatic tumors, including prostate cancer (Hou et al., 2013; Zhang et al., 2014), lung cancer (Awad et al., 2017; Breitenbuecher et al., 2017), neuroblastoma (Pajtler et al., 2017), and non-Hodgkin's lymphoma (Vose et al., 2013) to name a few. These studies suggest elevated levels of PLK1 expression in highly metastatic and advanced cancers, leads to chromosome instability and aneuploidy (Yamamoto et al., 2006), providing these cells an advantage to overgrow and invade tissues. By inhibiting PLK1 activity in these cells, it is hypothesized that the cells will suffer cell cycle arrest, leading to cell death and hindered tumor growth, allowing for increased survival (Raab et al., 2015). Initial studies using 2D tissue culture and mouse models of various cancers yielded promising results. The inhibitor BI2536 impeded tumor growth in a mouse xenograph models (Steegmaier, Hoffmann, Baum, Lenart, et al., 2007). The overall survival of the animals significantly increased compared to controls, suggesting PLK1 inhibitors would be promising cancer therapeutics in clinical trials.

Despite these results, clinical trials for PLK1 therapeutics have not yet been successful as monotherapy treatments, but appear to work best in clinical trials within a chemotherapeutic cocktail (Yim, 2013). One reason for this is that PLK1 inhibition causes sensitivity to other pathway inhibitors, such as androgen signaling inhibitors, preventing prostate cancer tumor growth (Zhang et al., 2014). An alternative method for targeting PLK1 activity in these cells is to better understand how PLK1 is regulated in cells, specifically through binding scaffolds as described above. The PLK1 scaffold Gravin is commonly misregulated in advanced prostate cancer and its depletion has been shown to increase PLK1 activity (Canton et al., 2012; Colicino et al., 2018). If these kinase-scaffold interactions can be disrupted instead of the kinase itself, there is the potential to increase the efficacy of PLK1 drug therapeutics.

## 6.3 | Current gaps of knowledge in research

Despite the new and innovated tools and technologies available, there is still a lot to learn about PLK1 regulation and function at its various subcellular locales during division. For instance, while a few newer studies have emerged looking at PLK1 during cytokinesis and abscission, it is still unclear whether PLK1 is active and functional during abscission and whether there is a direct role for PLK1 to ensure proper cleavage of the cytokinetic bridge. It has been suggested that PLK1 works as a negative-feedback and checkpoint regulator at this final stage of division, ensuring that ESCRT-complex components are properly recruited, and the cell is prepared to undergo abscission. Despite these studies, a lot more work needs to be done in order to measure PLK1 dynamics and activity at these sites, to determine specific PLK1 binding scaffolds and downstream phosphorylation targets, and to test whether PLK1 has a direct role in ensuring abscission. The development of a midbody-localized PLK1 FRET biosensor would provide an opportunity to further study the spatial and temporal activity of PLK1 at the cytokinetic midbody. From here, PLK1's interactions with CEP55 and its role in cytokinesis and abscission can be more clearly understood. While some of the tools are available and predictions have been made on a number of candidates for binding scaffolds and phosphorylation targets, many of these candidates have not been confirmed. By utilizing a combination of innovative tools, including chemical genetics and FRET-biosensors, with the addition of super resolution microscopy, it is possible to determine PLK1's direct, and indirect, roles in ensuring successful division at mitotic centrosomes, kinetochores, and the cytokinetic midbody.

## ACKNOWLEDGMENTS

The Hehnly lab is currently supported by the Department of Defense, Grant W81XWH-17-1-0241 (to H.H), and the NIH Grants, R01GM127621 (to H.H.) and R00GM107355 (to H.H). This work was supported by the U.S. Army Medical Research Acquisition Activity through the FY 16 Prostate Cancer Research Programs under Award No. W81XWH-17-1-0241. Opinions, interpretations, conclusions and recommendations are those of the author and are not necessarily endorsed by the Department of Defense. We also thank the Carol Baldwin Research Foundation of Central New York for their support of this project. We thank Patrina Pellet (previously at G.E.) for assistance obtaining SIM images.

## ORCID

*Erica G. Colicino* https://orcid.org/0000-0002-3333-1370

## REFERENCES


Agromayor, M., Carlton, J. G., Phelan, J. P., Matthews, D. R., Carlin, L. M., Ameer-Beg, S., … Martin-Serrano, J. (2009). Essential role of hIST1 in cytokinesis. *Molecular Biology of the Cell*, *20*, 1374–1387. http://doi.org/10.1091/mbc.E08

Andrysik, Z., Bernstein, W. Z., Deng, L., Myer, D. L., Li, Y.-Q., Tischfield, J. A., … Mustapha Bahassi, E. (2010). The novel mouse polo-like kinase 5 responds to DNA damage and localizes in the nucleolus. *Nucleic Acids Research*, *38*, 2931–2943.

Awad, M. M., Chu, Q. S. C., Gandhi, L., Stephenson, J. J., Govindan, R., Bradford, D. S., … Socinski, M. A. (2017). An open-label, phase II study of the polo-like kinase-1 (Plk-1) inhibitor, BI 2536, in patients with relapsed small cell lung cancer (SCLC). *Lung Cancer*, *104*, 126–130. http://doi.org/10.1016/j.lungcan.2016.12.019

Bastos, R. N., & Barr, F. A. (2010). Plk1 negatively regulates Cep55 recruitment to the midbody to ensure orderly abscission. *Journal of Cell Biology*, *191*(4), 751–760. http://doi.org/10.1083/jcb.201008108

Beck, J., Maerki, S., Posch, M., Metzger, T., Persaud, A., Scheel, H., … Sumara, I. (2013). Ubiquitylation-dependent localization of PLK1 in mitosis. *Nature Cell Biology*, *15*(4), 430–439. http://doi.org/10.1038/ncb2695

Bishop, A. C., Ubersax, J. A., Petsch, D. T., Matheos, D. P., Grayk, N. S., Blethrow, J., … Shokat, K. M. (2000). A chemical switch for inhibitor-sensitive alleles of any protein kinase. *Cell*, *407*(September), 395–401. http://doi.org/10.1038/35030148

Breitenbuecher, F., Von Pawel, J., Sebastian, M., Kortsik, C., Ting, S., Kasper, S., … Schuler, M. (2017). Comprehensive biomarker analyses in patients with advanced or metastatic non-small cell lung cancer prospectively treated with the polo-like kinase 1 inhibitor BI2536. *Oncology Research and Treatment*, *40*, 435–439. http://doi.org/10.1159/000475503

Bruinsma, W., Aprelia, M., García-Santisteban, I., Kool, J., Xu, Y., & Medema, R. (2016). Inhibition of Polo-like kinase 1 during the DNA damage response is mediated through loss of Aurora A recruitment by Bora. *Oncogene*, *36*, 1840–1848.

Bruinsma, W., Aprelia, M., Kool, J., Macurek, L., Lindqvist, A., & Medema, R. H. (2015). Spatial separation of Plk1 phosphorylation and activity. *Frontiers in Oncology*, *5*(June), 1–8. http://doi.org/10.3389/fonc.2015.00132

Bruinsma, W., Macurek, L., Freire, R., Lindqvist, A., Medema, R. H., Archambault, V., … Matsumura, F. (2014). Bora and Aurora-a continue to activate Plk1 in mitosis. *Journal of Cell Science*, *127*(Pt 4), 801–811. http://doi.org/10.1242/jcs.137216

Bruinsma, W., Raaijmakers, J. A., & Medema, R. H. (2012). Switching polo-like kinase-1 on and off in time and space. *Trends in Biochemical Sciences*, *37*(12), 534–542. http://doi.org/10.1016/j.tibs.2012.09.005

Bryan Tsou, M.-F., Wang, W.-J., George, K. A., Uryu, K., Stearns, T., & Jallepalli, P. V. (2009). Polo kinase and Separase regulate the mitotic licensing of centriole duplication in human cells. *Developmental Cell*, *17*, 344–354. http://doi.org/10.1016/j.devcel.2009.07.015

Burkard, M. E., Maciejowski, J., Rodriguez-Bravo, V., Repka, M., & Lowery, D. M. (2009). Plk1 self-organization and priming phosphorylation of HsCYK-4 at the spindle Midzone regulate the onset of division in human cells. *PLoS Biology*, *7*(5), 1000111. http://doi.org/10.1371/journal.pbio.1000111

Burkard, M. E., Randall, C. L., Larochelle, S., Zhang, C., Shokat, K. M., Fisher, R. P., & Jallepalli, P. V. (2007). Chemical genetics reveals the requirement for polo-like kinase 1 activity in positioning RhoA and triggering cytokinesis in human cells. *Proceedings of the National Academy of Sciences of the United States of America*, *104*(11), 4383–4388. http://doi.org/10.1073/pnas.0701140104

Canton, D. A., Keene, C. D., Swinney, K., Langeberg, L. K., Nguyen, V., Pelletier, L., … Scott, J. D. (2012). Gravin is a transitory effector of polo-like kinase 1 during cell division. *Molecular Cell*, *48*, 547–559. http://doi.org/10.1016/j.molcel.2012.09.002

Chang, J., Cizmecioglu, O., Hoffmann, I., & Rhee, K. (2010). PLK2 phosphorylation is critical for CPAP function in procentriole formation during the centrosome cycle. *The EMBO Journal*, *29*, 2395–2406. http://doi.org/10.1038/emboj.2010.118

Chen, C.-T., Hehnly, H., & Doxsey, S. J. (2012). Orchestrating vesicle transport, ESCRTs and kinase surveillance during abscission. *Nature Reviews Molecular Cell Biology*, *13*, 483–488. http://doi.org/10.1038/nrm3395

Chen, C.-T., Hehnly, H., Yu, Q., Farkas, D., Zheng, G., Redick, S. D., … Doxsey, S. (2014). A unique set of centrosome proteins requires pericentrin for spindle-pole localization and spindle orientation. *Current Biology: CB*, *24*(19), 2327–2334. http://doi.org/10.1016/j.cub.2014.08.029

Choi, Y.-K., Liu, P., Sze, S. K., Dai, C., & Qi, R. Z. (2010). CDK5RAP2 stimulates microtubule nucleation by the γ-tubulin ring complex. *The Journal of Cell Biology*, *191*(6), 1089–1095. http://doi.org/10.1083/jcb.201007030

Colicino, E. G., Garrastegui, A. M., Freshour, J., Santra, P., Post, D. E., Kotula, L., & Hehnly, H. (2018). Gravin regulates centrosome function through PLK1. *Molecular Biology of the Cell*, *29*(5), 532–541.

De Cárcer, G., Escobar, B., Higuero, A. M., García, L., Ansón, A., Pérez, G., … Malumbres, M. (2011). Plk5, a polo box domain-only protein with specific roles in neuron differentiation and Glioblastoma suppression. *Molecular and Cellular Biology*, *31*(6), 1225–1239. http://doi.org/10.1128/MCB.00607-10

De Cárcer, G., Manning, G., & Malumbres, M. (2011). From Plk1 to Plk5: Functional evolution of polo-like kinases. *Cell Cycle*, *10*(14), 2255–2262. http://doi.org/10.4161/cc.10.14.16494

Delaval, B., & Doxsey, S. J. (2010). Pericentrin in cellular function and disease. *Journal of Cell Biology*, *188*(2), 181–190. http://doi.org/10.1083/jcb.200908114

Descombes, P., & Nigg, E. A. (1998). The polo-like kinase Plx1 is required for M phase exit and destruction of mitotic regulators in Xenopus egg extracts. *The EMBO Journal*, *17*(5), 1328–1335.

Doxsey, S. J., Steln, P., Evans, L., Calarco, P. D., & Kirschnefi, M. (1994). Pericentrin, a highly conserved centrosome protein involved in microtubule organization. *Cell*, *76*, 639–650.

Eckerdt, F., & Strebhardt, K. (2006). Polo-like kinase 1: Target and regulator of anaphase-promoting complex/Cyclosome-dependent proteolysis anaphase-promoting complex/Cyclosome activity: Ordered proteolysis of mitotic proteins, including polo-like kinase 1. *Cancer Research*, *66*(14), 6895–6903.

Elia, A. E. H., Cantley, L. C., & Yaffe, M. B. (2003). Proteomic screen finds pSer/pThr-binding domain localizing Plk1 to mitotic substrates. *Science (New York, N.Y.)*, *299*(5610), 1228–1231. http://doi.org/10.1126/science.1079079

Elia, A. E. H., Rellos, P., Haire, L. F., Chao, J. W., Ivins, F. J., Hoepker, K., … Yaffe, M. B. (2003). The molecular basis for Phosphodependent substrate targeting and regulation of Plks by the polo-box domain. *Cell*, *115*, 83–95.

Elia, N., Sougrat, R., Spurlin, T. A., Hurley, J. H., & Lippincott-Schwartz, J. (2011). Dynamics of endosomal sorting complex required for transport (ESCRT) machinery during cytokinesis and its role in abscission. *Proceedings of the National Academy of Sciences of the United States of America*, *108*(12), 4846–4851. http://doi.org/10.1073/pnas.1102714108

Elizabeth, R., Gutteridge, A., Ndiaye, M. A., Liu, X., & Ahmad, N. (2016). Plk1 inhibitors in cancer therapy: From laboratory to clinics. *Molecular Cancer Therapeutics*, *15*(7), 1427–1435.

Elowe, S., Hümmer, S., Uldschmid, A., Li, X., & Nigg, E. A. (2007). Tension-sensitive Plk1 phosphorylation on BubR1 regulates the stability of kinetochore–microtubule interactions. *Genes & Development*, *21*, 2205–2219. http://doi.org/10.1101/gad.436007

Enserink, J. M., & Kolodner, R. D. (2010). Open access review BioMed central an overview of Cdk1-controlled targets and processes. *Cell Division*, *5*, 11.

Fabbro, M., Zhou, B.-B., Takahashi, M., Sarcevic, B., Lal, P., Graham, M. E., … Khanna, K. K. (2005). Cdk1/Erk2-and Plk1-dependent phosphorylation of a centrosome protein, Cep55, is required for its recruitment to Midbody and cytokinesis. *Developmental Cell*, *9*, 477–488. http://doi.org/10.1016/j.devcel.2005.09.003

Fenton, B., & Glover, D. M. (1993). A conserved mitotic kinase active at late anaphase—Telophase in syncytial drosophila embryos. *Nature*, *363*(6430), 637–640. http://doi.org/10.1038/363637a0

Fuller, B. G., Lampson, M. A., Foley, E. A., Rosasco-Nitcher, S., Le, K. V., Tobelmann, P., … Kapoor, T. M. (2008). Midzone activation of aurora B in anaphase produces an intracellular phosphorylation gradient. *Nature*, *453*(7198), 1132–1136. http://doi.org/10.1038/nature06923

Gasic, I., Nerurkar, P., & Meraldi, P. (2015). Centrosome age regulates kinetochore–microtubule stability and biases chromosome mis-segregation. *eLife*, *4*, e07909. http://doi.org/10.7554/eLife.07909

Golsteyn, R. M., Mundt, K. E., Fry, A. M., & Nigg, E. A. (1995). Cell cycle regulation of the activity and subcellular localization of plk1, a human protein kinase implicated in mitotic spindle function. *Journal of Cell Biology*, *129*, 1617. http://doi.org/10.1083/jcb.129.6.1617

Goto, H., Kiyono, T., Tomono, Y., Kawajiri, A., Urano, T., Furukawa, K., … Inagaki, M. (2006). Complex formation of Plk1 and INCENP required for metaphase-anaphase transition. *Nature Cell Biology*, *8*(2), 180–187. http://doi.org/10.1038/ncb1350

Guizetti, J., Schermelleh, L., Mäntler, J., Maar, S., Poser, I., Leonhardt, H., … Gerlich, D. W. (2011). Cortical constriction during abscission involves helices of ESCRT-III-dependent filaments. *Science*, *331*, 1616–1620.

Habedanck, R., Stierhof, Y.-D., Wilkinson, C. J., & Nigg, E. A. (2005). The polo kinase Plk4 functions in centriole duplication. *Nature Cell Biology*, *7*(11), 1140–1146. http://doi.org/10.1038/ncb1320

Hanafusa, H., Kedashiro, S., Tezuka, M., Funatsu, M., Usami, S., Toyoshima, F., & Matsumoto, K. (2015). PLK1-dependent activation of LRRK1 regulates spindle orientation by phosphorylating CDK5RAP2. *Nature Cell Biology*, *17*(8), 1024–1035. http://doi.org/10.1038/ncb3204

Hartwell, L. H., Mortimer, R. K., L O, J. C., CuLo, M., & Esposito, R. E. (1973). Genetic control of the cell division cycle in yeast: v. genetic analysis of cdc mutants. *Genetics*, *74*(2), 267–286.

Hatano, T., Sluder, G., Brummelkamp, T. R., Bernards, R., Agami, R., Crasta, K., … Coutavas, E. (2012). The interrelationship between APC/-C and Plk1 activities in centriole disengagement. *Biology Open*, *1*(11), 1153–1160. http://doi.org/10.1242/bio.20122626

Hehnly, H., Canton, D., Bucko, P., Langeberg, L. K., Ogier, L., Gelman, I., … Scott, J. D. (2015). A mitotic kinase scaffold depleted in testicular seminomas impacts spindle orientation in germ line stem cells. *eLife*, *4*, e09384. http://doi.org/10.7554/eLife.09384

Hood, E. A., Kettenbach, A. N., Gerber, S. A., & Compton, D. A. (2012). Plk1 regulates the kinesin-13 protein Kif2b to promote faithful chromosome segregation. *Molecular and Cellular Biology*, *23*(12), 2264–2274. http://doi.org/10.1091/mbc.E11-12-1013

Hou, X., Li, Z., Huang, W., Li, J., Staiger, C., Kuang, S., … Liu, X. (2013). Plk1-dependent microtubule dynamics promotes androgen receptor signaling in prostate cancer. *The Prostate*, *73*(12), 1352–1363. http://doi.org/10.1002/pros.22683

Hu, C.-K., Özlü, N., Coughlin, M., Steen, J. J., & Mitchison, T. J. (2012). Plk1 negatively regulates PRC1 to prevent premature midzone formation before cytokinesis. *Molecular and Cellular Biology*, *23*(14), 2702–2711. http://doi.org/10.1091/mbc.E12-01-0058

Hung, H. F., Hehnly, H., & Doxsey, S. (2016). The mother centriole appendage protein cenexin modulates lumen formation through spindle orientation. *Current Biology*, *26*(6), 793–801. http://doi.org/10.1016/j.cub.2016.01.025

Hyun, S.-Y., Hwang, H.-I., Hwan, H.-I., & Jang, Y.-J. (2014). Polo-like kinase-1 in DNA damage response. *BMB Reports*, *47*(5), 249–255. http://doi.org/10.5483/bmbrep.2014.47.5.061

Kachaner, D., Garrido, D., Mehsen, H., Normandin, K., Lavoie, H., & Archambault, V. (2017). Coupling of polo kinase activation to nuclear localization by a bifunctional NLS is required during mitotic entry. *Nature Communications*, *8*, 1701. http://doi.org/10.1038/s41467-017-01876-8

Kamranvar, S. A., Gupta, D. K., Huang, Y., Gupta, R. K., Johansson, S., Kamranvar, S. A., … Johansson, S. (2016). Integrin signaling via FAK-Src controls cytokinetic abscission by decelerating PLK1 degradation and subsequent recruitment of CEP55 at the midbody. *Oncotarget*, *7*(21), 30820–30830.

Kang, Y. H., Park, J.-E., Yu, L.-R., Soung, N.-K., Yun, S.-M., Bang, J. K., … Lee, K. S. (2006). Self-regulated Plk1 recruitment to kinetochores by the Plk1-PBIP1 interactions is critical for proper chromosome segregation. *Molecular Cell*, *24*, 409–422. http://doi.org/10.1016/j.molcel.2006.10.016

Kishi, K., van Vugt, M. A. T. M., Okamoto, K., Hayashi, Y., & Yaffe, M. B. (2009). Functional dynamics of polo-like kinase 1 at the centrosome. *Molecular and Cellular Biology*, *29*(11), 3134–3150. http://doi.org/10.1128/MCB.01663-08

Kleylein-Sohn, J., Westendorf, J., Le Clech, M., Habedanck, R., Stierhof, Y.-D., & Nigg, E. A. (2007). Article Plk4-induced centriole biogenesis in human cells. *Developmental Cell*, *13*, 190–202. http://doi.org/10.1016/j.devcel.2007.07.002

Kolobova, E., Roland, J. T., Lapierre, L. A., Williams, J. A., Mason, T. A., & Goldenring, J. R. (2017). The C-terminal region of A-kinase anchor protein 350 (AKAP350A) enables formation of microtubule-nucleation centers and interacts with pericentriolar proteins. *The Journal of Biological Chemistry*, *292*, 20394–20409. http://doi.org/10.1074/jbc.M117.806018

Kong, D., Farmer, V., Shukla, A., James, J., Gruskin, R., Kiriyama, S., & Loncarek, J. (2014). Centriole maturation requires regulated Plk1 activity during two consecutive cell cycles. *Journal of Cell Biology*, *206*(7), 855–865. http://doi.org/10.1083/jcb.201407087

Kothe, M., Kohls, D., Low, S., Coli, R., Cheng, A. C., Jacques, S. L., … Ding, Y.-H. (2007). Structure of the catalytic domain of human polo-like kinase 1. *Biochemistry*, *46*(20), 5960–5971.

Langeberg, L. K., & Scott, J. D. (2015). Signalling scaffolds and local organization of cellular behaviour. *Nature Reviews. Molecular Cell Biology*, *16*(4), 232–244. http://doi.org/10.1038/nrm3966

Lee, H.-J., Hwang, H.-I., & Jang, Y.-J. (2010). Mitotic DNA damage response: Polo-like Kinase-1 is dephosphorylated through ATM-Chk1 pathway. *Cell Cycle*, *9*, 2389–2398. http://doi.org/10.4161/cc.9.12.11904org/10.4161/cc.9.12.11904

Lee, K. H., Johmura, Y., Yu, L.-R., Park, J.-E., Gao, Y., Bang, J. K., … Lee, K. S. (2012). Identification of a novel Wnt5a–CK1ε–Dvl2–Plk1-mediated primary cilia disassembly pathway. *The EMBO Journal*, *31144*, 3104–3117. http://doi.org/10.1038/emboj.2012.144

Lee, K., & Rhee, K. (2011). PLK1 phosphorylation of pericentrin initiates centrosome maturation at the onset of mitosis. *Journal of Cell Biology*, *195*(7), 1093–1101. http://doi.org/10.1083/jcb.201106093

Lee, K. S., & Erikson, R. L. (1997). Plk is a functional homolog of *Saccharomyces cerevisiae* Cdc5, and elevated Plk activity induces multiple septation. *Structure*, *17*(6), 3408–3417.

Lee, K. S., Oh, D.-Y., Kang, Y. H., & Park, J.-E. (2008). Self-regulated mechanism of Plk1 localization to kinetochores: Lessons from the Plk1-PBIP1 interactions. *Cell Division*, *3*, 4. http://doi.org/10.1186/1747-1028-3-4

Lee, K. S., Yuan, Y.-L. O., Kuriyama, R., & Erikson, R. L. (1995). Plk is an M-phase-specific protein kinase and interacts with a Kinesin-like protein, CHO1/MKLP-1. *Molecular and Cellular Biology*, *15*(12), 7143–7151.

Lee, M., Kim, I. S., Park, K. C., Kim, J., Baek, S. H., & Kim, K. I. (2018). Mitosis-specific phosphorylation of Mis18α by Aurora B kinase enhances kinetochore recruitment of polo-like kinase. *Oncotarget*, *9*(2), 1563–1576. http://doi.org/10.18632/oncotarget.22707

Lenart, P., Petronczki, M., Steegmaier, M., Di Fiore, B., Lipp, J. J., Hoffmann, M., … Peters, J. M. (2007). The small-molecule inhibitor BI 2536 reveals novel insights into mitotic roles of polo-like kinase 1. *Current Biology*, *17*(4), 304–315. http://doi.org/10.1016/j.cub.2006.12.046

Lera, R. F., & Burkard, M. E. (2012). High mitotic activity of polo-like kinase 1 is required for chromosome segregation and genomic integrity in human epithelial cells. *Journal of Biological Chemistry*, *287*(51), 42812–42825. http://doi.org/10.1074/jbc.M112.412544

Lera, R. F., Potts, G. K., Suzuki, A., Johnson, J. M., Salmon, E. D., Coon, J. J., & Burkard, M. E. (2016). Decoding polo-like kinase 1 signaling along the kinetochore–centromere axis. *Nature Chemical Biology*, *12*(April), 1–10. http://doi.org/10.1038/nchembio.2060

Leung, G. C., Hudson, J. W., Kozarova, A., Davidson, A., Dennis, J. W., & Sicheri, F. (2002). The Sak polo-box comprises a structural domain sufficient for mitotic subcellular localization. *Nature Structural Biology*, *9*(10), 719–724. http://doi.org/10.1038/nsb848

Liu, D., Davydenko, O., & Lampson, M. A. (2012). Polo-like kinase-1 regulates kinetochore-microtubule dynamics and spindle checkpoint

silencing. *The Journal of Cell Biology*, *198*(4), 491–499. http://doi.org/10.1083/jcb.201205090

Liu, J., & Zhang, C. (2017). The equilibrium of ubiquitination and deubiquitination at PLK1 regulates sister chromatid separation. *Cellular and Molecular Life Sciences*, *74*(12), 2127–2134. http://doi.org/10.1007/s00018-017-2457-5

Llamazares, S., Moreira, A., Tavares, A., Girdham, C., Spruce, B. A., Gonzalez, C., … Sunkel, C. E. (1991). Polo encodes a protein kinase homolog required for mitosis in drosophila. *Genes & Development*, *5*, 2153–2165.

Lon Carek, J., Hergert, P., & Khodjakov, A. (2010). Centriole reduplication during prolonged interphase requires Procentriole maturation governed by Plk1. *Current Biology*, *20*, 1277–1282. http://doi.org/10.1016/j.cub.2010.05.050

Lowery, D. M., Clauser, K. R., Hjerrild, M., Lim, D., Alexander, J., Kishi, K., … Yaffe, M. B. (2007). Proteomic screen defines the polo-box domain interactome and identifies Rock2 as a Plk1 substrate. *The EMBO Journal*, *26*(9), 2262–2273. http://doi.org/10.1038/sj.emboj.7601683

Macůrek, L., Lindqvist, A., Lim, D., Lampson, M. a., Klompmaker, R., Freire, R., … Medema, R. H. (2008). Polo-like kinase-1 is activated by aurora a to promote checkpoint recovery. *Nature*, *455*(7209), 119–123. http://doi.org/10.1038/nature07185

Maia, A. R. R., Garcia, Z., Kabeche, L., Barisic, M., Maffini, S., Macedo-Ribeiro, S., … Maiato, H. (2012). Cdk1 and Plk1 mediate a CLASP2 phospho-switch that stabilizes kinetochore-microtubule attachments. *Journal of Cell Biology*, *199*(2), 285–301. http://doi.org/10.1083/jcb.201203091

Martin, B. T., & Strebhardt, K. (2006). Polo-like kinase 1 target and regulator of transcriptional control. *Cell Cycle*, *5*(24), 2881–2885.

Miyamoto, T., Akutsu, S. N., Fukumitsu, A., Morino, H., Masatsuna, Y., Hosoba, K., … Matsuura, S. (2017). PLK1-mediated phosphorylation of WDR62/MCPH2 ensures proper mitotic spindle orientation. *Human Molecular Genetics*, *26*(22), 4429–4440. http://doi.org/10.1093/hmg/ddx330

Morita, E., Sandrin, V., Chung, H.-Y., Morham, S. G., Gygi, S. P., Rodesch, C. K., & Sundquist, W. I. (2007). Human ESCRT and ALIX proteins interact with proteins of the midbody and function in cytokinesis. *The EMBO Journal*, *26*, 4215–4227. http://doi.org/10.1038/

Murugan, R. N., Park, J.-E., Kim, E.-H., Shin, S. Y., Cheong, C., Lee, K. S., & Bang, J. K. (2011). Plk1-targeted small molecule inhibitors: Molecular basis for their potency and specificity. *Molecules and Cells*, *32*(3), 209–220. http://doi.org/10.1007/s10059-011-0126-3

Nasmyth, K., & Nurse, P. (1981). Cell division cycle mutants altered in DNA replication and mitosis in the fission yeast Schizosaccharomyces pombe. *Molecular & General Genetics*, *182*, 119–124.

Neef, R., Gruneberg, U., Kopajtich, R., Li, X., Nigg, E. A., Sillje, H., & Barr, F. A. (2007). Choice of Plk1 docking partners during mitosis and cytokinesis is controlled by the activation state of Cdk1. *Nature Cell Biology*, *9*(4), 436–444. http://doi.org/10.1038/ncb1557

Nigg, E. A., & Stearns, T. (2011). The centrosome cycle: Centriole biogenesis duplication and inherent asymmetries. *Nature Cell Biology*, *13*(10), 1154–1160. http://doi.org/10.1038/ncb2345

Nishino, M., Kurasawa, Y., Evans, R., Lin, S.-H., Brinkley, B. R., & Yu-Lee, L.-Y. (2006). Report NudC is required for Plk1 targeting to the kinetochore and chromosome Congression. *Current Biology*, *16*, 1414–1421. http://doi.org/10.1016/j.cub.2006.05.052

Ohta, M., Ashikawa, T., Nozaki, Y., Kozuka-Hata, H., Goto, H., Inagaki, M., … Kitagawa, D. (2014). Direct interaction of Plk4 with STIL ensures formation of a single procentriole per parental centriole. *Nature Communications*, *5*, 6267. http://doi.org/10.1038/ncomms6267

Ouyanga, B., Wangb, Y., & Daia, W. (1999). *Caenorhabditis elegans* contains structural homologs of human prk and plk. *DNA Sequence*, *10*, 109–113.

Pajtler, K. W., Sadowski, N., Ackermann, S., Althoff, K., Schönbeck, K., Batzke, K., … Schulte, J. H. (2017). The GSK461364 PLK1 inhibitor exhibits strong antitumoral activity in preclinical neuroblastoma models. *Oncotarget*, *8*(4), 6730–6741. http://doi.org/10.18632/oncotarget.14268

Park, C. H., Park, J.-E., Kim, T.-S., Kang, Y. H., Soung, N.-K., Zhou, M., … Lee, K. S. (2015). Mammalian polo-like kinase 1 (Plk1) promotes proper chromosome segregation by phosphorylating and delocalizing the PBIP1CENP-Q complex from kinetochores. *Journal of Biological Chemistry*, *290*(13), 8569–8581. http://doi.org/10.1074/jbc.M114.623546

Park, J.-E., Soung, N.-K., Johmura, Y., Kang, Y. H., Liao, C., Lee, K. H., … Lee, K. S. (2010). Polo-box domain: A versatile mediator of polo-like kinase function. *Cellular and Molecular Life Sciences*, *67*, 1957–1970. http://doi.org/10.1007/s00018-010-0279-9

Park, S.-Y., Park, J.-E., Kim, T.-S., Hee Kim, J., Kwak, M.-J., Ku, B., … Lee, K. S. (2014). Molecular basis for unidirectional scaffold switching of human Plk4 in centriole biogenesis. *Nature Structural and Molecular Biology*, *21*(8), 696–703. http://doi.org/10.1038/nsmb.2846

Qi, W., Tang, Z., & Yu, H. (2006). Phosphorylation-and polo-box– Dependent binding of Plk1 to Bub1 is required for the kinetochore localization of Plk1 □ D. *Molecular Biology of the Cell*, *17*, 3705–3716. http://doi.org/10.1091/mbc.E06

Raab, M., Krämer, A., Hehlgans, S., Sanhaji, M., Kurunci-Csacsko, E., Dötsch, C., … Strebhardt, K. (2015). Mitotic arrest and slippage induced by pharmacological inhibition of polo-like kinase 1. *Molecular Oncology*, *9*(1), 140–154. http://doi.org/10.1016/j.molonc.2014.07.020

Sanhaji, M., Ritter, A., Belsham, H. R., Friel, C. T., Roth, S., Louwen, F., & Yuan, J. (2014). Polo-like kinase 1 regulates the stability of the mitotic centromere-associated kinesin in mitosis. *Oncotarget*, *5*(10), 3130–3144.

Santamaria, A., Wang, B., Elowe, S., Malik, R., Zhang, F., Bauer, M., … Nigg, E. a. (2011). The Plk1-dependent phosphoproteome of the early mitotic spindle. *Molecular & Cellular Proteomics : MCP*, *10*(1), M110.004457. http://doi.org/10.1074/mcp.M110.004457

Saurin, A. T. (2018). Kinase and phosphatase cross-talk at the kinetochore. *Frontiers in Cell and Developmental Biology*, *6*(June), 62.

Seeburg, D. P., Pak, D., & Sheng, M. (2005). Polo-like kinases in the nervous system. *Oncogene*, *24*, 292–298. http://doi.org/10.1038/sj.onc.1208277

Seki, A., Coppinger, J. A., Jang, C.-Y., Yates, J. R., & Fang, G. (2008). Bora and the kinase Aurora a cooperatively activate the kinase Plk1 and control mitotic entry. *Science (New York, N.Y.)*, *320*(5883), 1655–1658. http://doi.org/10.1126/science.1157425

Shukla, A., Kong, D., Sharma, M., Magidson, V., & Loncarek, J. (2015). Plk1 relieves centriole block to reduplication by promoting daughter centriole maturation. *Nature Communications*, *6*, 8077. http://doi.org/10.1038/ncomms9077

Shyang Fong, C., Kim, M., Tony Yang, T., Liao, J.-C., & Bryan Tsou, M.-F. (2014). SAS-6 assembly templated by the lumen of cartwheel-less centrioles precedes centriole duplication. *Developmental Cell*, *30*, 238–245. http://doi.org/10.1016/j.devcel.2014.05.008

Sillibourne, J. E., & Bornens, M. (2010). Polo-like kinase 4: the odd one out of the family. *Cell Division*, *5*, 25.

Slevin, L. K., Nye, J., Pinkerton, D. C., Buster, D. W., Rogers, G. C., & Slep, K. C. (2012). The structure of the Plk4 cryptic polo box reveals two tandem polo boxes required for centriole duplication. *Structure*, *20*(11), 1905–1917. http://doi.org/10.1016/j.str.2012.08.025

Smits, V. A. J., Klompmaker, R., Arnaud, L., Rijksen, G., Nigg, E. A., & Medema, R. H. (2000). Polo-like kinase-1 is a target of the DNA damage checkpoint. *Nature Cell Biology*, *2*, 672–676.

Somers, W. G., & Saint, R. (2003). A RhoGEF and rho family GTPase-activating protein complex links the contractile ring to cortical microtubules at the onset of cytokinesis. *Developmental Cell*, *4*, 29–39.

Sonnen, K. F., Gabryjonczyk, A.-M., Anselm, E., Stierhof, Y.-D., & Nigg, E. A. (2013). Human Cep192 and Cep152 cooperate in Plk4 recruitment and centriole duplication. *Journal of Cell Science*, *126*, 3223–3233. http://doi.org/10.1242/jcs.129502

Soung, N.-K., Kang, Y. H., Kim, K., Kamijo, K., Yoon, H., Seong, Y.-S., … Lee, K. S. (2006). Requirement of hCenexin for proper mitotic functions of polo-like kinase 1 at the centrosomes. *Molecular and Cellular Biology*, *26*(22), 8316–8335. http://doi.org/10.1128/MCB.00671-06

Soung, N.-K., Park, J.-E., Yu, L.-R., Lee, K. H., Lee, J.-M., Bang, J. K., … Lee, K. S. (2009). Plk1-dependent and -independent roles of an ODF2 splice variant, hCenexin1, at the centrosome of somatic cell. *Developmental Cell*, *16*(4), 539–550. http://doi.org/10.1016/j.devcel.2009.02.004

Steegmaier, M., Hoffmann, M., Baum, A., Lenart, P., Petronczki, M., Krssak, M., … Rettig, W. J. (2007). BI 2536, a potent and selective

inhibitor of polo-like kinase 1, inhibits tumor growth in vivo. *Current Biology*, *17*(4), 316–322. http://doi.org/10.1016/j.cub.2006.12.037

Steegmaier, M., Hoffmann, M., Baum, A., Ter Lé Ná, R., Petronczki, P., Krssak, M., … Rettig, W. J. (2007). Report BI 2536, a potent and selective inhibitor of polo-like kinase 1, inhibits tumor growth in vivo. *Current Biology*, *17*, 316–322. http://doi.org/10.1016/j.cub.2006.12.037

Suijkerbuijk, S. J. E., Vleugel, M., Teixeira, A., & Kops, G. J. P. L. (2012). Integration of kinase and phosphatase activities by BUBR1 ensures formation of stable kinetochore-microtubule attachments. *Developmental Cell*, *23*, 745–755. http://doi.org/10.1016/j.devcel.2012.09.005

Sun, S., Sun, L., Zhou, X., Wu, C., Wang, R., Lin, S.-H., & Kuang, J. (2016). Phosphorylation-dependent activation of the ESCRT function of ALIX in Cytokinetic abscission and retroviral budding. *Developmental Cell*, *36*, 331–343. http://doi.org/10.1016/j.devcel.2016.01.001

Sunkel, C. E., & Glover, D. M. (1988). Polo, a mitotic mutant of drosophila displaying abnormal spindle poles. *Journal of Cell Science*, *89*, 25–38.

Thomas, Y., Cirillo, L., Panbianco, C., Martino, L., Tavernier, N., Schwager, F., … Quan, J. (2016). Cdk1 phosphorylates SPAT-1/bora to promote Plk1 activation in C. elegans and human cells. *Cell Reports*, *15*(3), 510–518. http://doi.org/10.1016/j.celrep.2016.03.049

Van De Weerdt, B. C. M., Littler, D. R., Klompmaker, R., Huseinovic, A., Fish, A., Perrakis, A., & Medema, R. H. (2008). Polo-box domains confer target specificity to the polo-like kinase family. *Biochimica et Biophysica Acta*, *1783*(6), 1015–1022.

Van Vugt, M. A. T. M., Brá, A., & Medema, R. H. (2004). Polo-like Kinase-1 controls recovery from a G2 DNA damage-induced arrest in mammalian cells. *Molecular Cell*, *15*, 799–811.

Vertii, A., Bright, A., Delaval, B., Hehnly, H., & Doxsey, S. (2015). New frontiers: Discovering cilia-independent functions of cilia proteins. *EMBO Reports*, *16*(10), 1275–1287. http://doi.org/10.15252/embr.201540632

Vose, J. M., Friedberg, J. W., Waller, E. K., Cheson, B. D., Juvvigunta, V., Fritsch, H., … Younes, A. (2013). The Plk1 inhibitor BI 2536 in patients with refractory or relapsed non-Hodg...: EBSCOhost. *Leukemia and Lymphoma*, *54*(4), 708–713. http://doi.org/10.3109/10428194.2012.729833

Wakida, T., Ikura, M., Kuriya, K., Ito, S., Shiroiwa, Y., Habu, T., … Furuya, K. (2017). The CDK-PLK1 axis targets the DNA damage checkpoint sensor protein RAD9 to promote cell proliferation and tolerance to genotoxic stress. *eLife*, *6*, e29953. http://doi.org/10.7554/eLife.29953

Wang, G., Chen, Q., Zhang, X., Zhang, B., Zhuo, X., Liu, J., … Zhang, C. (2013). PCM1 recruits Plk1 to the pericentriolar matrix to promote primary cilia disassembly before mitotic entry. *Journal of Cell Science*, *126*(Pt 6), 1355–1365. http://doi.org/10.1242/jcs.114918

Wolfe, B. A., Takaki, T., Petronczki, M., & Glotzer, M. (2009). Polo-like kinase 1 directs assembly of the HsCyk-4 RhoGAP/Ect2 RhoGEF complex to initiate cleavage furrow formation. *PLoS Biology*, *7*(5), 1000110. http://doi.org/10.1371/journal.pbio.1000110

Wong, O. K., & Fang, G. (2007). Cdk1 phosphorylation of BubR1 controls spindle checkpoint arrest and Plk1-mediated formation of the 3F3/2 epitope. *Journal of Cell Biology*, *179*(4), 611–617. http://doi.org/10.1083/jcb.200708044

Wong, Y. L., Anzola, J. V., Davis, R. L., Yoon, M., Motamedi, A., Kroll, A., … Oegema, K. (2015). Reversible centriole depletion with an inhibitor of Polo-like kinase 4. *Science*, *348*(6239), 1155–1160.

Woodruff, J. B., Ferreira Gomes, B., Widlund, O., Mahamid, J., Honigmann, A., & Hyman, A. A. (2017). The centrosome is a selective condensate that nucleates microtubules by concentrating tubulin. *Cell*, *169*, 1066–1077. http://doi.org/10.1016/j.cell.2017.05.028

Yamamoto, Y., Matsuyama, H., Kawauchi, S., Matsumoto, H., Nagao, K., Ohmi, C., … Sasaki, K. (2006). Laboratory investigation overexpression of polo-like kinase 1 (PLK1) and chromosomal instability in bladder cancer. *Oncology*, *70*, 231–237. http://doi.org/10.1159/000094416

Yang, D., Rismanchi, N., Benoı̈t Renvoisé, B., Lippincott-Schwartz, J., Blackstone, C., & Hurley, J. H. (2008). Structural basis for midbody targeting of spastin by the ESCRT-III protein CHMP1B. *Nature Structural & Molecular Biology*, *15*, 1278–1286. http://doi.org/10.1038/nsmb.1512

Yim, H. (2013). Current clinical trials with polo-like kinase 1 inhibitors in solid tumors. *Anti-Cancer Drugs*, *24*(10), 999–1006. http://doi.org/10.1097/CAD.0000000000000007

Zhang, B., Wang, G., Xu, X., Yang, S., Zhuang, T., Wang, G., … Zhang, C. (2016). DAZ-interacting protein 1 (dzip1) phosphorylation by polo-like kinase 1 (plk1) regulates the centriolar satellite localization of the bbsome protein during the cell cycle * □ S. *The Journal of Biological Chemistry*, *292*(4), 1351–1360. http://doi.org/10.1074/jbc.M116.765438

Zhang, Z., Hou, X., Shao, C., Li, J., Cheng, J.-X., Kuang, S., … Liu, X. (2014). Plk1 inhibition enhances the efficacy of androgen signaling blockade in castration-resistant prostate cancer. *Cancer Research*, *74*(22), 6635–6647. http://doi.org/10.1158/0008-5472.CAN-14-1916

Zimmerman, W. C., & Erikson, R. L. (2007). Polo-like kinase 3 is required for entry into S phase. *Proceedings of the National Academy of Sciences of the United States of America*, *104*(6), 1847–1852.

Zimmerman, W. C., Sillibourne, J., Rosa, J., & Doxsey, S. J. (2004). Mitosis-specific anchoring of tubulin complexes by Pericentrin controls spindle organization and mitotic entry. *Molecular Biology of the Cell*, *15*(8), 3642–3657. http://doi.org/10.1091/mbc.E03-11-0796

**How to cite this article:** Colicino EG, Hehnly H. Regulating a key mitotic regulator, polo-like kinase 1 (PLK1). *Cytoskeleton*. 2018;75:481–494. https://doi.org/10.1002/cm.21504

# Chromosome misalignment is associated with PLK1 activity at cenexin-positive mitotic centrosomes

Erica G. Colicino[a,b,†], Katrina Stevens[c], Erin Curtis[a], Lindsay Rathbun[a], Michael Bates[a], Julie Manikas[a], Jeffrey Amack[b], Judy Freshour[a], and Heidi Hehnly[a,*]
[a]Biology Department, Syracuse University, Syracuse, NY 13210; [b]Department of Cell and Developmental Biology, Upstate Medical University, Syracuse, NY 13210; [c]Biology Department, Clarkson University, Potsdam, NY 13699

**ABSTRACT** **The mitotic kinase, polo-like kinase 1 (PLK1), facilitates the assembly of the two mitotic spindle poles, which are required for the formation of the microtubule-based spindle that ensures appropriate chromosome distribution into the two forming daughter cells. Spindle poles are asymmetric in composition. One spindle pole contains the oldest mitotic centriole, the mother centriole, where the majority of cenexin, the mother centriole appendage protein and PLK1 binding partner, resides. We hypothesized that PLK1 activity is greater at the cenexin-positive older spindle pole. Our studies found that PLK1 asymmetrically localizes between spindle poles under conditions of chromosome misalignment, and chromosomes tend to misalign toward the oldest spindle pole in a cenexin- and PLK1-dependent manner. During chromosome misalignment, PLK1 activity is increased specifically at the oldest spindle pole, and this increase in activity is lost in cenexin-depleted cells. We propose a model where PLK1 activity elevates in response to misaligned chromosomes at the oldest spindle pole during metaphase.**

**Monitoring Editor**
Yukiko Yamashita
University of Michigan

Received: Dec 26, 2018
Revised: Mar 28, 2019
Accepted: Apr 25, 2019

## INTRODUCTION

Mitotic cell division is a process whereby genetic material is duplicated, separated, and packaged to yield two daughter cells. This process relies heavily on the spatial and temporal synchronization of signaling activity at the mitotic spindle, a structure that segregates the chromosomes and guides them toward the daughter cells. The mitotic kinase, polo-like kinase 1 (PLK1), is a major regulator of this process that works to ensure bipolar spindle formation and chromosome alignment at the metaphase plate. This is accomplished by PLK1-scaffold interactions at the mitotic centrosomes/spindle poles, which modulate the recruitment of centrosome components SAS-4, γ-tubulin, γ-TuRC, pericentrin, and CEP215 (reviewed in Colicino and Hehnly, 2018). Their recruitment is initiated after PLK1-dependent SAS-4 phosphorylation (Ramani *et al.*, 2018). This phosphorylation allows SAS-4 expansion to occur, followed by the recruitment of CEP215 and γ-tubulin and subsequent expansion of the pericentriolar material (PCM), playing a crucial role in mitotic centrosome/spindle pole formation during division (Ramani *et al.*, 2018). However, it is unclear whether PLK1 is additionally regulated between the two spindle poles during cell division.

Owing to the nature of centriole duplication, the two spindle poles are inherently asymmetric from one another. The oldest (mother) spindle pole is enriched with the centriole appendage protein cenexin, compared to the youngest spindle pole (daughter; Vertii *et al.*, 2015; Hung *et al.*, 2016). During interphase, mother centriole appendages assist in centrosome positioning (Hung *et al.*, 2016) and primary cilia formation by anchoring the oldest centriole (known here as the basal body) to the cell membrane to form

This article was published online ahead of print in MBoC in Press (http://www.molbiolcell.org/cgi/doi/10.1091/mbc.E18-12-0817) on May 1, 2019.

E.C. and H.H. designed and E.C., M.B., L.R., K.S., J.M., and H.H. conducted experiments and analyzed the data. J.A. provided zebrafish embryos and husbandry knowledge. J.F. constructed all vectors utilized. E.C. and H.H. wrote the manuscript, contributing to multiple rounds of edits.

†Present address: Department of Cell and Developmental Biology, University of Michigan Medical School, Ann Arbor, MI 48109.

*Address correspondence to: Heidi Hehnly (hhehnly@syr.edu).

Abbreviations used: CENPA, centromere protein A; CEP164, centrosome protein 164; CEP215, centrosome protein 215; CFP, cyan fluorescent protein; DAPI, 4′,6-diamidino-2-phenylindole; DDR, DNA damage repair; FRAP, fluorescence recovery after photobleaching; FRET, fluorescence resonance energy transfer; γ-TuRC, γ-tubulin ring complex; GFP, green fluorescent protein; GSD, ground state depletion; HPF, hours postfertilization; LUT, look-up table; PACT, pericentrin AKAP centrosomal targeting; PCM, pericentriolar material; PLK1, Polo-like kinase 1; ROI, region of Interest; RPE, retinal pigment epithelial; SAS-4, spindle assembly abnormal protein 4; shRNA, short-hairpin RNA; SIM, structured illumination microscopy; YFP, yellow fluorescent protein.

© 2019 Colicino *et al.* This article is distributed by The American Society for Cell Biology under license from the author(s). Two months after publication it is available to the public under an Attribution–Noncommercial–Share Alike 3.0 Unported Creative Commons License (http://creativecommons.org/licenses/by-nc-sa/3.0).

"ASCB®," "The American Society for Cell Biology®," and "Molecular Biology of the Cell®" are registered trademarks of The American Society for Cell Biology.

the primary cilia (reviewed in Kobayashi and Dynlacht, 2011, and Vertii *et al.*, 2016). Prior to mitotic onset, PLK1 is recruited to the basal body where it assists in ciliary disassembly (Wang *et al.*, 2013). Cenexin regulates appendage formation and has also been identified as a PLK1 binding partner (Soung *et al.*, 2006, 2009). Previous work utilizing ground state depletion (GSD) identified a modest, but significant, enrichment of PLK1 at the mother (cenexin-positive) spindle pole in fixed in vitro metaphase cells (Hehnly *et al.*, 2015). This study suggests an inherent asymmetry in PLK1 distribution that is dependent on centrosome age. During division, cenexin has been implicated in multiple processes, including modulating preferential chromosome misalignment toward the oldest spindle pole in the event of mitotic error (Gasic *et al.*, 2015). Knowing this, we wanted to test the hypothesis that PLK1 localization and activity is asymmetrically regulated between the two spindle poles through the presence of cenexin at the mother spindle pole, which can modulate directional chromosome misalignment.

Using a multidisciplinary approach, we found a significant asymmetry in PLK1 localization and activity between spindle poles in in vivo zebrafish studies and in vitro tissue culture. From here, we tested whether the propensity for chromosomes to misalign toward one spindle pole altered PLK1 activity. We further examined whether altering PLK1 activity influences the preferential misalignment of lagging chromosomes toward the oldest spindle pole.

## RESULTS

### Asymmetric distribution of PLK1 in zebrafish and mammalian cells

In mammalian dividing cells, PLK1 is up-regulated during mitosis. During this time, it is enriched at spindle poles and kinetochores, specifically from prometaphase to metaphase (Kishi *et al.*, 2009; Colicino and Hehnly, 2018). Following metaphase exit, PLK1 transitions from kinetochores to the cytokinetic furrow, where it is subsequently concentrated at the forming midbody (Burkard *et al.*, 2007; Kishi *et al.*, 2009; Colicino *et al.*, 2018; modeled in Supplemental Figure 1A). The subcellular distribution of PLK1 in mammalian cells has predominately been studied in in vitro cell culture models. However, in vitro systems do not always represent what is happening in vivo. Here, we examine the temporal and spatial regulation of PLK1 during division first in a developing vertebrate embryo (Figure 1, A–E) and then in in vitro cell culture (Figure 1, F–I). Fertilized embryos were injected with 100 pg of PLK1-mCherry mRNA. Injected embryos were imaged using confocal microscopy 4.5 h postfertilization (hpf). At this time, embryonic cells are proliferating asynchronously (Kimmel *et al.*, 1995), and proliferating cells can be distinguished via PLK1 expression (Supplemental Figure 1, A–D). By magnifying the PLK1-mCherry–positive subpopulation, a distinct subcellular distribution of PLK1-mCherry at spindle poles and kinetochores was noted (Supplemental Figure 1, D and E). The spatial and temporal distribution of PLK1-mCherry in a single dividing cell was monitored over a 360 s time span. PLK1-mCherry transitions from spindle pole and kinetochore localization in metaphase to cytokinetic furrow localization during cytokinesis where it becomes concentrated at the cytokinetic midbody (Figure 1A and Supplemental Video 1).

Upon investigation of the integrated intensity of PLK1-mCherry between spindle poles in metaphase cells within the zebrafish embryo, we noted that one spindle pole has a significantly larger proportion of PLK1-mCherry compared with the other (Figure 1Ba′; Fire look-up table [LUT]). This is clearly demonstrated when the maximum projection of a single metaphase cell (Figure 1Ba′) is presented as a three-dimensional (3D) surface plot (Figure 1Bb′), where each peak represents a spindle pole (labeled with 1 and 2). The spindle pole peak on the left (1) presents with 10% greater PLK1 fluorescence intensity than its partnering spindle pole peak on the right (2; Figure 1Bb′). To validate this finding, we measured PLK1 fluorescence intensity between spindle pole pairs over 49 metaphase cells from 10 embryos. The spindle pole with the highest intensity was binned as pole 1 and the pole with the lowest intensity was binned as pole 2. From this data set, one spindle pole consistently contained 10.31 ± 1.14% less PLK1-mCherry compared with the other (Figure 1C). We then examined whether this asymmetry was present throughout a 150 s time course of a prometaphase cell transitioning through metaphase (Figure 1, D and E). This was measured by placing a region of interest (ROI) over spindle poles 1 and 2. The integrated intensity of PLK1-mCherry within this region was plotted over 150 s with images taken every 30 s. The graph demonstrates that spindle poles present with asymmetric PLK1 distribution as cells exit prometaphase (Figure 1E; beginning at 60 s time point). These findings suggest an inherent asymmetry in the amount of PLK1 between the two spindle poles that is similar to the asymmetry reported under in vitro fixed cell conditions using GSD (Hehnly *et al.*, 2015).

To determine whether this inherent PLK1 asymmetry between metaphase spindle poles is conserved in live mammalian cells, we employed a retinal pigment epithelial (RPE) cell line that stably expresses GFP-PLK1 at endogenous levels (Colicino *et al.*, 2018). Fluorescence recovery after photobleaching (FRAP) was performed. To do this, a ROI was placed over both spindle poles (Figure 1F), where a 488-nm laser was applied. Upon application of the laser, GFP-PLK1 fluorescence within the regions was bleached. After 1.6 s, GFP-PLK1 signal returns to that region (Figure 1F and Supplemental Video 2). A 3D surface plot was performed for the metaphase cell pre-FRAP (–1.2 s), during the FRAP (0 s), and post-FRAP (1.6 s; Figure 1F). At –1.2 s (pre-FRAP), pole 1 contained significantly more GFP-PLK1 than the other (pole 2). At 0 s, GFP-PLK1 at both poles was successfully bleached. At 1.6 s, pole 1 returned to have an elevated amount of GFP-PLK1 compared with spindle pole 2 (Figure 1F), suggesting an increased exchange of GFP-PLK1 at pole 1. Along these same lines, we determined over multiple metaphase cells that spindle pole 2 contained 14.70 ± 4.12% less GFP-PLK1 compared with pole 1 (Figure 1G). These findings are strikingly similar to the differences in GFP-PLK1 between the two spindle poles observed in metaphase cells within the zebrafish embryo, where one pole had 10.31 ± 1.14% less PLK1 than the other (Figure 1C). Together, this suggests a conserved mechanism for an asymmetric distribution of PLK1 between the two spindle poles.

Our findings demonstrate an asymmetry in PLK1 distribution between the two spindle poles; however, a difference in distribution does not necessarily confer a difference in PLK1 activity. To test activity, we utilized a centrosome-localized PLK1 activity fluorescence resonance energy transfer (FRET) biosensor that we developed and controlled for in Colicino *et al.*, 2018. This biosensor can be successfully utilized under either live or fixed conditions (Colicino *et al.*, 2018). The PLK1 activity FRET biosensor is composed of monomeric cyan fluorescent protein (CFP) and yellow fluorescent protein (YFP) flanking a c-jun PLK1 substrate sequence and an FHA2-phosphobinding domain, anchored to centrosomes by the pericentrin-AKAP450 centrosomal-targeting (PACT) domain using a 10 amino acid linker (Figure 1H; Colicino *et al.*, 2018). Active-PLK1 phosphorylates the c-jun region, causing a conformational change in the biosensor and a decrease in FRET between CFP and YFP. We plotted the inverse FRET ratio, such that an increase in this ratio would correspond to an increase in PLK1 activity (Figure 1I; Colicino *et al.*, 2018). Using this biosensor, we measured the inverse FRET ratio in dividing HeLa cells and binned, from a single metaphase

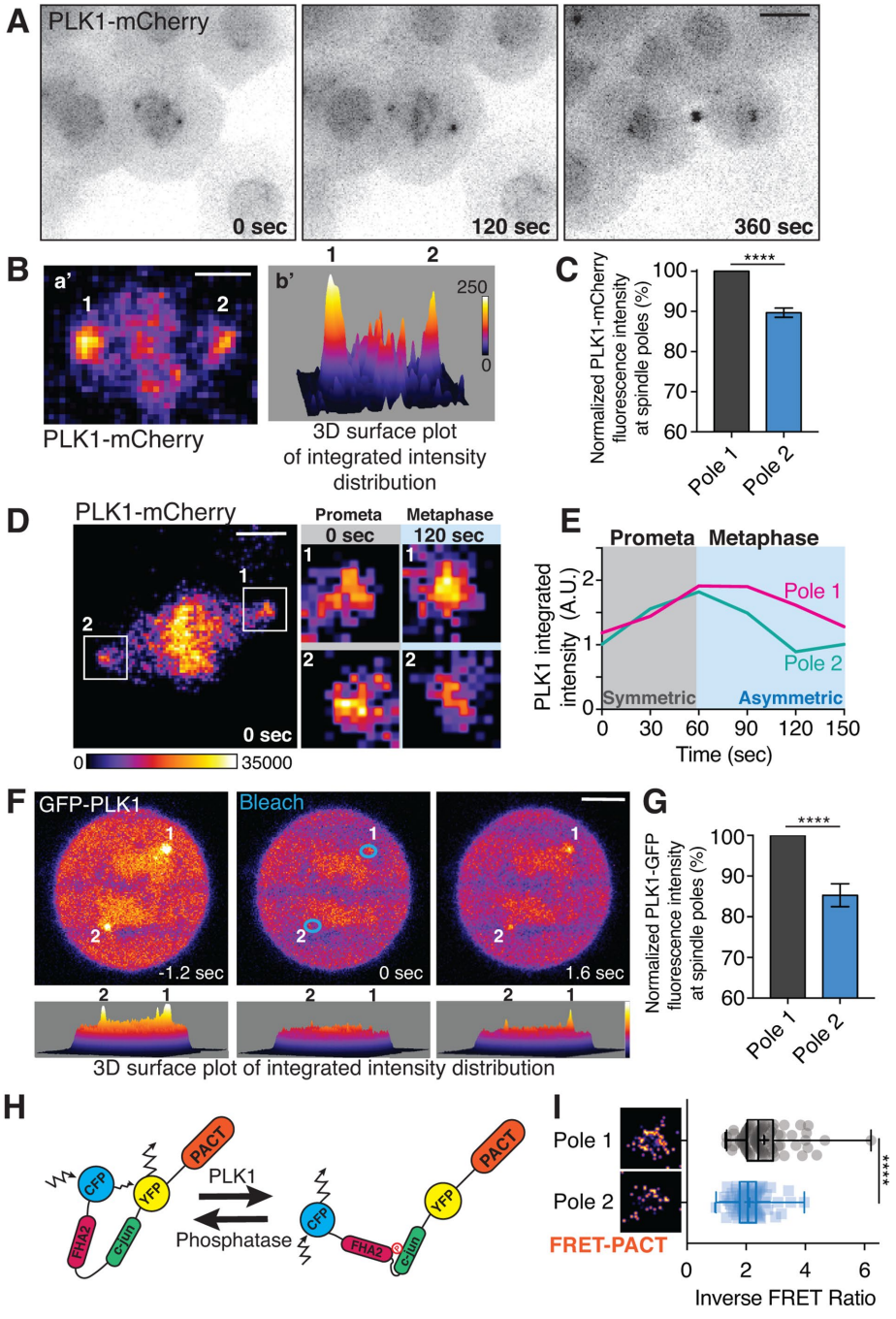



**FIGURE 1:** PLK1 asymmetric distribution between spindle poles is conserved in vivo (zebrafish) and in vitro (mammalian cell culture). (A–E) Data from a 4.5 hpf embryo expressing PLK1-mCherry. (A) Confocal maximum projections of a single mitotic cell taken from prometaphase through cytokinesis expressing PLK1-mCherry. Images taken every 30 s, over 6 min. Bar = 10 μm. (Ba') Maximum projection of single metaphase cell expressing PLK1-mCherry. Bar = 5 μm. (Bb') 3D surface plot of metaphase cell (from a') displaying PLK1-mCherry integrated intensity measurements ranging between 0 and 250. Spindle poles marked 1 and 2. Fire-LUT (ImageJ). (C) PLK1-mCherry integrated intensity at the highest spindle pole (pole 1) was normalized to 100% and compared with the lowest spindle pole within a single mitotic spindle ($n = 49$ cells measured across 10 embryos ± SEM, Student's $t$ test, $p < 0.0001$). (D) Shown is a single prometaphase cell expressing PLK1-mCherry with poles 1 and 2 marked by a ROI at time point 0 s. PLK1-mCherry integrated intensity is displayed through a Fire-LUT where high intensity white pixels are 35,000 and lower intensity black pixels are 0. The ROIs where PLK1 intensity between poles 1 and 2 is symmetric is highlighted in gray (0 s). Where PLK1 intensity is asymmetric is highlighted in blue (120 s). Bar = 5 μm. (E) Line graph of PLK1 intensity over 2.5 min at poles 1 (magenta) and 2 (cyan) featured in D, illustrating periods of symmetric (gray) and asymmetric (blue) PLK1 intensity between the spindle poles. (F–I) Data from human retinal pigment epithelial (RPE) cells stably expressing GFP-PLK1. (F) Representative images of fluorescence recovery after photobleaching (FRAP) of GFP-PLK1 expressing RPE cells at spindle poles during metaphase (Fire-LUT, ImageJ). Bar = 5 μm. 3D surface plot of a single metaphase cell displaying GFP-PLK1 integrated intensity between the two spindle poles. Spindle poles 1 and 2 are marked. (G) GFP-PLK1 integrated intensity at the highest spindle pole (pole 1) was normalized to 100% and compared with the lowest spindle pole within a single mitotic spindle, over $n = 44$ cells in $n = 3$ experiments ± SEM, Student's paired $t$ test, $p < 0.001$. (H) Model of centrosome-localized PLK1-activity FRET biosensor where active PLK1 phosphorylates the substrate sequence c-jun (green), causing the FHA2 domain (magenta) to bind, and leading to a conformational change in the biosensor and subsequent loss of FRET. Increased phosphatase activity causes the biosensor to enter a relaxed conformation, allowing FRET (Colicino *et al.*, 2018). (I) Quantification of the inverse FRET ratio across multiple spindle poles displayed as a box and whisker plot. Pole 1 binned as mitotic centrosome with highest inverse FRET ratio (gray) compared with pole 2 (blue) from a single mitotic spindle. Representative of FRET ratio at a single mitotic centrosome shown (Fire-LUT, ImageJ). $n = 60$ cells, + indicating mean, and each data point representing a single mitotic centrosome, Student's paired $t$ test, $p < 0.001$.

mitotic spindle, the spindle pole with a higher inverse FRET ratio as spindle pole 1 and the spindle pole with a lower inverse FRET ratio as spindle pole 2. This was done over 60 metaphase cells, where we calculated that one spindle pole (pole 1) had a significantly greater inverse FRET ratio (median of 2.43) compared with the other (pole 2, median of 2.06; Figure 1I). Together, these data suggest that an asymmetry in PLK1 distribution and activity exists between the two spindle poles in metaphase cells.

### Chromosome misalignment drives asymmetry in PLK1 distribution

A possible mechanism to respond to misaligned chromosomes is to adjust PLK1 distribution between spindle poles. During prometaphase exit and metaphase, misaligned chromosomes can be found that realign with the metaphase plate (Figure 2A). During these situations, we imaged GFP-PLK1 RPE cells every 2 min across the full volume of the cell until it passed through anaphase (~20 min in duration). GFP-PLK1 intensity was then measured at each spindle

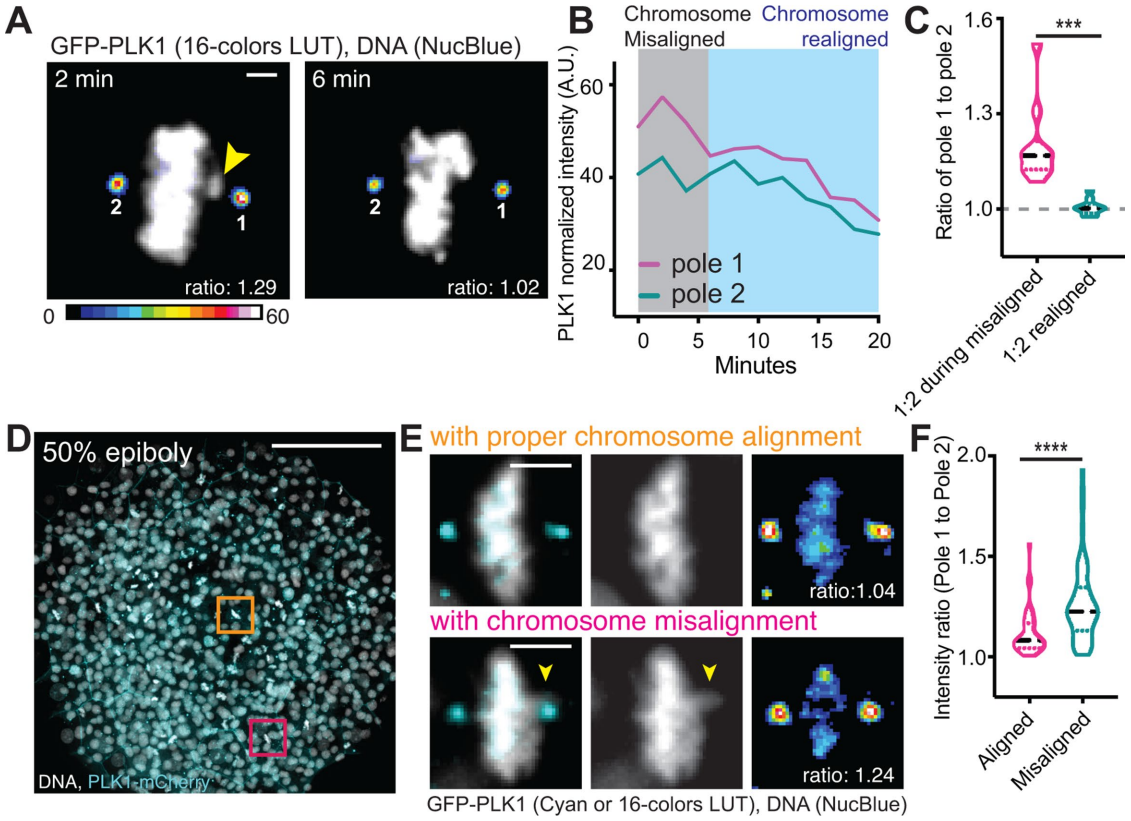



FIGURE 2: PLK1 asymmetric distribution between spindle poles is driven by chromosome misalignment. (A) GFP-PLK1 (16-color LUT, Image J) RPE cells treated with NucBlue to stain DNA (white) were imaged every 2 min. Shown is a time point with a misaligned chromosome (2 min, arrow) that then assembles within the metaphase plate by 6 min. Bar = 2 µm. The spindle pole on the side with the misaligned chromosome is marked as 1, and the opposite pole is 2. Ratio values for GFP-PLK1 between poles 1 and 2 shown in the lower right corner. (B) The intensity of poles 1 and 2 from A was measured over a 20-min time course and plotted. Chromosome misalignment marked on plot. (C) The ratio GFP-PLK1 intensity at the spindle pole (labeled 1) with a misaligned chromosome divided by the GFP-PLK1 intensity of spindle pole without a misaligned chromosome (labeled 2) was measured during misalignment (magenta) and postmisalignment (cyan) in the same cell over $n = 10$ live-cell data sets. Violin plot shown. Dashed line at median; dotted lines at interquartile range. Student's paired $t$ test; ***, $p < 0.001$. (D) Maximum projection of a zebrafish embryo expressing PLK1-mCherry (cyan) and NucBlue (white). Examples of metaphase cells with proper chromosome alignment (orange) and chromosome misalignment (magenta) denoted by boxes. Bar, 100 µm. (E) Example images of mitotic cells from D with proper chromosome alignment (top, orange box in D) and chromosome misalignment (bottom, magenta box in D). PLK1-mCherry (cyan) and NucBlue (white) shown in left and center images. PLK1-mCherry (16-color LUT) in right images to denote areas of high PLK1 intensities. Ratio values for PLK1-mCherry between mitotic spindle poles shown in the top right corner. Bar = 5 µm. (F) Violin plot depicting the ratio between the highest PLK1-intensity spindle pole over the lowest PLK1-intensity spindle pole in mitotic cells with an aligned metaphase plate (magenta) or misaligned (cyan). $n > 45$ cells/treatment across $n = 11$ embryos. Student's paired $t$ test; ****, $p < 0.0001$.

pole over time. The spindle pole with the misaligned chromosome in closest proximity was binned as spindle pole 1 and the other as spindle pole 2. When a misaligned chromosome occurred, spindle pole 1 contained an elevated GFP-PLK1 signal compared with spindle pole 2 (Figure 2, A and B). To examine whether this was a consistent phenomenon, a ratio was calculated for GFP-PLK1 intensity at the spindle pole with a misaligned chromosome (pole 1) over the spindle pole without the misaligned chromosome (pole 2) during time points of misalignment compared with time points postmisalignment over 10 dividing cells (Figure 2C). During misalignment, a mean ratio of 1.33 occurs compared with postmisalignment where a mean ratio is at 1.01 (Figure 2C), suggesting that asymmetry in PLK1 between mitotic spindle poles is due to adjustments in chromosome alignment.

Next, we tested whether this occurs in vivo by examining division in a zebrafish embryo expressing PLK1-mCherry and chromosomes stained with 4′,6-diamidino-2-phenylindole (DAPI) or NucBlue. In a fixed, 50% epiboly embryo (Figure 2D), we noted metaphase cells with misaligned chromosomes compared with cells with a clearly aligned metaphase plate (Figure 2E). Under these conditions, we calculated a ratio of the spindle pole with highest intensity over the pole with lowest intensity and determined that the mean ratio is significantly higher under conditions of misaligned chromosomes (mean at 1.27) compared with dividing cells with an aligned plate (mean at 1.12; Figure 2F). Taken together, these studies suggest that chromosome misalignment is causing an elevated asymmetric distribution of PLK1 at spindle poles both in tissue culture and in vivo.

### Determining oldest from youngest mitotic spindle pole and PLK1 distribution between the two

Chromosomes preferentially misalign toward the oldest spindle pole, the one containing the oldest mitotic centriole (Gasic *et al.*, 2015). In our studies, we utilized HeLa cells that stably express GFP-centrin to

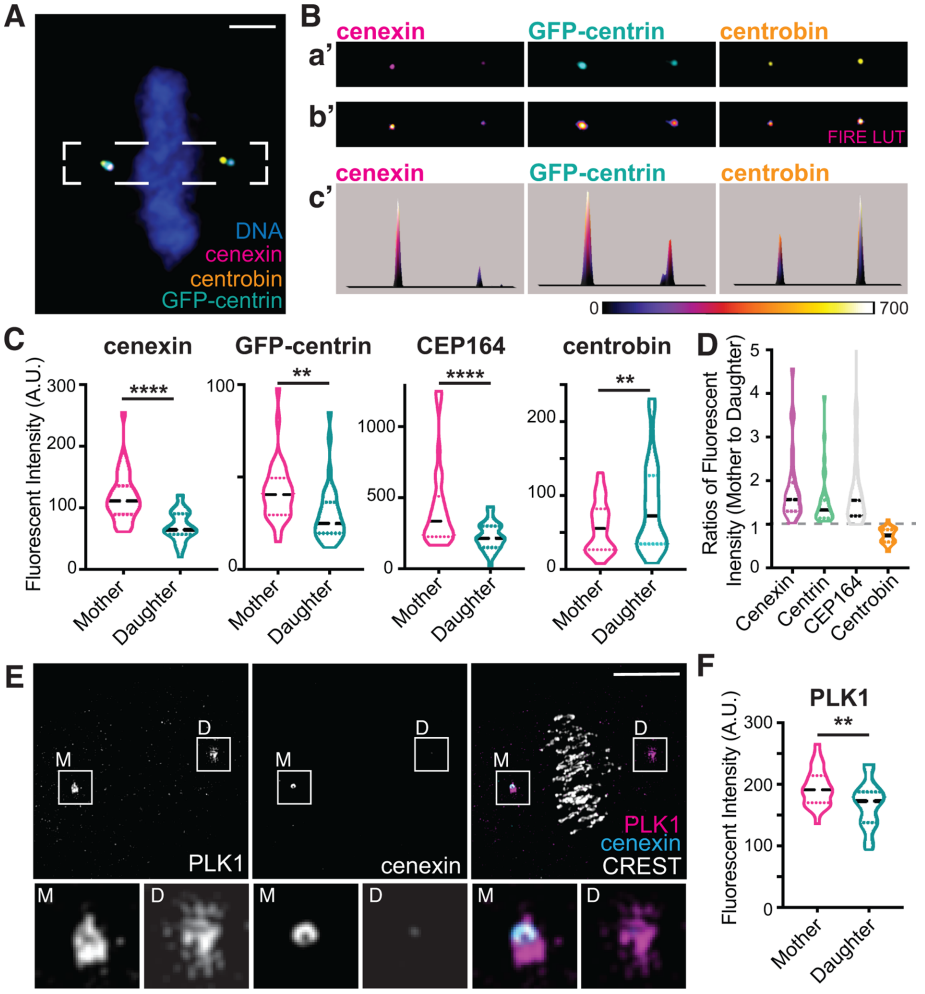



FIGURE 3: PLK1 distribution between the oldest (mother) and youngest (daughter) spindle poles. (A) Immunofluorescence staining of HeLa GFP-centrin cells at metaphase, centrioles (centrin, cyan), cenexin (magenta), centrobin (gold), and DNA (blue). Bar = 3 μm. (B) Insets from A showing cenexin (magenta), GFP-centrin (cyan), and centrobin (gold; Ba'). Fire-LUT depicting intensities of cenexin, GFP-centrin, and centrobin (Bb'). 3D profile plot of each pole. Heat map of intensity ranges (Bc'). (C) The intensity of cenexin, GFP-centrin, CEP164, and centrobin was measured at the mother and daughter spindle pole. Violin plot shown, black dashed line at median. Representative of $n = 3$ experiments, $n > 30$ cells measured/group. Student's paired $t$ test; **, $p < 0.01$; ****, $p < 0.0001$. (D) Measured fluorescence intensities were used to calculate a ratio for each metaphase cell where the mother spindle pole intensity was divided by that of the daughter spindle pole. Violin plot shown, black dashed line at median. Representative of $n = 3$ experiments, $n > 30$ cells/group. (E) Structured illumination micrograph (SIM) volumetric projection of a single metaphase HeLa cell immunolabeled for PLK1 (magenta), cenexin (cyan), and CREST (gray). Mother spindle pole (M) and daughter spindle pole (D). White insets depict single mitotic centrosomes. Bar = 5 μm. (F) PLK1 fluorescence intensity was measured at the mother and daughter spindle pole (determined by GFP-centrin) across $n = 30$ cells. Violin plot shown, black dashed line at median. Student's paired $t$ test; **, $p < 0.01$.

distinguish mother from daughter spindle poles. GFP-centrin is enriched at the oldest spindle pole (mother) compared with the youngest spindle pole (daughter) due to the nature of centriole duplication. When new protein synthesis of centrin occurs, new centrioles incorporate freshly translated centrin. Thus, the oldest centriole has more centrin accumulated (Piel *et al.*, 2000; Wang *et al.*, 2009; Kuo *et al.*, 2011). Additional markers used to distinguish between the oldest and youngest pole were two mother centriole appendage proteins, cenexin (a subdistal appendage protein; Ishikawa *et al.*, 2005; Hehnly *et al.*, 2012; Hung *et al.*, 2016) and CEP164 (a distal appendage protein; Schmidt *et al.*, 2012; Hung *et al.*, 2016), along with the daughter centriole protein centrobin (Januschke *et al.*, 2011; Hehnly *et al.*, 2015). When a single centrosome duplicates to two spindle poles, one spindle pole will inherit the mother centriole, while the other spindle pole does not (Hung *et al.*, 2016; Vertii *et al.*, 2018). The oldest mitotic centriole is positive for cenexin and CEP164 and is enriched for GFP-centrin (Figure 3, A–C, and Supplemental Figure 2, A and B). The youngest spindle pole has elevated amounts of the daughter centriole marker, centrobin (Figure 3, A–C; Hehnly *et al.*, 2015). We then calculated a ratio between mother and daughter spindle poles of CEP164, cenexin, GFP-centrin, and centrobin. In these studies the mother was distinguished by its elevated amounts of GFP-centrin (Piel *et al.*, 2000; Wang *et al.*, 2009; Kuo *et al.*, 2011). CEP164, cenexin, and centrin were enriched on the mother (ratios >1; an equal distribution of 1 is at the dashed line), whereas centrobin was enriched on the daughter (ratio <1; Figure 3D).

Cenexin has been identified to interact with PLK1 (Soung *et al.*, 2006, 2009). Using structured illumination microscopy (SIM) we found that cenexin was organized on one spindle pole (mother, M) in a specific "ring-like" pattern, and PLK1 organized in a similar pattern (Figure 3E). This finding suggests that cenexin may be organizing a population of PLK1 specifically on one of the two spindle poles. When we measured the integrated fluorescence intensity of endogenous PLK1 at mother and daughter spindle poles in HeLa GFP-centrin cells, we found that the mother spindle pole (the one with the most GFP-centrin) contained significantly more PLK1 than the daughter spindle pole (Figure 3, E and F).

## PLK1 activity increases at the oldest spindle pole when a lagging chromosome is in close proximity

We measured PLK1 activity at spindle poles in cells expressing the centrosome-localized PLK1 activity FRET-biosensor (Figure 1H; Colicino *et al.*, 2018). We did these studies with nocodazole synchronized and released cells under fixed conditions so that we could analyze more cells and induce misaligned chromosomes (Crasta *et al.*, 2012). Cells were fixed so that mother and daughter spindle poles could be distinguished, and kinetochores visualized. To identify the mother and daughter spindle poles, we used the molecular marker centrobin (Figure 3, B–D) or centrin (Supplemental Figure 2B). Kinetochores were denoted by immunostaining for CREST. We measured PLK1 activity under conditions of normal chromosome alignment, misaligned chromosomes toward the mother spindle pole, or misaligned chromosomes toward the daughter spindle pole (Figure 4A). Misaligned chromosomes were determined by identifying kinetochores outside the metaphase plate (yellow arrowheads in Figure 4A). These unaligned

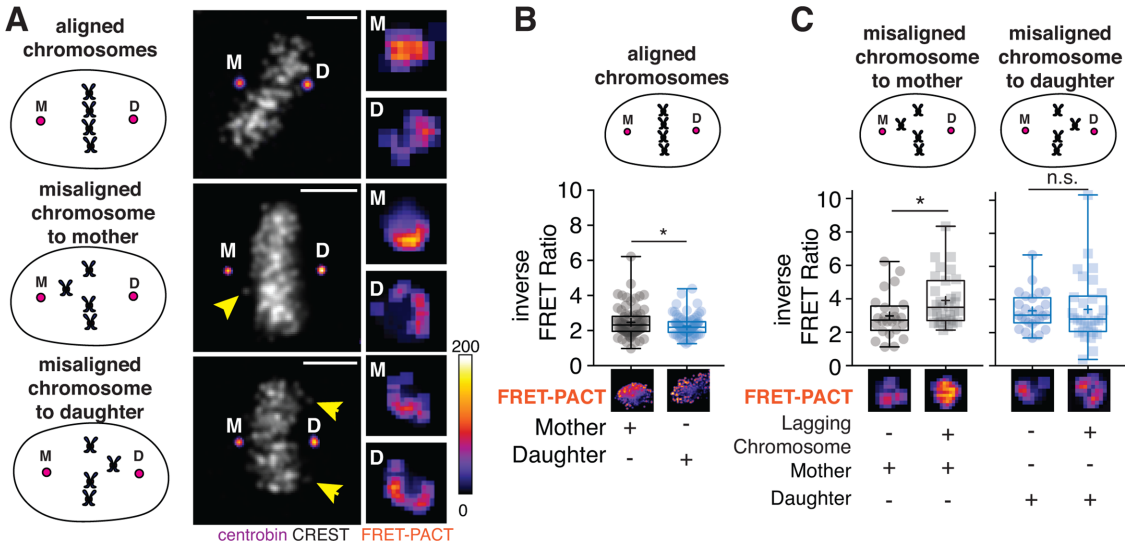



FIGURE 4: PLK1 activity increases at the oldest spindle pole (mother) when a misaligned chromosome is in close proximity. (A) Models depicting conditions of normal chromosome alignment (top), misaligned chromosome to the mother spindle pole (center), and misaligned chromosome to the daughter spindle pole (bottom). Representative maximum confocal projections of metaphase HeLa cells immunostained for centrobin (magenta) and DAPI (white). Insets show inverse FRET ratio of the PLK1-FRET biosensor (right, Fire-LUT; ImageJ). The mother (M) and daughter (D) spindle poles labeled respectively. Bars = 5 μm. (B) Significantly greater PLK1 activity FRET ratios are measured at the mother (gray) spindle pole compared with the daughter (blue) under conditions of normal chromosome alignment. $n = 79$ cells over $n = 3$ experiments. Data shown as a box and whisker plot, + indicating mean, and each data point representing a single spindle pole. Student's paired $t$ test, $p = 0.0139$. (C) Greater PLK1 activity FRET ratios are measured at the mother (gray) spindle pole when there is a misaligned chromosome in close proximity, but no change in PLK1 activity is measured when chromosomes misalign toward the daughter (blue). $n > 20$ cells over $n = 3$ experiments, data shown as a box and whisker plot, + indicating mean, and each data point representing a single spindle pole. Student's unpaired $t$ test, lagging chromosomes to mother ($p = 0.0022$), lagging chromosomes to daughter ($p = 0.7044$).

chromosomes were positive for the mitotic kinase Aurora B (Supplemental Figure 2C). Aurora B is at its highest concentration between two sister chromatids when misaligned chromosomes are not under appropriate tension (Lampson and Cheeseman, 2011). Under conditions of normal chromosome alignment, a slight yet significant increase in PLK1 activity was measured at the mother spindle pole (median of 2.32) compared with the daughter (median of 2.19; Figure 4B). We next compared PLK1 activity at the mother spindle pole with and without a misaligned chromosome (Figure 4C, left) to the PLK1 activity at the daughter pole with and without a misaligned chromosome (Figure 4C, right). In the event of a misaligned chromosome toward the mother, PLK1 activity measured significantly higher (median of 3.50) compared with conditions where there were no detectable misaligned chromosomes (Figure 4C, left). In the event of a misaligned chromosome at the daughter spindle pole, there was no significant difference in PLK1 activity (Figure 4C, right). From this, we conclude that PLK1 activity can increase at the oldest spindle pole specifically when a chromosome misaligns in that direction.

### An increase in PLK1 activity at the mother spindle pole is cenexin dependent

To determine whether an increase in PLK1 activity at the mother spindle pole in the event of a lagging chromosome is cenexin-dependent, we utilized a previously published cenexin-depleted HeLa cell line (Hung *et al.*, 2016). Immunostaining (Figure 5, A and B) and immunoblotting (Figure 5C) confirmed cenexin depletion by short hairpin RNA (shRNA). We noted that in control shRNA–treated cells, 24.98 ± 3.83% of their mitotic cells presented with misaligned chromosomes, whereas in cenexin shRNA–treated cells, this percentage significantly increased to 39.3 ± 4.00% (Figure 5, A and D, refer to arrow, and Table 1).

We next examined cells synchronized in metaphase using the anaphase promoting complex inhibitor, ProTAME (10 μM), or the microtubule destabilizing drug, nocodazole (100 nM). In control cells treated with ProTAME, 19.93 ± 4.45% of mitotic cells had misaligned chromosomes (Figure 5D and Table 1). In ProTAME synchronized cenexin-depleted cells there was a threefold increase compared with control (64.9 ± 10.60%; Figure 5D and representative images in Supplemental Figure 2D). The misalignment observed in ProTAME synchronized cells was severe with misaligned chromosomes accumulating at both poles (Supplemental Figure 2D). A similar increase in the percentage of mitotic cells with misaligned chromosomes was observed in cenexin-depleted cells synchronized in nocodazole (48.47 ± 5.40%) when compared with controls (38.80 ± 6.28%; Table 1). Together these studies suggest that cenexin loss is causing defects in chromosome alignment.

We next tested whether cenexin localization at the mother spindle pole drives preferential distribution of PLK1 activity. The centrosome-localized PLK1 FRET activity biosensor was expressed in cenexin-depleted HeLa cells. These studies were performed under fixed conditions with cells that were nocodazole synchronized and released. Under conditions of normal chromosome alignment, there was no significant difference in the inverse FRET ratios between the mother (median of 2.184) and daughter spindle pole (median of 2.16; Figure 5E). When a misaligned chromosome was present toward the mother spindle pole, there was no significant increase in PLK1 activity at this site (Figure 5F, left). Additionally, there was no increase in PLK1 activity at the daughter when a misaligned chromosome was present (Figure 5F, right). To directly

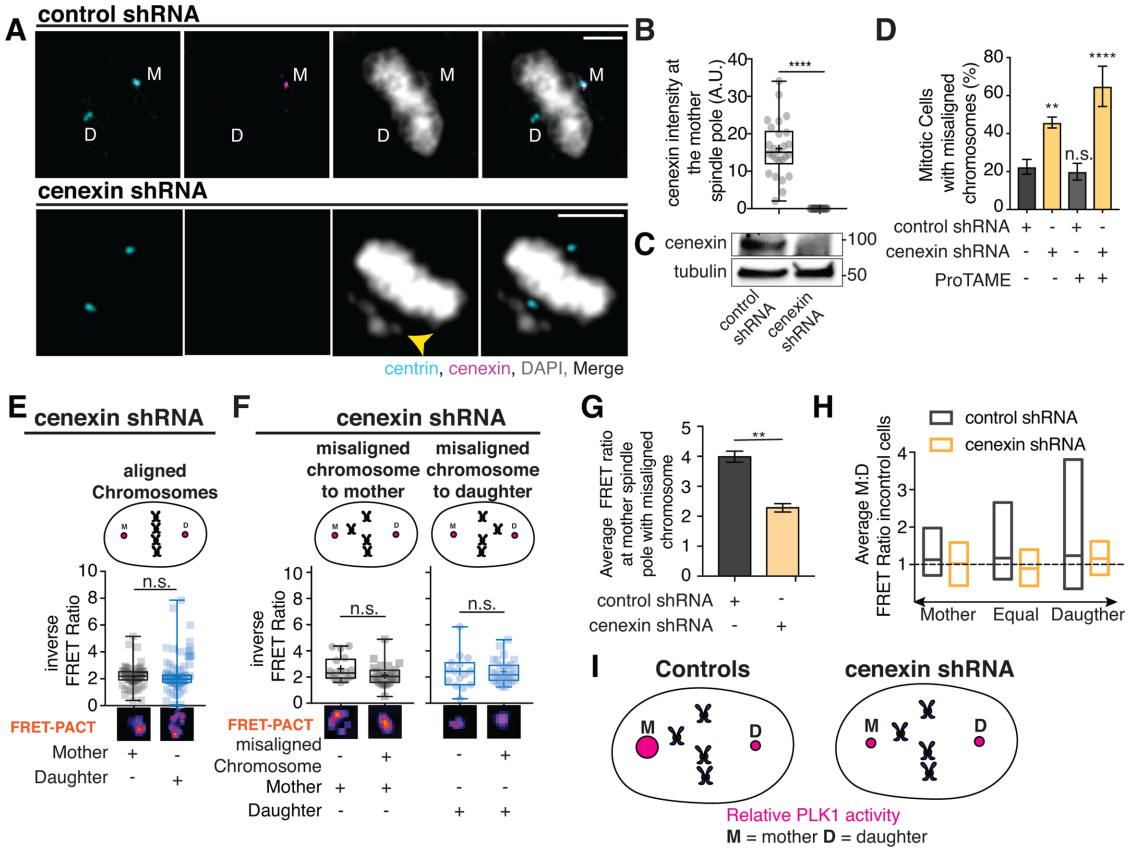



FIGURE 5: An increase in PLK1 activity at the oldest spindle pole (mother) in the event of a misaligned chromosome is cenexin dependent. (A) Maximum confocal projections of control shRNA and cenexin shRNA HeLa cells immunostained for centrin (cyan), cenexin (magenta), and DAPI (gray). Yellow arrowhead indicates misaligned chromosomes. Bars = 5 μm. (B) Cenexin fluorescence intensity at the mother spindle pole in control shRNA and cenexin shRNA HeLa cells. Data shown as a box and whisker plot over $n > 26$ cells, + indicating mean, and each data point representing a single spindle pole. Representative from $n = 3$ experiments. Student's $t$ test, $p < 0.0001$. (C) Western blot of HeLa cells expressing a control nontargeting shRNA or a cenexin shRNA. Tubulin loading control shown below. (D) Bar graph depicting percent (%) metaphase cells with misaligned chromosomes in control and cenexin-depleted cells under control conditions or after ProTAME (10 μM) synchronization in metaphase. $n = 3$ experiments ± SEM. With a one-way ANOVA applying multiple comparisons to control shRNA, cenexin shRNA-treated (**, $p = 0.0023$) and cenexin shRNA-treated plus ProTAME (****, $p < 0.0001$) are significant. (E) PLK1 activity FRET ratios between the mother (gray) and daughter (blue) spindle poles in cenexin-depleted cells when chromosomes are properly aligned. $n > 80$ cells over $n = 3$ experiments, data shown as a box and whisker plot, + indicating mean, and each data point representing a single spindle pole. Student's paired $t$ test, $p = 0.3504$. (F) PLK1 activity in cenexin-depleted cells in the presence of a misaligned chromosome toward the mother (gray) spindle pole or the daughter (blue) spindle pole. $n > 40$ cells over $n = 3$ experiments, data shown as a box and whisker plot, + indicating mean, and each data point representing a single spindle pole. Student's unpaired $t$ test, misaligned chromosome to mother ($p = 0.0719$), misaligned chromosome to daughter ($p = 0.9415$). (G) Bar graph representing average PLK1 FRET ratio at the mother spindle pole in cenexin-depleted cells compared with controls in the event of a misaligned chromosome toward the mother spindle pole across $n = 3$ experiments ± SEM, Student's $t$ test, $p = 0.0018$. (H) Ratio of PLK1 FRET between the mother and daughter (FRET ratios at mother/FRET ratios at daughter) were compared in control cells (gray) and cenexin-depleted cells (gold) under conditions of equal chromosome misalignment toward both spindle poles, asymmetry in misaligned chromosomes toward the mother spindle pole, or asymmetry in misaligned chromosomes toward the daughter spindle pole. Black dotted line at $y = 1$ represents equal FRET ratios between mother and daughter spindle poles. $n > 56$ cells in graph measured over $n = 3$ experiments. Range of data shown as a box plot; center bar represents mean. (I) Model illustrating an increase in PLK1 activity (magenta) in control cells, which does not occur in cenexin-depleted cells.

compare the differences in activity at the mother spindle pole when a misaligned chromosome is present in cells treated with control shRNA or cenexin shRNA, the average inverse FRET ratios for PLK1 were calculated over $n = 3$ experiments. A significantly higher average inverse FRET ratio was calculated in control cells (3.99 ± 0.19) compared with cenexin-depleted cells (2.28 ± 0.14; Figure 5G). These studies suggest a mechanism where PLK1 activity at the oldest spindle pole can respond to chromosome misalignment in a cenexin-dependent manner. If cenexin is absent, an increase in overall misalignment occurs (Figure 5D and Table 1).

We examined how PLK1 activity was distributed between the two spindle poles when more than one chromosome misaligns. The inverse FRET ratio at the mother spindle pole and the inverse FRET ratio at the daughter spindle pole were calculated and presented as a mother to daughter ratio (M:D). If there are consistently equal activities between the two spindle poles, a tight range of values that

| | % metaphase cells with misaligned chromosomes | % of misaligned metaphase cells with chromosomes toward mother | % of misaligned metaphase cells with chromosomes toward both poles |
|---|---|---|---|
| Control shRNA | 24.98 ± 3.83 | 58.08 ± 4.28 | 20.10 ± 5.32 |
| Control shRNA+ 100 nM nocodazole | 38.88 ± 6.28 | 57.49 ± 11.79 | 24.75 ± 11.81 |
| Control shRNA+ 10 μM ProTAME | 19.93 ± 4.45 | 56.79 ± 4.90 | 18.55 ± 12.01 |
| Control shRNA+ 100 nM BI2536 | 44.63 ± 3.70 | 41.42 ± 0.72 | 36.48 ± 3.20 |
| Cenexin shRNA | 39.3 ± 4.00 | 42.9 ± 2.80 | 31.37 ± 1.90 |
| Cenexin shRNA+ 100 nM nocodazole | 48.47 ± 5.40 | 16.86 ± 0.90 | 65.45 ± 4.90 |
| Cenexin shRNA+ 100 nM BI2536 | 61.00 ± 3.40 | 54.33 ± 5.21 | 18.07 ± 3.36 |

The mitotic index, percent of mitotic cells that had chromosomes misaligned toward the mother spindle pole, and the percent of mitotic cells that had chromosomes misaligned toward both spindle poles are shown. These measurements were completed for control shRNA HeLa cells as well as cenexin shRNA HeLa cells treated with 100 nm of nocodazole, 10 μm of ProTAME, or 100 nm of BI2536. Percentages are mean percentages over $n > 3$ experiments ± SEM.

**TABLE 1:** Cenexin and PLK1 regulate directional chromosome misalignment during metaphase.

organize around 1 should be calculated. The ratios presented were calculated under three different conditions: 1) when chromosome misalignment was equal to each pole (e.g., one chromosome toward the daughter and one chromosome toward the mother); 2) asymmetric mother misalignment (e.g., >2 chromosomes toward the mother and <2 chromosomes toward the daughter), and asymmetric daughter misalignment (e.g., <2 chromosomes toward the mother and >2 chromosomes toward the daughter). In control cells, we found a range in activity that always trends above 1 under all conditions. However, in cenexin-depleted cells, a tighter trend that concentrated around a value of 1 was calculated (Figure 5H). This graph suggests that in control cells under both symmetric and asymmetric chromosome misalignment conditions, there is a bias in PLK1 activity toward the mother spindle pole. This bias is lost, however, when cenexin is depleted (Figure 5H). From here, we present a model where PLK1 acts as a sensor to correct for chromosome misalignment at the cenexin-positive oldest spindle pole (mother; Figure 5I).

### Chromosomes predominately misalign toward the oldest spindle pole in a cenexin- and PLK1-dependent manner

A previous report demonstrated an inherent bias for chromosomes to preferentially misalign toward the oldest spindle pole (mother) in a cenexin-dependent manner (Gasic *et al.*, 2015). This suggests a reason for a sensing mechanism to be in place specifically at the mother spindle pole. To confirm and expand upon the findings of Gasic *et al.* (2015), we utilized control and cenexin-depleted HeLa cells stably expressing GFP-centrin (to determine centrosome age; Figure 3, A–D, and Supplemental Figure 3, A and B; Piel *et al.*, 2000; Kuo *et al.*, 2011) and mCherry-CENPA (to follow chromosome missegregation by marking kinetochores; Posch *et al.*, 2010; Gasic *et al.*, 2015). The number of chromosomes (marked by mCherry-CENPA) that misaligned were evaluated by live-cell video microscopy (Supplemental Figure 3, C and D, and Supplemental Video 3). We found a preferential directionality in misaligned chromosomes toward the mother (53.7%), compared with the daughter (19.5%), and toward both spindle poles (26.8%; Supplemental Figure 3C). Notably, we found that anywhere between 1 and 6 chromosomes can misalign toward the mother, whereas ≤2 chromosomes tend to misalign toward the daughter under control conditions (Supplemental Figure 3C). These studies were confirmed over four experiments where 54.17 ± 6.59% of cells presented with preferential chromosome misalignment toward the mother (Supplemental Figure 3D). However, this preferential misalignment is disrupted in cells where cenexin is depleted by shRNA (Supplemental Figure 3D). Together, the results suggest that chromosomes preferentially misalign toward the oldest spindle pole in a cenexin-dependent manner.

Because chromosomes preferentially misalign toward the oldest spindle pole (mother), and PLK1 activity is significantly increased at the mother in the presence of misaligned chromosomes, it is possible that directional chromosome misalignment occurs in a PLK1- and cenexin-dependent manner. To test this, we treated both control and cenexin-depleted cells with the PLK1 inhibitor, BI2536 (100 nM), fixed, and then scored metaphase cells that had misaligned chromosomes toward the mother, daughter, or both spindle poles (Figure 4A). In control cells, chromosomes tend to misalign toward the mother (58.08 ± 4.28% of cells; Figure 6, B and C, and Table 1). This preferential misalignment occurs under two methods of synchronization, either with 100 nM nocodazole followed by 20–30 min release (57.49% ± 11.79% mitotic cells misalign chromosomes toward the mother) or using 10 μM of ProTAME (56.79 ± 4.90% mitotic cells misalign chromosomes toward mother; Table 1). However, there was a significant decrease in the percentage of cells that misalign chromosomes toward the mother in cenexin-depleted cells (39.30 ± 4.00%; Figure 6, B and C, and Table 1), with an increase to both spindle poles (31.37 ± 1.90%, compared with controls at 20.10 ± 5.32%; Figure 6, B and C, and Table 1). With PLK1 inhibition (100 nM BI2536), the percentage of cells with preferential chromosome misalignment toward the mother significantly dropped to 44.63 ± 3.70% (Figure 6, B and C, and Table 1). These studies suggest that either PLK1 inhibition (BI2536 treatment), or cenexin depletion, causes an increased probability for chromosomes to misalign toward both spindle poles compared with just the mother.

To test whether PLK1 and cenexin might be acting together to modulate the direction of chromosome misalignment, we treated cenexin-depleted cells with the PLK1 inhibitor BI2536 and compared with control shRNA–treated cells, cells treated with BI2536 alone, and cenexin shRNA–treated cells. Strikingly, in cells treated with both cenexin shRNA and BI2536, cells are restored to control conditions, with 54.33 ± 5.21% of mitotic cells with misaligned chromosomes going toward the mother and only 18.07 ± 3.36% of cells with misaligned chromosomes toward both spindle poles (Figure 6, B and C, and Table 1). Of note, under these conditions 61 ± 3.40% of the total population of metaphase cells have misaligned chromosomes compared with BI2536- (44.63 ± 3.70%) or cenexin shRNA–treated (39.3 ± 4.0%; Table 1) cells.

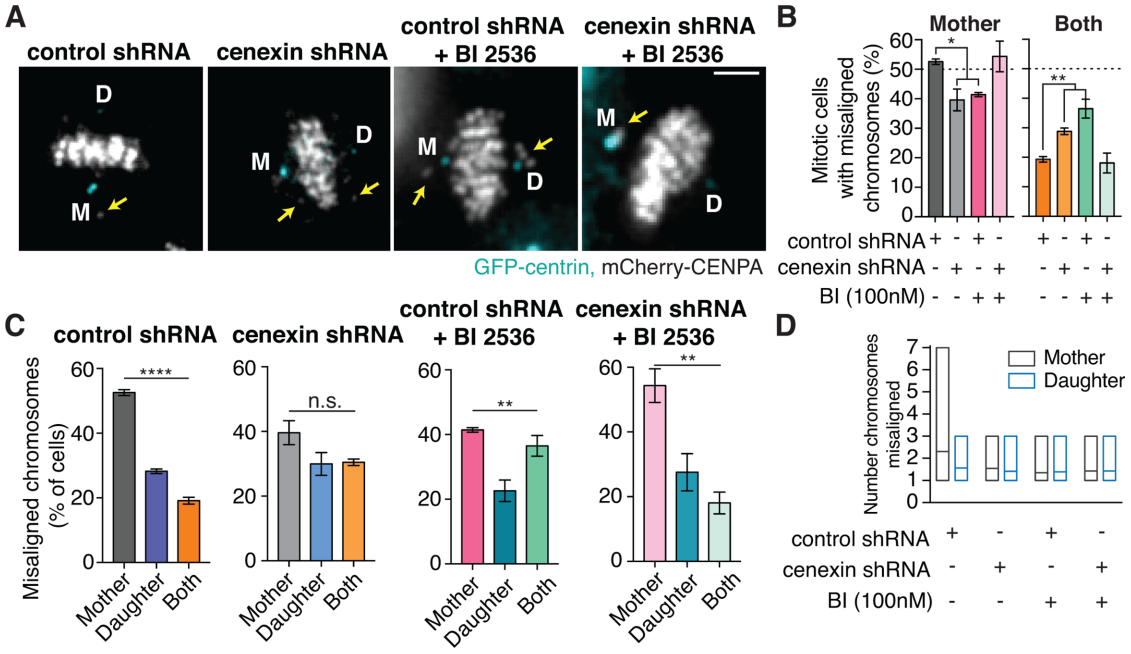



FIGURE 6: Chromosomes predominately misalign toward the oldest spindle pole in a PLK1- and cenexin-dependent manner. (A) Maximum confocal projections of HeLa cells stably expressing centrin-GFP, CENPA-mCherry, and either a control or cenexin shRNA, treated with 100 nM BI2536. Yellow arrows depict lagging chromosomes. Bar = 5 μm. (B) Bar graph quantifying percentage of cells that display misaligned chromosomes toward the mother spindle pole (left) or both spindle poles (right) in control and cenexin-depleted cells ± 100 nM BI2536 treatment. Dotted line at 50% represents randomization. $n = 3$ experiments ± SEM, one-way ANOVA (*, $p = 0.0131$; **, $p = 0.0028$). (C) Quantification of misaligned chromosome directionality (%) in control and cenexin-depleted HeLa cells ± 100 nM BI2536 treatment. $n > 50$ cells over $n = 3$ experiments ± SEM; a one-way ANOVA was performed for each condition: control shRNA ($p < 0.0001$), cenexin shRNA ($p = 0.1099$), control shRNA +BI ($p = 0.0063$), cenexin shRNA +BI ($p = 0.0047$). (D) Number of individual misaligned chromosomes toward either the mother (gray) or daughter (blue) spindle poles under conditions where chromosomes misalign in both directions. $n > 5$ experiments, range of data shown as a box plot, and center bar represents mean.

To test whether there is a bias under conditions where there is chromosome misalignment toward both spindle poles, the number of chromosomes toward the mother and daughter were scored per cell (Figure 6D). Control cells presented with a tendency for more chromosomes to misalign toward the mother spindle pole (anywhere from one to seven chromosomes, noted by CREST staining) compared with the side of the cell with the daughter (one to three chromosomes; Figure 6D). This trend toward the mother, however, is diminished when cells are treated with a cenexin shRNA, BI2536, or both cenexin shRNA and BI2536. Under these conditions, there is equal chromosome segregation to both sides of the spindle (anywhere from one to three chromosomes). This result suggests that, even under conditions of chromosome misalignment toward both spindle poles, there is still a bias for chromosomes to misalign toward the oldest spindle pole in a cenexin- and PLK1-dependent manner.

## DISCUSSION

Through this study, we determined that if chromosomes misalign, these chromosomes are more likely to misalign toward the oldest spindle pole (mother). Upon misalignment toward the mother, one cellular response that occurs is a cenexin-dependent increase in PLK1 activity at this site. On the basis of this result, we present a model where cenexin and PLK1 work together in response to misaligned chromosomes. We propose this model based on the known interaction between PLK1 and cenexin (Soung *et al.*, 2006, 2009), and our studies that identified PLK1 in a ring-like structure at the mother spindle pole colocalizing with the ring-like structure cenexin forms (Figure 3E). Additionally, we find that PLK1 inhibition or cenexin depletion causes chromosomes to no longer preferentially misalign toward the mother (Figure 6, A–C, and Table 1). Instead, chromosomes tend to misalign more toward both spindle poles (Figure 6, B and C, and Table 1). However, if we combine PLK1 inhibition with cenexin depletion, we restore the propensity for chromosomes to misalign toward the mother (Figure 6, B and C, and Table 1), but cause an increased percentage of mitotic cells to have misaligned chromosomes (61.00 ± 3.40% compared with cenexin depletion at 39.3 ± 4.0%). From these studies we propose a model that PLK1 and cenexin work together as a sensor to correct and respond to chromosome misalignment.

Another potential model is that the mother spindle pole is driving chromosomes to misalign toward itself and is not necessarily acting as a sensor to fix a misaligned chromosome. If this were the case, we would propose that depleting cenexin would decrease chromosome misalignment toward the mother, but not affect overall chromosome misalignment. Here, we find that cenexin depletion significantly decreases chromosome misalignment toward the mother spindle pole (Figure 6B and Table 1), but causes a subsequent increase in the total percentage of cells that present with misaligned chromosomes toward both spindle poles (Figure 6, B and C, and Table 1). We did not find a condition that preferentially forced chromosomes to misalign toward the daughter spindle

pole. These data support our first proposed model that PLK1 and cenexin work as a sensor to respond to and fix chromosome misalignment.

We predict that in order for PLK1 and cenexin to act as a sensor to fix misaligned chromosomes, a feedback mechanism needs to be in place to alert the spindle pole to a misaligned chromosome in close proximity. Active PLK1 resides at the kinetochore of misaligned chromosomes, acting as a mitotic checkpoint until proper microtubule attachments have been made and the error has been rectified (Liu *et al.*, 2012). To date, distinct, independent pools of active PLK1 have not been identified between spindle poles and kinetochores. This leaves the potential for active-PLK1 to cross-communicate or exchange between the kinetochores and centrosomes, alerting the oldest spindle pole of a misaligned chromosome. This would allow the spindle pole closest to the lagging chromosome to become hyperactivated through increased PLK1 activity. This increase in PLK1 activity could potentially recruit more PCM components to nucleate more microtubules to correct the misaligned chromosome. PLK1 activity has been associated with recruiting PCM proteins such as pericentrin, CEP215, and γ-tubulin (Lee and Rhee, 2011; Kong *et al.*, 2014; Ramani *et al.*, 2018). Each of these components is also known to be enriched at the oldest spindle pole and CEP215 and pericentrin form a complex with the mother centriole appendage protein, centriolin (Conduit and Raff, 2010; Conduit *et al.*, 2010; Chen *et al.*, 2014). Thus, increased PLK1 activity specifically at the mother spindle pole can lead to pericentriolar material remodeling specifically at this spindle pole.

Our finding that a bias exists in chromosome misalignment toward the mother spindle pole may have evolutionary implications. For instance, previous studies have determined using the *Drosophila* germline that the mother spindle pole is inherited by the daughter cell that remains stem, while the daughter spindle pole is inherited by the cell destined for differentiation (Yamashita *et al.*, 2007). When stem cells divide, these divisions are responsible for repopulating the stem-cell niche, as well as providing cells that will differentiate. This preference for the mother to be inherited by the cell which remains within the stem cell population could shed light on why the oldest spindle pole preferentially misaligns chromosomes during division. Stem cells are better equipped to cope with aneuploidy compared with differentiated cells (reviewed in Garcia-Martinez *et al.*, 2016), due to the importance of these cells in maintaining genome integrity. To combat aneuploidy, stem cells have multiple forms of defense. These defenses include increased expression of DNA damage repair (DDR), which can repair the genomic errors associated with aneuploidy (Maynard *et al.*, 2008) and p53-driven apoptosis or spontaneous differentiation, which removes the aneuploid cell from the stem cell population to retain genomic integrity (Jain *et al.*, 2012). An alternative viewpoint in this argument is that stem cells provide an opportunity to pass on "cultural adaptations" that may arise as the result of aneuploidy (Enver *et al.*, 2005). This would allow stem cells to develop an advantage due to this new, unique genome, allowing for adaptations in differentiated cells previously unavailable. Together, this could explain why our studies showed a preferential, directional misalignment of chromosomes toward the mother.

In conclusion, our studies utilize both a zebrafish embryonic model and an in vitro cell culture model to demonstrate an asymmetry in PLK1 distribution and activity between the two spindle poles. Here, we argue that this asymmetry is conserved and occurs predominately during instances of chromosome misalignment toward the mother spindle pole.

## MATERIALS AND METHODS

### Antibodies and chemical inhibitors

For Western blot analysis and immunofluorescence imaging, the following antibodies were used: mouse anti-PLK1 (E-2; Santa Cruz; sc-55504; 1:250), rabbit anti-cenexin (Proteintech; 12058-1-AP; 1:250), mouse anti–α-tubulin monoclonal antibody (Proteintech; 66031-1-Ig; 1:10,000), human anti-CREST (Antibodies; 15-234-0001; 1:1000), mouse anti-centrin clone 20H5 (Millipore Sigma; 04-1624; 1:1000), rabbit anti-CEP164 (Novus Biologicals; NBP1-81445; 1:50), and mouse anti-centrobin (Abcam; ab70448; 1:500). Horseradish peroxidase (HRP)-conjugated antibodies: donkey anti-mouse immunoglobulin G (IgG) (H+L; Jackson ImmunoResearch Labs; 715-035-150), donkey anti-rabbit IgG (H+L; Jackson ImmunoResearch Labs; 711-035-152), and mouse anti-GAPDH (1:10,000, Sigma Aldrich; 45-9295). Fluorescent secondary antibodies include Alexa Fluor donkey anti–mouse 488 (Life Technologies; A21202), 568 (Life Technologies; A10037), and 647 (Life Technologies; A31571); Alexa Fluor donkey anti–rabbit 488 (Life Technologies; A21206), 568 (Life Technologies; A10042), 647 (Life Technologies; A31573), rhodamine-conjugated donkey anti-human (Jackson Immunoresearch; 709-025-149), and DyLight 649-conjugated goat anti-human (Jackson Immunoresearch; 109-495-064). Chemical inhibitors include nocodazole used on cells at 100 nM (Fisher; AC358240500), ProTAME (Fisher; I44001M) used on cells at 10 µM, and BI2536 (Selleck Chemicals; S1133-5 mg) used on cells at 100 nM.

### Zebrafish

Zebrafish embryos (provided by Jeffrey Amack's laboratory, SUNY Upstate Medical University) were injected with 100–150 pg PLK1-mCherry mRNA immediately following fertilization. Injected zebrafish were then grown at 30°C until 4.5 h postfertilization. For live imaging, embryos were mounted in MatTek dishes using 2% agar and imaged at 30°C. For fixed imaging, embryos were fixed at 4.5 hpf in 4% paraformaldehyde (PFA) + 0.5% Triton X-100 overnight at 4°C. The following day, embryos were washed in phosphate-buffered saline (PBS) + 0.5% Tween for 20 min, dechorionated, and placed in NucBlue fixed cell stain from Ready Probes (Thermo Fisher Scientific; R37606) for 30 min before imaging.

### Cell culture

HeLa cells expressing either control or cenexin shRNA (Hung *et al.*, 2016) and PLK1-GFP RPE cells were used throughout this study. For live-cell imaging, a GFP-centrin/ mCherry-CENPA HeLa cell line was used, a kind gift from Patrick Meraldi, Department of Cell Physiology and Metabolism, Université de Genève (Gasic *et al.*, 2015). All cultures were grown in 1X DMEM (Life Technologies) supplemented with 10% Seradigm FBS (VWR) and 1% penicillin–streptomycin (10,000 U/ml; Life Technologies) and maintained at 37°C with 5% $CO_2$. Cells were synchronized as noted with either nocodazole (100 nM) or ProTAME (10 µM). For nocodazole synchronization, cells were incubated for at least 6 h in nocodazole to synchronize in prometaphase and then washed with fresh media three times and incubated for 20 min for cells to synchronize in metaphase. With ProTAME synchronization, cells were incubated for 6 h and then immediately fixed.

### shRNA and plasmid constructs

Control shRNA and cenexin shRNA (Hung *et al.*, 2016) were infected in HeLa cells stably expressing GFP-centrin and mCherry-CENPA to create a stable cenexin-depleted cell line. Lentiviruses used to generate the stable cell lines used the protocol of Hung *et al.* (2016). FRET experiments were performed using a centrosome-localized

PLK1 FRET-biosensor. This previously characterized biosensor was localized to the centrosome through fusion to the PACT domain (Colicino *et al.*, 2018). pCS2-PLK1-mCherry constructs were generated and verified through sequencing.

### Immunofluorescence 2D cultures

Cells were plated on #1.5 coverslips until they reached 90% confluence, and fixed using either methanol (–20°C; described in Colicino *et al.*, 2018) or 4% PFA containing 0.5% Triton X-100 at room temperature for 30 min. Cells were washed, blocked with PBSΔT (PBS, 1% bovine serum albumin, 0.5% Triton X-100), and incubated with primary antibodies for 1 h at room temperature. Cultures were washed three times with PBSΔT and incubated with secondary antibodies for 1 h at room temperature. Coverslips were rinsed with di$H_2O$ and mounted on glass slides using either Vectashield (Vector Laboratories; H-1000) or Prolong Diamond with DAPI mounting media (Thermo Fisher Scientific; P36971).

### FRET

HeLa cells expressing either control or cenexin shRNA (Hung *et al.*, 2016) were transfected with PLK1 FRET-PACT sensor using Mirus Bio TransIT-X transfection reagent. After 48 h, cells were treated with 100 nM nocodazole and synchronously released into metaphase after 6 h to induce lagging chromosomes. Cells were imaged live or then fixed using 4% PFA containing 0.5% Triton X-100 at room temperature for 30 min. Cells were immunostained for centrobin (1:500) or centrin (1:1000) to distinguish between the spindle poles and CREST (1:1000) to visualize kinetochores. Coverslips were then mounted in vectashield and imaged using a Leica DMi8 STP800 (Leica, Bannockburn, IL) equipped with an 89 North–LDI laser, Photometrics Prime-95B camera, Crest Optics: X-light V2 Confocal Unit spinning disk, using a HC PL APO 63×/1.40 NA oil CS2 objective. For these experiments, $YFP^{ex}\rightarrow YFP^{em}$ control images were taken, using a 520-excitation laser. $CFP^{ex}\rightarrow YFP^{em}$ was imaged using a 445-excitation laser. The $YFP^{ex}\rightarrow YFP^{em}/CFP^{ex}\rightarrow YFP^{em}$ FRET ratio was calculated using ImageJ Ratio-Plus plug-in after background subtraction and averaged over multiple cells. Experiments were repeated multiple times with similar results.

### Imaging

Zebrafish and tissue culture cells were imaged using a Leica SP8 scanning confocal microscope (Leica, Bannockburn, IL) or a Leica DMi8 equipped with a X-light V2 Confocal Unit spinning disk. The Leica SP8 was equipped with an HC PL APO 40×/1.10 W CORR CS2 objective equipped with Leica LAS-X software (Leica). The Leica DMi8 STP800 (Leica, Bannockburn, IL) equipped with a Lumencor SPECTRA X (Lumencor, Beaverton, OR) with a Hamamatsu ORCA-flash 4.0 V2 CMOS C11440-22CU camera or 89 North–LDI laser with a Photometrics Prime-95B camera taken with a Crest Optics: X-light V2 Confocal Unit spinning disk. Optics used were either HC PL APO 63×/1.40 NA oil CS2, HC PL APO 40×/1.10 NA WCS2 CORR, a 40 × 1.15 N.A. Lamda S LWD, or 100×/1.4 N.A. HC Pl Apo oil emersion objective. Metamorph or VisiView software was used to acquire images. Superresolution 3D-SIM images were acquired on a DeltaVision OMX V4 (GE Healthcare) equipped with a 60×/1.42 NA PlanApo oil immersion lens (Olympus), 405-, 488-, 568-, and 642-nm solid-state lasers and sCMOS cameras. Image stacks of 5–6 µm with 0.125-µm-thick z-sections and 15 images per optical slice (three angles and five phases) were acquired using immersion oil with a refractive index of 1.518. Images were reconstructed using Wiener filter settings of 0.003 and optical transfer functions measured specifically for each channel with SoftWoRx 6.1.3 (GE Healthcare). Images from different color channels were registered using parameters generated from a gold grid registration slide (GE Healthcare) and SoftWoRx 6.1.3 (GE Healthcare).

### Image analysis

z-Steps (0.2 µm) of cell volumes are presented as maximum projections using ImageJ. Integrated intensities were measured on sum projections as described in Hoffman *et al.* (2001). Line scans were performed by calculating the normalized fluorescence intensity across a single line; poles were determined as the oldest if they had elevated centrin (as reported in Kuo *et al.*, 2011). Spindle pole integrated intensities were measured from sum confocal projections. Background fluorescence was measured based on values from control shRNA–treated cells and subtracted from both control and cenexin shRNA–treated cells. A ROI was placed over spindle poles (marked with GFP-centrin or cenexin, depending) and the fluorescence intensity was measured. The same ROI was used for all images. Graphs and statistical analysis (unpaired Student's *t* tests or analysis of variance [ANOVA] as labeled) were completed using Graphpad Prism software. Error bars represent ± SEM; $p < 0.05$ were considered to be statistically significant. All images were set to a resolution of 300 DPI or greater after image analysis from raw data.

To quantify PLK1 intensity ratios between poles in zebrafish embryos, a maximum projection was created using a z-stack that encompassed both spindle poles of a metaphase cell. A ROI was drawn around one pole of a single cell within an embryo using FIJI/ImageJ. The same ROI was used for all images. The mean intensity was calculated by subtracting the minimum intensity from that measured region. A ratio was calculated by dividing the value of the pole with the smaller intensity by the value of the pole with the larger intensity. This yielded a value greater or equal to 1. Graphs and statistical analysis (unpaired Student's *t* tests or ANOVA analysis as labeled) were completed using Graphpad Prism software.

## ACKNOWLEDGMENTS

This work was supported by National Institutes of Health Grants no. R00GM107355 and no. R01GM127621 (to H.H.) and the Carol Baldwin Foundation of Central New York (to H.H. while at SUNY Upstate Medical University). This work was supported by the U.S. Army Medical Research Acquisition Activity through the FY 16 Prostate Cancer Research Programs under Award no. W81XWH-17-1-0241 (to H.H.). Opinions, interpretations, conclusions, and recommendations are those of the authors and are not necessarily endorsed by the Department of Defense. We thank Patrick Meraldi for providing us the centrin-GFP/CENPA-mCherry HeLa cell line (Gasic *et al.*, 2015) and Patrina Pellet (previously at G.E.) for assistance obtaining SIM images. We thank Dan Bergstralh (University of Rochester), Wenyi Feng, Leszek Kotula, and David Pruyne (SUNY Upstate Medical University) for careful edits and suggestions on earlier versions of this article.

## REFERENCES

Burkard ME, Randall CL, Larochelle S, Zhang C, Shokat KM, Fisher RP, Jallepalli PV (2007). Chemical genetics reveals the requirement for Polo-like kinase 1 activity in positioning RhoA and triggering cytokinesis in human cells. Proc Natl Acad Sci USA 104, 4383–4388.

Chen CT, Hehnly H, Yu Q, Farkas D, Zheng G, Redick S, Hung HF, Samtani R, Jurczyk A, Akbarian S, *et al.* (2014). A unique set of centrosome proteins requires pericentrin for spindle-pole localization and spindle orientation. Curr Biol 24, 2327–2334.

Colicino EG, Garrastegui AM, Freshour J, Santra P, Post DE, Kotula L, Hehnly H (2018). Gravin regulates centrosome function through PLK1. Mol Biol Cell 29, 532–541.

Colicino EG, Hehnly H (2018). Regulating a key mitotic regulator, polo-like kinase 1 (PLK1). Cytoskeleton (Hoboken) 75, 481–494.
Conduit PT, Brunk K, Dobbelaere J, Dix CI, Lucas EP, Raff JW (2010). Centrioles regulate centrosome size by controlling the rate of Cnn incorporation into the PCM. Curr Biol 20, 2178–2186.
Conduit PT, Raff JW (2010). Cnn dynamics drive centrosome size asymmetry to ensure daughter centriole retention in *Drosophila* neuroblasts. Curr Biol 20, 2187–2192.
Crasta K, Ganem NJ, Dagher R, Lantermann AB, Ivanova EV, Pan Y, Nezi L, Protopopov A, Chowdhury D, Pellman D (2012). DNA breaks and chromosome pulverization from errors in mitosis. Nature 482, 53–58.
Enver T, Soneji S, Joshi C, Brown J, Iborra F, Omtoft T, Thykjaer T, Maltby E, Smith K, Abu Dawud R, *et al*. (2005). Cellular differentiation hierarchies in normal and culture-adapted human embryonic stem cells. Hum Mol Genet 14, 3129–3140.
Garcia-Martinez J, Bakker B, Schukken KM, Simon JE, Foijer F (2016). Aneuploidy in stem cells. World J Stem Cells 8, 216–222.
Gasic I, Nerurkar P, Meraldi P (2015). Centrosome age regulates kinetochore-microtubule stability and biases chromosome mis-segregation. Elife 4, 1.
Hehnly H, Canton D, Bucko P, Langeberg LK, Ogier L, Gelman I, Santana LF, Wordeman L, Scott JD (2015). A mitotic kinase scaffold depleted in testicular seminomas impacts spindle orientation in germ line stem cells. Elife 4, e09384.
Hehnly H, Chen C-T, Powers CM, Liu H-L, Doxsey S (2012). The centrosome regulates the Rab11-dependent recycling endosome pathway at appendages of the mother centriole. Curr Biol 22, 1944–1950.
Hoffman DB, Pearson CG, Yen TJ, Howell BJ, Salmon ED (2001). Microtubule-dependent changes in assembly of microtubule motor proteins and mitotic spindle checkpoint proteins at PtK1 kinetochores. Mol Biol Cell 12, 1995–2009.
Hung H-F, Hehnly H, Doxsey S (2016). The mother centriole appendage protein cenexin modulates lumen formation through spindle orientation. Curr Biol 26, 793–801.
Ishikawa H, Kubo A, Tsukita S, Tsukita S (2005). Odf2-deficient mother centrioles lack distal/subdistal appendages and the ability to generate primary cilia. Nat Cell Biol 7, 517–524.
Jain AK, Allton K, Iacovino M, Mahen E, Milczarek RJ, Zwaka TP, Kyba M, Barton MC (2012). p53 regulates cell cycle and MicroRNAs to promote differentiation of human embryonic stem cells. PLoS Biol 10, e1001268–16.
Januschke J, Llamazares S, Reina J, Gonzalez C (2011). Drosophila neuroblasts retain the daughter centrosome. Nat Comm 2, 243.
Kimmel CB, Ballard WW, Kimmel SR, Ullmann B, Schilling TF (1995). Stages of embryonic development of the zebrafish. Dev Dyn 203, 253–310.
Kishi K, van Vugt MATM, Okamoto K-I, Hayashi Y, Yaffe MB (2009). Functional dynamics of Polo-like kinase 1 at the centrosome. Mol Cell Biol 29, 3134–3150.
Kobayashi T, Dynlacht BD (2011). Regulating the transition from centriole to basal body. J Cell Biol 193, 435–444.
Kong D, Farmer V, Shukla A, James J, Gruskin R, Kiriyama S, Loncarek J (2014). Centriole maturation requires regulated Plk1 activity during two consecutive cell cycles. J Cell Biol 206, 855–865.
Kuo TC, Chen CT, Baron D, Onder TT, Loewer S, Almeida S, Weismann CM, Xu P, Houghton JM, Gao FB, *et al*. (2011). Midbody accumulation through evasion of autophagy contributes to cellular reprogramming and tumorigenicity. Nat Cell Biol 13, 1214–1223.
Lampson MA, Cheeseman IM (2011). Sensing centromere tension: aurora B and the regulation of kinetochore function. Trends Cell Biol 21, 133–140.
Lee K, Rhee K (2011). PLK1 phosphorylation of pericentrin initiates centrosome maturation at the onset of mitosis. J Cell Biol 195, 1093–1101.
Liu D, Davydenko O, Lampson MA (2012). Polo-like kinase-1 regulates kinetochore-microtubule dynamics and spindle checkpoint silencing. J Cell Biol 198, 491–499.
Maynard S, Swistowska AM, Lee JW, Liu Y, Liu S-T, Da Cruz AB, Rao M, de Souza-Pinto NC, Zeng X, Bohr VA (2008). Human embryonic stem cells have enhanced repair of multiple forms of DNA damage. Stem Cells 26, 2266–2274.
Piel M, Meyer P, Khodjakov A, Rieder CL, Bornens M (2000). The respective contributions of the mother and daughter centrioles to centrosome activity and behavior in vertebrate cells. J Cell Biol 149, 317–330.
Posch M, Khoudoli GA, Swift S, King EM, Deluca JG, Swedlow JR (2010). Sds22 regulates aurora B activity and microtubule-kinetochore interactions at mitosis. J Cell Biol 191, 61–74.
Ramani A, Mariappan A, Gottardo M, Mandad S, Urlaub H, Avidor-Reiss T, Riparbelli M, Callaini G, Debec A, Feederle R, *et al*. (2018). Plk1/Polo phosphorylates Sas-4 at the onset of mitosis for an efficient recruitment of pericentriolar material to centrosomes. Cell Rep 25, 3618–3630.e6.
Schmidt KN, Kuhns S, Neuner A, Hub B, Zentgraf H, Pereira G (2012). Cep164 mediates vesicular docking to the mother centriole during early steps of ciliogenesis. J Cell Biol 199, 1083–1101.
Soung N-K, Kang YH, Kim K, Kamijo K, Yoon H, Seong YS, Kuo YL, Miki T, Kim SR, Kuriyama R, *et al*. (2006). Requirement of hCenexin for proper mitotic functions of polo-like kinase 1 at the centrosomes. Mol Cell Biol 26, 8316–8335.
Soung N-K, Park J-E, Yu L-R, Lee KH, Lee J-M, Bang JK, Veenstra TD, Rhee K, Lee KS (2009). Plk1-dependent and -independent roles of an ODF2 splice variant, hCenexin1, at the centrosome of somatic cells. Dev Cell 16, 539–550.
Vertii A, Bright A, Delaval B, Hehnly H, Doxsey S (2015). New frontiers: discovering cilia-independent functions of cilia proteins. EMBO Rep 16, 1275–1287.
Vertii A, Hung H-F, Hehnly H, Doxsey S (2016). Human basal body basics. Cilia 5, 13.
Vertii A, Kaufman PD, Hehnly H, Doxsey S (2018). New dimensions of asymmetric division in vertebrates. Cytoskeleton (Hoboken) 75, 87–102.
Wang G, Chen Q, Zhang X, Zhang B, Zhuo X, Liu J, Jiang Q, Zhang C (2013). PCM1 recruits Plk1 to the pericentriolar matrix to promote primary cilia disassembly before mitotic entry. J Cell Sci 126, 1355–1365.
Wang X, Tsai J-W, Imai JH, Lian W-N, Vallee RB, Shi S-H (2009). Asymmetric centrosome inheritance maintains neural progenitors in the neocortex. Nature 461, 947–955.
Yamashita YM, Mahowald AP, Perlin JR, Fuller MT (2007). Asymmetric inheritance of mother versus daughter centrosome in stem cell division. Science 315, 518–521.

# Supplemental Materials

***Molecular Biology of the Cell***

Colicino et al.

**SUPPLEMENTAL FIGURE LEGENDS**

# Chromosome misalignment is associated with PLK1 activity at cenexin-positive mitotic centrosomes.

Erica G. Colicino[1,2], Katrina Stevens[3], Erin Curtis[1], Lindsay Rathbun[1], Michael Bates[1], Julie Manikas[1], Jeffery Amack[2], Judy Freshour[1], and Heidi Hehnly[1]

[1] Department of Biology, Syracuse University Syracuse, NY

[2] Department of Cell and Developmental Biology, Upstate Medical University Syracuse, NY

[3] Department of Biology, Clarkson University Potsdam, NY

Correspondence to: hhehnly@syr.edu

**Supplemental Figure 1.**

**(A)** Model depicting PLK1 (magenta) localization to spindle poles, kinetochores, and cytokinetic midbody. DNA = blue. **(B)** Model depicting zebrafish embryo 4.5 hours post fertilization (hpf)**.** Drawn inset represents area imaged in (**C**) along the yolk boundary. **(C)** A maximum confocal projection is presented for PLK1-mCherry. Bar = 50μm. Inset of single metaphase cell. Bar = 5μm. Magenta dotted line represents yolk boundary. **(D)** PLK1-mCherry expression at 4.5hpf. Cells positive for PLK1-mCherry are indicative of dividing cells. Bar = 10μm. Inset marked 1 is magnified in (**E**). **(E)** A maximum confocal projection of a single metaphase cell expressing PLK1-mCherry at spindle poles and kinetochores. Bar = 5μm.

**Supplemental Figure 2. (A)** Immunofluorescence staining of Hela cells at metaphase; centrioles (centrin, cyan), CEP164 (magenta), and CREST (grey). M depicts mother spindle pole, and D depicts daughter spindle pole. Bar = 5μm. **(B)** Top, maximum confocal images of fixed individual HeLa cells with misaligned chromosomes that are stained for CREST (red) and centrin (green) and mounted in Prolong containing DAPI shown in metaphase. The images depict either a misaligned chromosome to the mother (M) mitotic centrosome (left image), or a misaligned chromosome to the daughter (D) mitotic centrosome (right image). Bottom, line scan bisecting the two spindle poles, illustrating centrin concentration predominately localized to the mother (M) spindle pole compared to the daughter (D). Bar = 5 μm. **(C)** A maximum confocal projection of a HeLa cell stained for centrin (cyan), Aurora B (magenta), and CREST (grey). A misaligned chromosome misaligning towards the older (mother) spindle pole is positive for Aurora B between two CREST puncta. 3X zoom of inset in **(a')**. Bar = 5 μm. **(D)** Maximum confocal projections of control shRNA and cenexin shRNA treated HeLa cells that were synchronized at metaphase in proTAME (10 mM). Cells were stained for centrin (cyan), Aurora B (magenta), and CREST (grey). Bar = 5 μm.

**Supplemental Figure 3. (A)** Maximum confocal micrographs of single HeLa cells stably expressing CENPA-mCherry (black) and either control or cenexin shRNA from prometaphase/metaphase through telophase. Bars = 5μm. **(B)** Maximum projection micrographs of centrin-GFP (magenta) from corresponding images of CENPA-mCherry in A. Line graphs (below) bisecting the two spindle poles, representing greater centrin concentrations at the mother (M) compared to the daughter (D) in both control and cenexin-depleted cells. Bar = 5μm. **(C)** The number and directionality of misaligned chromosomes toward the mother (gray), daughter (blue) or both (orange) mitotic centrosomes was counted in control and cenexin-depleted HeLa cells. Each mark along the x-axis represents a single cell. Data represents a single representative experiment. **(D)** Bar graphs quantifying percentage of cells with directional chromosome misalignment toward either the mother, daughter, or both mitotic centrosomes from live-cell imaging. (n=4 experiments± S.E.M, One-way ANOVA, Control shRNA ($p=0.0069$) and cenexin shRNA ($p=0.8331$)).

**Video 1. PLK1-mCherry is enriched at spindle poles, kinetochores, and cytokinetic midbody in live zebrafish embryos.**

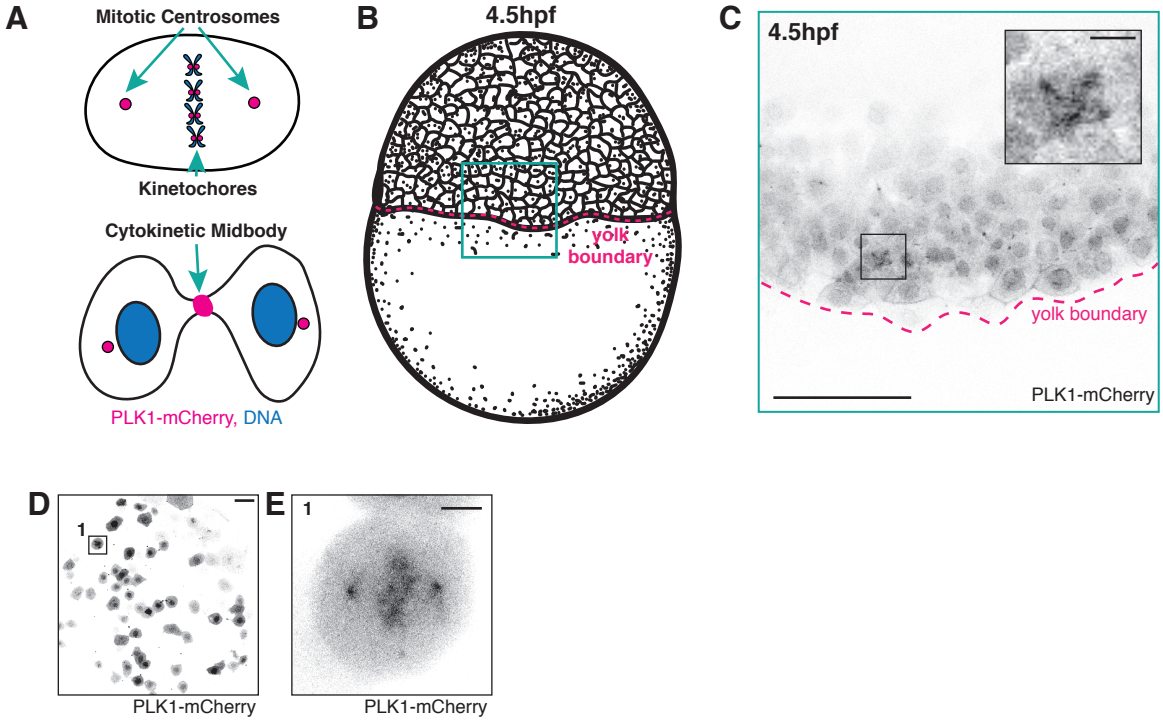
Maximum confocal micrographs of a single mitotic cell in a live zebrafish embryo (4.5 hpf) expressing PLK1-mCherry from prometaphase through cytokinesis. Images from every 60 seconds, over 6 minutes. Bar = 10μm.

**Video 2. PLK1-GFP asymmetrically distributes and is exchanged at the two spindle poles during metaphase.**

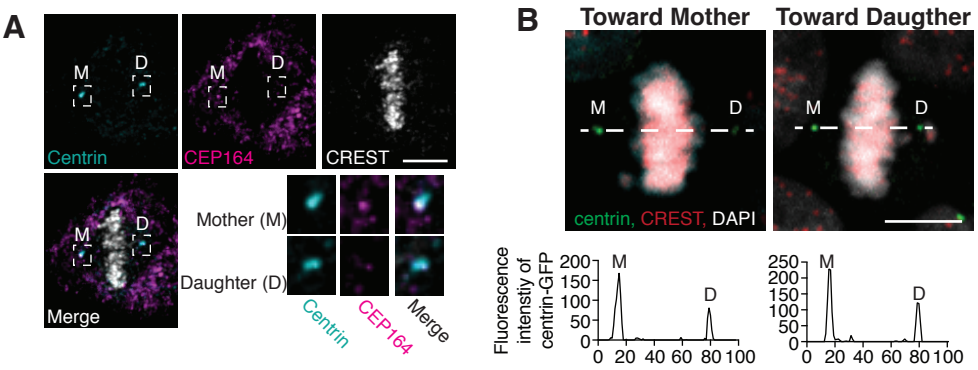
Fluorescence recovery after photobleaching of RPE cells stably expressing GFP-PLK1 at mitotic centrosomes during metaphase. Images taken every 113 milliseconds for 18 seconds. (Fire-LUT, ImageJ). Bar = 5μm.

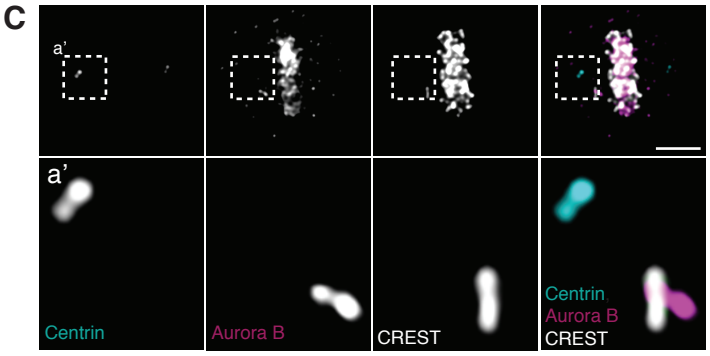
**Video 3. Chromosomes predominately misalign toward the oldest spindle pole in a cenexin-dependent manner.**

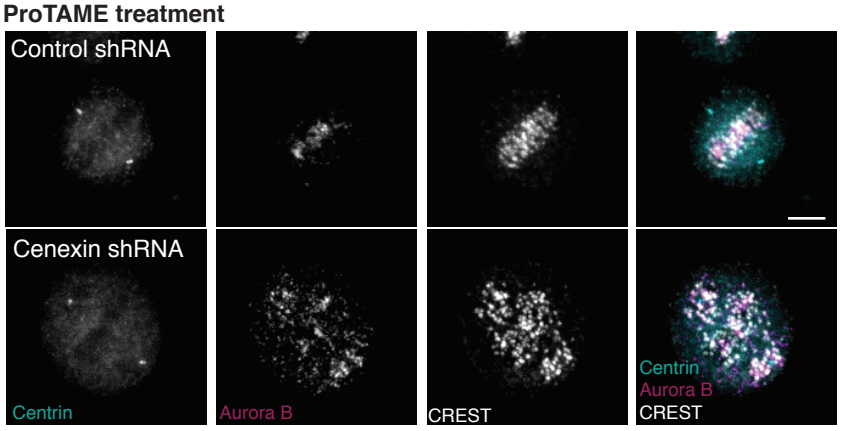
Maximum confocal micrographs of single HeLa cells stably expressing CENPA-mCherry (black) and either control (left) or cenexin (right) shRNA from prometaphase/metaphase through cytokinesis. Images taken every 3 seconds for 84 seconds. Bar = 5μm.



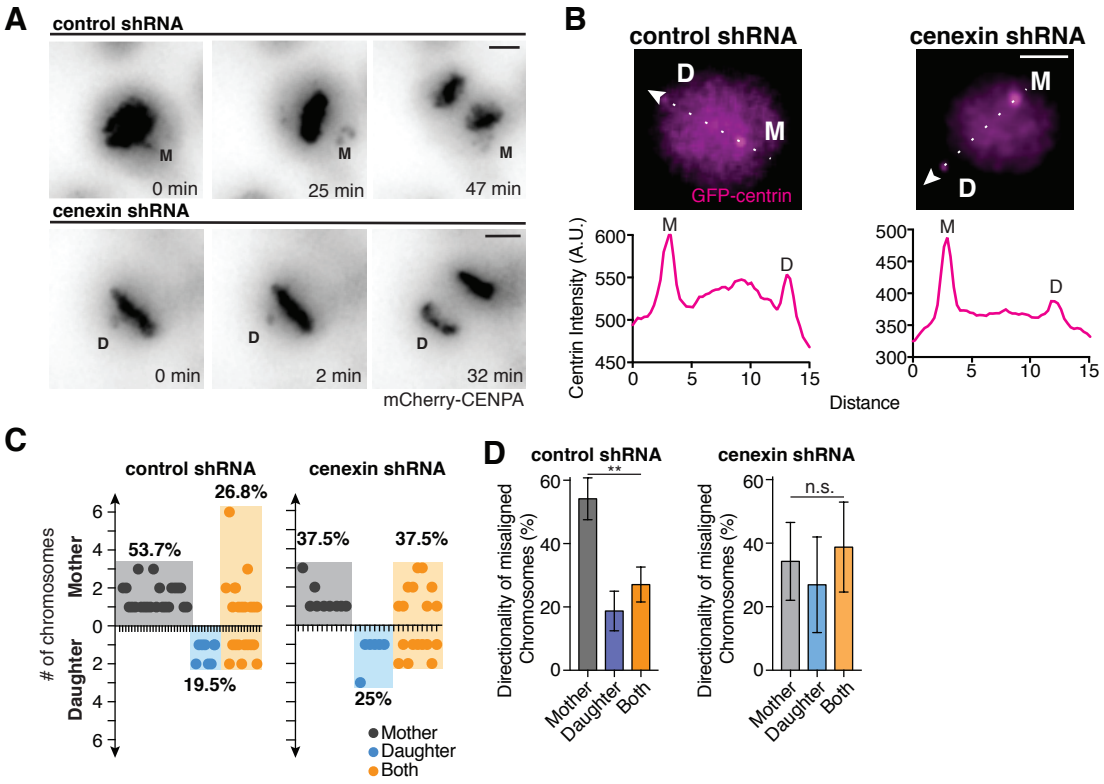

**Supplemental Figure 1.**




**Supplemental Figure 2.**




**Supplemental Figure 3.**